

DEVELOPMENT OF CATALYSTS FOR TRANSESTERIFICATION OF
PALM OIL AND HYDROGENATION OF METHYL LEVULINATE TO
GAMMA-VALEROLACTONE



CHAIANUN PANSAKDANON

A Thesis Submitted in Partial Fulfillment of the Requirements for the
Degree of Doctor of Philosophy in Chemistry
Suranaree University of Technology
Academic Year 2023

การพัฒนาตัวเร่งปฏิกิริยาสำหรับทรานส์เอสเทอร์ิฟิเคชันของน้ำมันปาล์ม และ
การเติมไฮโดรเจนของเมทิลเลวุลิเนตไปเป็นแกมมาวาเลโรแลกโตน



นายไชยอนันต์ พันธุ์ศักดิ์านนท์

วิทยานิพนธ์นี้เป็นส่วนหนึ่งของการศึกษาตามหลักสูตรปริญญาวิทยาศาสตรดุษฎีบัณฑิต
สาขาวิชาเคมี
มหาวิทยาลัยเทคโนโลยีสุรนารี
ปีการศึกษา 2566

DEVELOPMENT OF CATALYSTS FOR TRANSESTERIFICATION OF PALM OIL AND
HYDROGENATION OF METHYL LEVULINATE TO GAMMA-VALEROLACTONE

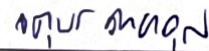
Suranaree University of Technology has approved this submitted in partial fulfillment
of the requirements for the Degree of Doctor of Philosophy.

Thesis Examining Committee



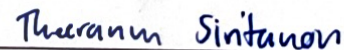
(Assoc. Prof. Dr. Anyanee Kamkaew)

Chairperson



(Prof. Dr. Jatuporn Wittayakun)

Member (Thesis advisor)



(Assoc. Prof. Dr. Theeranun Siritanon)

Member



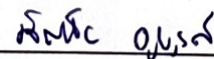
(Assoc. Prof. Dr. Sanchai Prayoonpokarach)

Member



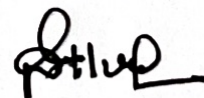
(Asst. Prof. Dr. Natkanin Supamathanon)

Member



(Dr. Sanchai Kuboon)

Member



(Prof. Dr. Santi Maensiri)

Dean of Institute of Science



(Assoc. Prof. Dr. Yupaporn Ruksakulpiwat)

Vice Rector for Academic Affairs
and Quality Assurance

ไชยอนันต์ พันธุ์ศักดิ์กานนท์ : การพัฒนาตัวเร่งปฏิกิริยาสำหรับทรานส์เอสเทอร์ิฟิเคชันของ
น้ำมันปาล์มและการเติมไฮโดรเจนของเมทิลเลวูลิเนตไปเป็นแกมมาวาเลโรแลกโตน

(DEVELOPMENT OF CATALYSTS FOR TRANSESTERIFICATION OF PALM OIL AND
HYDROGENATION OF METHYL LEVULINATE TO GAMMA-VALEROLACTONE)

อาจารย์ที่ปรึกษา : ศาสตราจารย์ ดร.จตุพร วิทยาคุณ, 78 หน้า

คำสำคัญ: โพลีเอสเตอร์/ ซีโอไลต์/ ตัวเร่งปฏิกิริยา/ ความเป็นผลึก/ ทรานส์เอสเทอร์ิฟิเคชัน/
น้ำมันปาล์ม/ เมทิลเลวูลิเนต/ วาเลโรแลกโตน/ นิกเกิล/ คอปเปอร์/ ไฮโดรจีเนชัน

จากการที่ความต้องการพลังงานทั่วโลกที่เพิ่มขึ้นอย่างต่อเนื่อง สวนทางกับการลดลงของ
เชื้อเพลิงจากฟอสซิล ทำให้การใช้พลังงานจากชีวมวลเป็นทางเลือกที่น่าสนใจอย่างมาก วิทยานิพนธ์
ฉบับนี้จึงมุ่งเน้นเกี่ยวกับการศึกษาและพัฒนาตัวเร่งปฏิกิริยาเพื่อใช้เปลี่ยนชีวมวลไปเป็นเชื้อเพลิง
ทางเลือกและสารเคมีมูลค่าสูง เช่น ไบโอดีเซลจากน้ำมันปาล์มและแกมมาวาเลโรแลกโตนจากเมทิล
เลวูลิเนต ตามลำดับ

ส่วนแรกของวิทยานิพนธ์ฉบับนี้เป็นการศึกษาถึงอิทธิพลจากความเป็นผลึกของซีโอไลต์ NaX
ที่ใช้เป็นวัสดุรองรับในตัวเร่งปฏิกิริยาโพลีเอสเตอร์ที่รองรับบนซีโอไลต์ NaX ซึ่งใช้ในการเร่งปฏิกิริยา
ทรานส์เอสเทอร์ิฟิเคชันของน้ำมันปาล์มและเมทานอลเพื่อสังเคราะห์ไบโอดีเซล โดยใช้วิธีการ
ปรับเปลี่ยนเวลาในการไฮโดรเทอร์มอลตั้งแต่ 0, 4, 8, 12, และ 24 ชั่วโมง ในการเตรียมซีโอไลต์ NaX
ให้มีความเป็นผลึกแตกต่างกัน และใช้วิธีการเอ็บซุ่มด้วยสารตั้งต้นจากบัพเฟอร์โพลีเอสเตอร์อะซิ
เตตร่วมกับวิธีอัลตราซาวด์ในการเตรียมตัวเร่งปฏิกิริยา จากผลการศึกษาพบว่า เมื่อเพิ่มเวลาไฮโดร
เทอร์มอล จะส่งผลให้ความเป็นผลึกของซีโอไลต์ NaX เพิ่มขึ้น โดยซีโอไลต์ NaX จะเริ่มมี
โครงสร้างผลึกที่สมบูรณ์เมื่อเวลาไฮโดรเทอร์มอลตั้งแต่ 8 ชั่วโมงเป็นต้นไป และเมื่อใช้ซีโอไลต์ NaX
มาเตรียมเป็นตัวเร่งปฏิกิริยา พบว่าความเป็นผลึกที่มากขึ้นยังส่งผลต่อความเป็นเบสที่มากขึ้นของ
ตัวเร่งปฏิกิริยา และส่งผลโดยตรงต่อการทดสอบการเร่งปฏิกิริยาทรานส์เอสเทอร์ิฟิเคชันของน้ำมัน
ปาล์มและเมทานอล โดยตัวเร่งปฏิกิริยาที่ใช้ซีโอไลต์ NaX ที่มีความเป็นผลึกมาก จะให้ผลิตภัณฑ์
เป็นไบโอดีเซลที่มากด้วยเช่นกัน

ส่วนที่สองของวิทยานิพนธ์ฉบับนี้ เป็นการศึกษาพฤติกรรมของการเร่งปฏิกิริยาของตัวเร่ง
ปฏิกิริยานิกเกิล (Ni) และทองแดง (Cu) ในรูปของโลหะเดี่ยวและโลหะผสม (NiCu) เพื่อใช้เป็นตัวเร่ง
ปฏิกิริยาการเติมไฮโดรเจนของเมทิลเลวูลิเนตไปเป็นแกมมาวาเลโรแลกโตน ผลการศึกษาพบว่า
ตัวเร่งปฏิกิริยาทั้ง Ni และ NiCu นั้นดีสำหรับการเติมไฮโดรเจนของเมทิลเลวูลิเนตไปเป็นสารมัธยันตร์
(แกมมาไฮดรอกซีเพนทานอีน) แต่มีเพียง NiCu เท่านั้นที่มีแนวโน้มที่จะเร่งการแปลงแกมมาไฮดรอก

ซีเพนทาโนเอตไปเป็นแกมมาวาเลโรแลกโทนผ่านกระบวนการการเกิดปฏิกิริยาเป็นวงแหวนได้ดีกว่าตัวเร่งปฏิกิริยา Ni และยังพบว่าตัวเร่งปฏิกิริยา NiCu ให้ประสิทธิภาพที่ดีแม้ที่อุณหภูมิการทำปฏิกิริยาต่ำกว่า 140 องศาเซลเซียส ซึ่งให้ผลได้แกมมาวาเลโรแลกโทนมากถึงร้อยละ 75 เมื่อใช้เวลาการเกิดปฏิกิริยาที่ 6 ชั่วโมง ในทางตรงกันข้าม ตัวเร่งปฏิกิริยา Ni แสดงประสิทธิภาพเชิงเปรียบเทียบกับตัวเร่งปฏิกิริยา NiCu ที่อุณหภูมิ 200 องศาเซลเซียส เท่านั้น แต่ที่อุณหภูมิ 160 องศาเซลเซียส ตัวเร่งปฏิกิริยา Ni ให้ผลได้แกมมาวาเลโรแลกโทนเพียงร้อยละ 28 และไม่สามารถเร่งปฏิกิริยาที่อุณหภูมิต่ำกว่านี้ได้ เมื่อใช้ผลการทดลองนี้ไปคำนวณหาค่าพลังงานกระตุ้น พบว่า ที่กระบวนการเกิดปฏิกิริยาเป็นวงแหวน เมื่อใช้ตัวเร่งปฏิกิริยาเป็น Ni นั้น มีค่าพลังงานกระตุ้นมากกว่าของตัวเร่งปฏิกิริยา NiCu ประมาณสองเท่า (ค่า $E_a^{K_2}$ คือ 121.7 และ 56.0 kJ·mol⁻¹ สำหรับ Ni และ NiCu ตามลำดับ) การศึกษานี้ให้หลักฐานที่ชัดเจนถึงความเหนือกว่าของตัวเร่งปฏิกิริยา NiCu ในการผลิตแกมมาวาเลโรแลกโทน



มหาวิทยาลัยเทคโนโลยีสุรนารี

สาขาวิชาเคมี
ปีการศึกษา 2566

ลายมือชื่อนักศึกษา วิวัฒน์ นามะวงษา
ลายมือชื่ออาจารย์ที่ปรึกษา อศุภร นามะวงษา

CHAIANUN PANSAKDANON : DEVELOPMENT OF CATALYSTS FOR TRANSESTERIFICATION OF PALM OIL AND HYDROGENATION OF METHYL LEVULINATE TO GAMMA-VALEROLACTONE. THESIS ADVISOR : PROF. JATUPORN WITTAYAKUN, Ph.D. 78 PP.

Keyword: Potassium/ Zeolite/ Catalyst/ Crystallinity/ Transesterification/ Palm oil/ Methyl levulinate/ Gamma-valerolactone/ Nickel/ Copper/ Hydrogenation

Given the continuous increase in global energy demand and the decreasing availability of fossil fuels, there is a growing interest in utilizing energy derived from biomass as an alternative source. This thesis therefore focuses on studying and developing catalysts for converting biomass into alternative fuels and high-value chemicals, such as biodiesel from palm oil and gamma-valerolactone from methyl levulinate, respectively.

The first part of this thesis investigates the influence of crystallinity of zeolite NaX in potassium-supported zeolite NaX catalysts and employs it in the transesterification reaction of palm oil and methanol to synthesize biodiesel. In this study, zeolite NaX samples were synthesized with varying hydrothermal treatment times of 0, 4, 8, 12, and 24 hours to achieve zeolite NaX with different degrees of crystallinity. Ultrasound-assisted impregnation with potassium acetate buffer was then employed to prepare the catalysts. The findings revealed that increasing the hydrothermal treatment time resulted in higher crystallinity of zeolite NaX, with complete crystallization observed at hydrothermal times of 8 hours or longer. The utilization of zeolite NaX with higher crystallinity as a catalyst support resulted in stronger basicity of the catalysts, directly enhancing the transesterification efficiency of palm oil to biodiesel.

In the second part of this thesis, the catalytic behavior of nickel (Ni) and copper (Cu) mono- and bimetallic (NiCu) catalysts was investigated for the hydrogenation of methyl levulinate to gamma-valerolactone. The study revealed that both Ni and NiCu catalysts are effective for the hydrogenation of methyl levulinate to gamma-hydroxypentanoate. However, NiCu has a better tendency to accelerate the conversion

ACKNOWLEDGEMENTS

I would like to express my gratitude and appreciation to all those who have helped me throughout my studies. First, I would like to thank my advisor, Prof. Dr. Jatuporn Wittayakun, for his kind support, stimulating suggestions and encouragement throughout my research and thesis writing.

I would like to thank Dr. Sanchai Kuboon from National Nanotechnology Center (NANOTEC), National Science and Technology Development Agency (NSTDA), Pathumthani, Thailand for his invaluable guidance, exceptional mentorship, and outstanding care throughout my research there. Prof. Dr. Frank Rößner is thanked for his supervision about MBOH reaction testing and supporting reactor and facilities for the experiments at Carl von Ossietzky Universität, Oldenburg, Germany.

I also thank the thesis examining committee including Assoc. Prof. Dr. Anyanee Kamkaew, Assoc. Prof. Dr. Sanchai Prayoonpokarach, Assoc. Prof. Dr. Theeranun Siritanon and Asst. Prof. Dr. Natkanin Supamathanon for their helpful suggestions. I would also like to thank all the lecturers at the School of Chemistry for their good attitude and useful advice, all the staff at the Center for Scientific and Technological Equipment for their assistance and suggestion for the use of instruments.

Finally, members in the Catalysis and Chemical Analysis Labs are thanked for their kindness and helpful suggestions in the experiments. My family and friends are thanked for their care, support, and understanding during this challenging journey.

This research and study were supported by a Science Achievement Scholarship of Thailand (SAST).

Chaianun Pansakdanon

CONTENTS

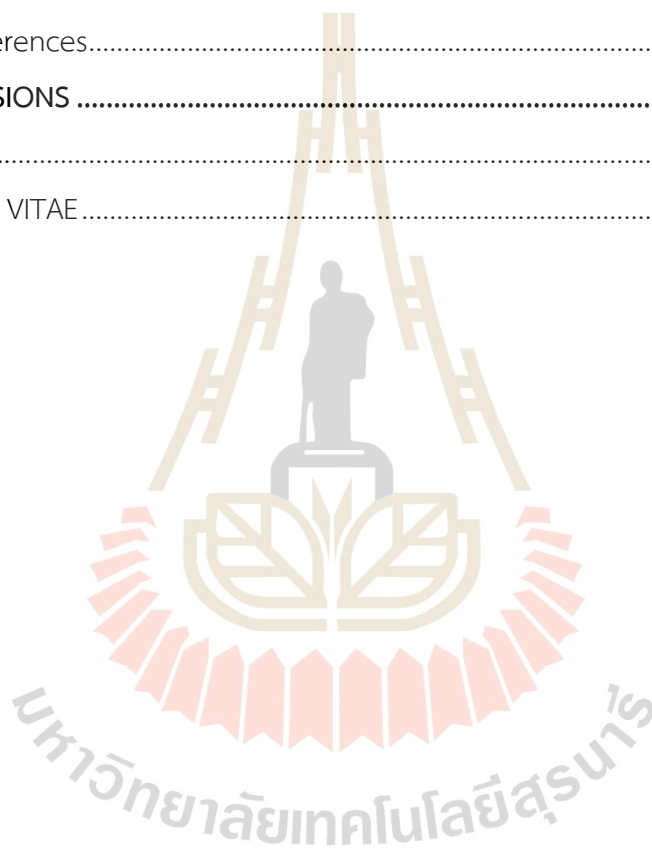
	Page
ABSTRACT IN THAI.....	I
ABSTRACT IN ENGLISH.....	III
ACKNOWLEDGEMENTS	V
CONTENTS	VI
LIST OF TABLES	IX
LIST OF FIGURES	X
LIST OF ABBREVIATIONS	XII
CHAPTER	
I INTRODUCTION	1
1.1 Introduction	1
1.2 References.....	3
II LITERATURE REVIEWS	7
2.1 Development of potassium-based catalyst for transesterification of palm oil to biodiesel	7
2.1.1 Biodiesel production	7
2.1.2 Potassium-based heterogeneous catalyst.....	8
2.1.3 Potassium catalysts on Faujasite (FAU) zeolite	8
2.2 Development of Ni and Cu catalysts in hydrogenation of methyl levulinate to gamma-valerolactone	11
2.2.1 Gamma-valerolactone production.....	11
2.2.2 Alcohol as hydrogen donors	13
2.2.3 Ni and Cu catalysts for hydrogenation of LA to GVL	13
2.2.4 GVL production from the hydrogenation of methyl levulinate.....	14
2.3 References.....	16

CONTENTS (Continued)

	Page
III INFLUENCE OF THE ZEOLITE NaX CRYSTALLINITY ON CATALYTIC PERFORMANCE OF K/NaX IN TRANSESTERIFICATION OF PALM OIL.....	23
3.1 Abstract.....	23
3.2 Introduction	24
3.3 Experimental.....	25
3.3.1 Chemicals.....	25
3.3.2 Synthesis of zeolite NaX with various hydrothermal time.....	26
3.3.3 Catalyst preparation.....	26
3.3.4 Catalyst characterization.....	27
3.3.5 Catalysts testing: Transesterification of palm oil	28
3.3.6 Catalysts stability.....	30
3.4 Results and discussion.....	30
3.4.1 Catalysts characterization.....	30
3.4.2 Catalysts performance on transesterification of palm oil.....	47
3.4.3 Catalysts stability.....	48
3.5 Conclusions.....	50
3.6 References.....	51
IV THE CATALYTIC BEHAVIOR OF NICKEL AND COPPER MONO/BIMETALLIC CATALYSTS IN HYDROGENATION OF METHYL LEVULINATE TO GAMMA-VALEROLACTONE.....	56
4.1 Abstract.....	56
4.2 Introduction	57
4.3 Experimental.....	59
4.3.1 Chemicals.....	59
4.3.2 Preparation of Ni metal, Cu metal and NiCu alloy catalysts.....	59
4.3.3 Catalysts characterization	60
4.3.4 Catalysts testing: Hydrogenation of ML.....	60

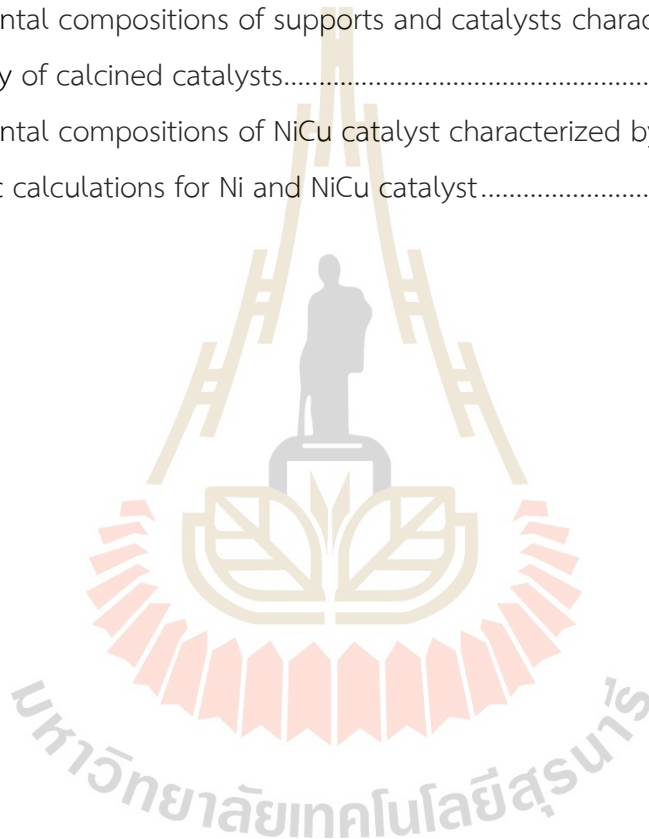
CONTENTS (Continued)

	Page
4.4 Results and discussion.....	61
4.4.1 Catalysts characterization	61
4.4.2 Catalytic behaviors of metal and alloy catalysts.....	63
4.5 Conclusions.....	68
4.6 References.....	68
V CONCLUSIONS	73
APPENDIX.....	74
CURRICULUM VITAE.....	78



LIST OF TABLES

Table	Page
3.1 BET surface area and micropore volume of supports and catalysts from N ₂ sorption analysis.....	36
3.2 Elemental compositions of supports and catalysts characterized by EDS	43
3.3 Basicity of calcined catalysts.....	47
4.1 Elemental compositions of NiCu catalyst characterized by EDS and XRF	63
4.2 Kinetic calculations for Ni and NiCu catalyst.....	67



LIST OF FIGURES

Figure	Page
2.1	Transesterification reaction of the triglycerides to fatty acid methyl esters.....7
2.2	Production of GVL from LA by hydrogenation and subsequent cyclization of HPA to GVL 12
2.3	Interactions of (a) primary and (b) secondary alcohol with a Ni. Reprinted (adapted) with permission from (Geboers et al., 2014) Copyright 2013 Elsevier B.V..... 13
2.4	Selectivity to (a) alkyl gamma-hydroxypentanoates and (b) gamma-valerolactone in function of reaction temperature (at full conversion of substrate). Reaction mixture: substrate (1.4 mmol), Raney Ni (0.3 g, dry basis), 2-propanol (7 mL). Reprinted (adapted) with permission from (Geboers et al., 2014) Copyright 2013 Elsevier B.V. 15
3.1	Apparatus set up for transesterification 29
3.2	XRD patterns of a) HT0 and HT4 and b) HT8, HT12 and HT24 31
3.3	Relative percentage crystallinity of all support samples 32
3.4	XRD patterns of a) K/HT0 and K/HT4 and b) K/HT8, K/HT12 and K/HT24..... 33
3.5	N ₂ sorption isotherms of (a) HT0, (b) HT4, (c) HT8, (d) HT12, and (e) HT24 compared to their potassium catalysts; filled symbol = adsorption and hollow symbol = desorption..... 35
3.6	SEM images of with 10k and 30k magnification of (a) HT0, (b) HT4, (c) HT8, (d) HT12, and (e) HT24 and 30k magnification of (f) K/HT0, (g) K/HT4, (h) K/HT8, (i) K/HT12, and (j) K/HT24..... 37
3.7	EDS elements mapping images of a) HT0 and b) K/HT0 38
3.8	EDS elements mapping images of a) HT4 and b) K/HT4 39
3.9	EDS elements mapping images of a) HT8 and b) K/HT8 40
3.10	EDS elements mapping images of a) HT12 and b) K/HT12 41
3.11	EDS elements mapping images of a) HT24 and b) K/HT24 42

LIST OF FIGURES (Continued)

Figure		Page
3.12	FTIR spectra of (a) supports, (b) as-prepared, and (c) calcined catalysts.....	45
3.13	CO ₂ -TPD profiles of a) supports and b) catalysts	56
3.14	GC chromatograms of biodiesel products from the conversion of palm oil obtained from a) K/HT0, b) K/HT4, c) K/HT8, d) K/HT12, e) K/HT24, and f) biodiesel yield at 60 °C for 3 h.	48
3.15	Comparison between fresh and spent catalysts by a) biodiesel yield, b) XRD, c) FTIR, and d) CO ₂ -TPD	50
4.1	XRD of the a) as-prepared catalysts and b) catalysts.....	61
4.2	H ₂ -TPR profile of (a) CuO (b) NiO and (c) NiCuO samples	62
4.3	SEM images of catalysts (a) Cu metal (b) Ni metal and (c) NiCu alloy catalyst and the EDS element mapping of (d) NiCu alloy (green indicates Ni and Cu is represented by orange)	63
4.4	Quantity profile of (a) ML and (b) GVL at 200 °C for no catalyst, Cu metal, Ni metal, and NiCu alloy	64
4.5	Quantity of reactant, product, and intermediate from the hydrogenation of ML in 2-propanol over time using NiCu catalyst at (a) 160 °C (b) 180 °C (c) 200 °C and Ni catalyst at (d) 160 °C (e) 180 °C and (f) 200 °C.....	65
4.6	A comparison of GVL quantity produced over NiCu catalyst at temperatures of 120–160 °C.....	66
4.7	Reaction scheme for GVL formation from ML	67

LIST OF ABBREVIATIONS

ML	Methyl levulinate
HPA	Gamma-hydroxypentanoate
GVL	Gamma-valerolactone
Ni	Nickel
Cu	Copper
NiCu	Nickel-copper alloy
DI	Deionized
GC-FID	Gas chromatography with flame ionization detector
XRD	X-ray diffraction
SEM	Scanning electron microscopy
EDS	Energy dispersive spectrometry
FTIR	Fourier-transform infrared spectroscopy
ATR	Attenuated total reflectance
CO ₂ -TPD	Temperature-programmed desorption of carbon dioxide
H ₂ -TPR	Temperature-programmed reduction by H ₂
XRF	X-ray fluorescence
BET	Brunauer-Emmett-Teller

CHAPTER I

INTRODUCTION

1.1 Introduction

Global energy demand is projected to increase by 2% annually, with consumption predicted to double that of 2001 by 2050 (Li et al., 2016). The gradual decline in fossil fuels has prompted a shift towards biomass valorization as an alternative to secure energy and chemical supplies (Zhang et al., 2016). Liquid biomass, such as edible and non-edible oils, can be converted into biodiesel to replace fossil fuels (Lee et al., 2014). Solid biomass, such as lignocellulose, can be converted into high-value chemicals such as 5-hydroxymethylfurfural (HMF), levulinic acid (LA), dimethylfuran (DMF), and gamma-valerolactone (GVL) (Ennaert et al., 2016; Teong et al., 2014). Therefore, biomass conversion to value-added chemicals and fuels using heterogeneous catalysts is a key concern in green chemistry (Chen et al., 2017). This thesis focuses on the development of solid catalysts for producing two prominent bio-based chemicals: biodiesel or fatty acid methyl ester (FAME) from liquid biomass, and GVL from solid biomass. The first part examines the impact of zeolite NaX crystallinity on the catalytic performance of K/NaX catalysts in the transesterification of palm oil. The second part investigates the catalytic behavior of nickel (Ni) and copper (Cu) mono/bimetallic (NiCu) catalysts in the hydrogenation of methyl levulinate (ML) to GVL.

Biodiesel or FAME, is typically synthesized through the transesterification process of triglycerides present in liquid biomass, including vegetable oils or animal fats. This procedure involves the utilization of alcohol and a catalyst (Meher et al., 2006). Heterogeneous catalysts play a pivotal role in this process, where carbonates and oxides of alkali and alkaline earth metals are predominant. These catalysts are frequently supported on materials characterized by high porosity and surface area,

such as SiO_2 , Al_2O_3 , and zeolites (Perego et al., 2017; Refaat, 2011; Romero et al., 2005). Numerous studies have investigated the use of potassium-supported zeolite catalysts for transesterification reactions, highlighting the notable properties of Faujasite (FAU) zeolites like NaX and NaY, which possess large surface areas and exhibit high thermal stability. These characteristics make them particularly intriguing for biodiesel production processes (Kosawatthanakun et al., 2022; Rakmae et al., 2016; Supamathanon et al., 2011; Verboekend et al., 2016).

Previous studies have compared various support materials for their efficacy in catalyzing transesterification reactions, revealing that zeolite NaX serves as a highly efficient catalyst for this process. Therefore, the first part of this research aims to develop and enhance understanding of the K/NaX catalyst by investigating how the crystallinity of zeolite NaX influences the transesterification process of palm oil.

Solid biomass, lignocellulose, presents an avenue for the production of biofuels and valuable chemicals through biorefinery processes (Alonso et al., 2012; Huber et al., 2006; Kumar et al., 2009). Among these chemicals, GVL has garnered significant attention due to its renewable, non-toxic, and biodegradable properties, serving various roles as a solvent, fuel additive, and precursor for bio-based polymers (Fegyverneki et al., 2010; Horváth et al., 2008; Liguori et al., 2015). GVL is conventionally synthesized via hydrogenation, where LA or its ester undergoes transformation in the presence of H_2 gas (Serrano-Ruiz et al., 2010). However, this method presents significant drawbacks, including the necessity of noble metal catalysts and the requirement for high-pressure H_2 , leading to economic challenges. Conversely, an alternative transfer hydrogenation method, employing alcohols and formic acid (FA) as hydrogen donors instead of H_2 , has gained widespread adoption (Deng et al., 2009; Hengne et al., 2012). While this method addresses the challenges associated with corrosive FA, the use of alcohols as hydrogen sources in catalytic transfer hydrogenation (CTH) of LA and its esters to GVL has emerged as a prominent trend (Tang et al., 2014; Yang et al., 2013).

Various solid heterogeneous and homogeneous metal catalysts have been developed for LA reduction, particularly noble metals like ruthenium, platinum, and palladium (Galletti et al., 2012; Yan et al., 2009; Upare et al., 2011). To reduce

operational costs, alternative non-noble metals such as Cu and Ni have been explored (Shimizu et al., 2014; Zhang et al., 2015). In a study by Cai et al. (2017), the CTH of ethyl levulinate (EL) to GVL, utilizing 10Cu-5Ni/Al₂O₃ as a catalyst, yielded a 97% GVL yield in 12 hours at 150 °C. While the bimetallic catalysts of Ni and Cu showed high catalytic activity and stability, it's essential to note that Cai et al. focused exclusively on metal-supported catalysts and pure support materials, neglecting the performance of pure nickel or copper catalysts. Consequently, the second part of this research aims to investigate the catalytic activity and selectivity of Ni and Cu during the CTH process of ML to GVL. Utilizing a sole NiCu alloy catalyst without support materials, the catalyst was prepared, characterized, and tested using 2-propanol as a hydrogen donor.

1.2 References

- Alonso, D. M., Wettstein, S. G., and Dumesic, J. A. (2012). Bimetallic catalysts for upgrading of biomass to fuels and chemicals. *Chemical Society Reviews*, 41(24), 8075-8098.
- Chen, S. S., Maneerung, T., Tsang, D. C. W., Ok, Y. S., and Wang, C.-H. (2017). Valorization of biomass to hydroxymethylfurfural, levulinic acid, and fatty acid methyl ester by heterogeneous catalysts. *Chemical Engineering Journal*, 328, 246-273.
- Deng, L., Li, J., Lai, D.-M., Fu, Y., and Guo, Q.-X. (2009). Catalytic conversion of biomass-derived carbohydrates into gamma-valerolactone without using an external H₂ supply. *Angewandte Chemie International Edition*, 48(35), 6529-6532.
- Ennaert, T., Van Aelst, J., Dijkmans, J., De Clercq, R., Schutyser, W., Dusselier, M., Verboekend, D., and Sels, B. F. (2016). Potential and challenges of zeolite chemistry in the catalytic conversion of biomass. *Chemical Society Reviews*, 45(3), 584-611.
- Fegyverneki, D., Orha, L., Láng, G., and Horváth, I. T. (2010). Gamma-valerolactone-based solvents. *Tetrahedron*, 66(5), 1078-1081.

- Galletti, A. M. R., Antonetti, C., De Luise, V., and Martinelli, M. (2012). A sustainable process for the production of gamma-valerolactone by hydrogenation of biomass-derived levulinic acid. *Green Chemistry*, 14(3), 688-694.
- Hengne, A. M., Biradar, N. S., and Rode, C. V. (2012). Surface species of supported ruthenium catalysts in selective hydrogenation of levulinic esters for bio-refinery application. *Catalysis Letters*, 142(6), 779-787.
- Horváth, I. T., Mehdi, H., Fábos, V., Boda, L., and Mika, L. T. (2008). Gamma-valerolactone: A sustainable liquid for energy and carbon-based chemicals. *Green Chemistry*, 10(2), 238-242.
- Huber, G. W., Iborra, S., and Corma, A. (2006). Synthesis of transportation fuels from biomass: Chemistry, catalysts, and engineering. *Chemical Reviews*, 106(9), 4044-4098.
- Kosawatthanakun, S., Pansakdanon, C., Sosa, N., Chanlek, N., Roessner, F., Prayoonpokarach, S., and Wittayakun, J. (2022). Comparative properties of K/NaX and K/NaY from ultrasound-assisted impregnation and performance in transesterification of palm oil. *ACS Omega*, 7(11), 9130-9141.
- Kumar, P., Barrett, D. M., Delwiche, M. J., and Stroeve, P. (2009). Methods for pretreatment of lignocellulosic biomass for efficient hydrolysis and biofuel production. *Industrial and Engineering Chemistry Research*, 48(8), 3713-3729.
- Lee, A. F., Bennett, J. A., Manayil, J. C., and Wilson, K. (2014). Heterogeneous catalysis for sustainable biodiesel production via esterification and transesterification. *Chemical Society Reviews*, 43(22), 7887-7916.
- Li, X., Luque-Moreno, L. C., Oudenhoven, S. R. G., Rehmann, L., Kersten, S. R. A., and Schuur, B. (2016). Aromatics extraction from pyrolytic sugars using ionic liquid to enhance sugar fermentability. *Bioresource Technology*, 216, 12-18.
- Liguori, F., Moreno-Marrodan, C., and Barbaro, P. (2015). Environmentally friendly synthesis of gamma-valerolactone by direct catalytic conversion of renewable sources. *ACS Catalysis*, 5(3), 1882-1894.
- Meher, L. C., Vidya Sagar, D., and Naik, S. N. (2006). Technical aspects of biodiesel production by transesterification: A review. *Renewable and Sustainable Energy Reviews*, 10(3), 248-268.

- Perego, C., Bosetti, A., Ricci, M., and Millini, R. (2017). Zeolite materials for biomass conversion to biofuel. *Energy and Fuels*, 31(8), 7721-7733.
- Rakmae, S., Keawkumay, C., Osakoo, N., Montalbo, K. D., de Leon, R. L., Kidkhunthod, P., Chanlek, N., Roessner, F., Prayoonpokarach, S., and Wittayakun, J. (2016). Realization of active species in potassium catalysts on zeolite NaY prepared by ultrasound-assisted impregnation with acetate buffer and improved performance in transesterification of palm oil. *Fuel*, 184, 512-517.
- Refaat, A. A. (2011). Biodiesel production using solid metal oxide catalysts. *International Journal of Environmental Science and Technology*, 8(1), 203-221.
- Romero, M. D., Ovejero, G., Rodríguez, A., and Gómez, J. M. (2005). Enhancement of the basic properties in FAU zeolites by impregnation with cesium hydroxide. *Microporous and Mesoporous Materials*, 81(1), 313-320.
- Serrano-Ruiz, J. C., Wang, D., and Dumesic, J. A. (2010). Catalytic upgrading of levulinic acid to 5-nonanone. *Green Chemistry*, 12(4), 574-577.
- Shimizu, K.-i., Kanno, S., and Kon, K. (2014). Hydrogenation of levulinic acid to gamma-valerolactone by Ni and MoO_x co-loaded carbon catalysts. *Green Chemistry*, 16(8), 3899-3903.
- Supamathanon, N., Wittayakun, J., and Prayoonpokarach, S. (2011). Properties of Jatropha seed oil from Northeastern Thailand and its transesterification catalyzed by potassium supported on NaY zeolite. *Journal of Industrial and Engineering Chemistry*, 17(2), 182-185.
- Tang, X., Zeng, X., Li, Z., Hu, L., Sun, Y., Liu, S., Lei, T., and Lin, L. (2014). Production of gamma-valerolactone from lignocellulosic biomass for sustainable fuels and chemicals supply. *Renewable and Sustainable Energy Reviews*, 40, 608-620.
- Teong, S. P., Yi, G., and Zhang, Y. (2014). Hydroxymethylfurfural production from bioresources: past, present and future. *Green Chemistry*, 16(4), 2015-2026.
- Upare, P. P., Lee, J.-M., Hwang, D. W., Halligudi, S. B., Hwang, Y. K., and Chang, J.-S. (2011). Selective hydrogenation of levulinic acid to gamma-valerolactone over carbon-supported noble metal catalysts. *Journal of Industrial and Engineering Chemistry*, 17(2), 287-292.

- Verboekend, D., Nuttens, N., Locus, R., Van Aelst, J., Verolme, P., Groen, J. C., Pérez-Ramírez, J., and Sels, B. F. (2016). Synthesis, characterisation, and catalytic evaluation of hierarchical faujasite zeolites: milestones, challenges, and future directions. *Chemical Society Reviews*, 45(12), 3331-3352.
- Yan, Z.-p., Lin, L., and Liu, S. (2009). Synthesis of gamma-valerolactone by hydrogenation of biomass-derived levulinic acid over Ru/C catalyst. *Energy and Fuels*, 23(8), 3853-3858.
- Yang, Z., Huang, Y.-B., Guo, Q.-X., and Fu, Y. (2013). RANEY® Ni catalyzed transfer hydrogenation of levulinate esters to gamma-valerolactone at room temperature. *Chemical Communications*, 49(46), 5328-5330.
- Zhang, J., Chen, J., Guo, Y., and Chen, L. (2015). Effective upgrade of levulinic acid into gamma-valerolactone over an inexpensive and magnetic catalyst derived from hydrotalcite precursor. *ACS Sustainable Chemistry and Engineering*, 3(8), 1708-1714.
- Zhang, X., Wilson, K., and Lee, A. F. (2016). Heterogeneously catalyzed hydrothermal processing of C5–C6 sugars. *Chemical Reviews*, 116(19), 12328-12368.



CHAPTER II

LITERATURE REVIEW

Literature review is divided into two parts including the development of potassium-based catalyst for transesterification of palm oil to biodiesel and development of Ni and Cu catalysts in hydrogenation of methyl levulinate to gamma-valerolactone.

2.1 Development of potassium-based catalyst for transesterification of palm oil to biodiesel

2.1.1 Biodiesel production

Biodiesel is produced by transesterification as shown in Figure 2.1. Triglycerides in oil react with alcohol, generally methanol, by using acid or base catalyst to produce fatty acid methyl esters which is also known as biodiesel (Boz et al., 2009).

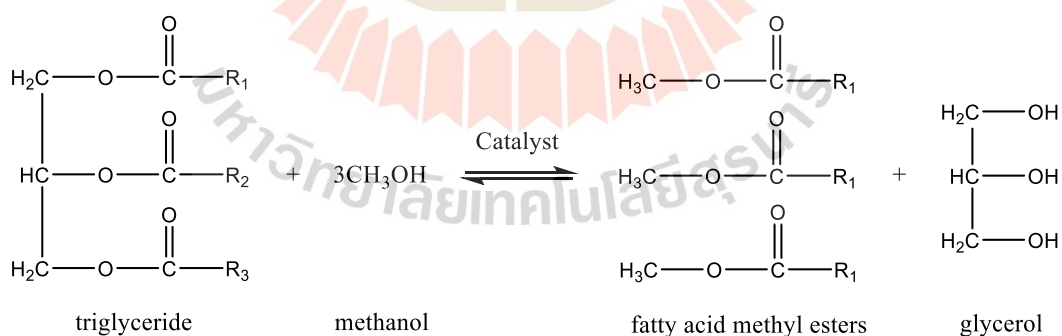


Figure 2.1 Transesterification reaction of the triglycerides to fatty acid methyl esters.

The transesterification reaction can be catalyzed by five distinct types of catalysts. The first category comprises alkali homogeneous catalysts, which are highly active and cost-effective, yet their purification process is notably laborious (Leung et

al., 2010; Vicente et al., 2004). Second, acid homogeneous catalysts are preferable for oils rich in free fatty acids (FFA), albeit characterized by lower reaction rates and challenging separation processes (Marchetti et al., 2007; Liu et al., 2010). Third, alkali heterogeneous catalysts necessitate a high alcohol-to-oil ratio for effectiveness, but these catalysts offer the advantage of being more environmentally benign by minimizing waste emissions (Highina et al., 2011; Zhang et al., 2010). The fourth type, acid heterogeneous catalysts, exhibit reduced corrosiveness and toxicity; however, they are more expensive and pose greater diffusional challenges compared to their homogeneous counterparts (Wan Omar et al., 2011). Lastly, enzymatic catalysts facilitate straightforward separation, regeneration, and reuse, despite their slower reaction rates and propensity for activity loss (Shimada et al., 2002).

2.1.2 Potassium-based heterogeneous catalyst

The predominant heterogeneous catalysts utilized in biodiesel production include carbonates and oxides of alkali and alkaline earth metals, which are supported on materials with high porosity and surface area, such as SiO_2 , Al_2O_3 , and zeolites (Perego et al., 2017; Refaat, 2011; Romero et al., 2005).

Sanchez et al. (2014) conducted a study where they varied the alkali and alkaline earth oxides on $\gamma\text{-Al}_2\text{O}_3$ supports to investigate the behavior of soybean oil transesterification with different $\gamma\text{-Al}_2\text{O}_3$ -based catalysts. Their findings indicated that $\text{K}/\gamma\text{-Al}_2\text{O}_3$ demonstrated superior performance compared to other catalysts tested. Additionally, Hindryawati et al. (2014) reported that potassium-based catalysts exhibit higher basicity and are more resistant to free fatty acid contamination in triglyceride sources compared to lithium and sodium alternatives.

2.1.3 Potassium catalysts on Faujasite (FAU) zeolite

Faujasite zeolites, designated as FAU, are crystalline aluminosilicates characterized by their unique structure, comprising sodalite cages and supercages, with a pore diameter of approximately 0.74 nm. This class of zeolites is divided into two main categories based on their chemical compositions: zeolite X and zeolite Y (Barthomeuf, 1996). The distinction between zeolite X and Y is primarily based on their

silicon to aluminum (Si/Al) ratios, which are in the ranges of 1-1.5 for zeolite X and 2-5 for zeolite Y, respectively. The incorporation of aluminum within the zeolite framework necessitates the presence of an equivalent number of extra-framework cations to maintain charge neutrality. Notably, zeolite NaX exhibits higher basic properties than zeolite NaY, attributed to their differing Si/Al ratios, which consequently influence their basicity and reactivity (Ma et al., 2021). These materials, particularly zeolite X and Y, have found extensive applications in various domains, including the transesterification process for biodiesel production. Their popularity in such applications can be ascribed to their straightforward synthesis, substantial surface area, voluminous pore structure, stability, and well-defined framework (Polisi et al., 2019; Zito et al., 2015).

Numerous studies have investigated catalysts featuring potassium supported on NaX and NaY for the transesterification of diverse oil sources including palm, soybean, sunflower, and Jatropha. Noiroj et al. (2009) evaluated the efficacy of KOH supported on Al_2O_3 and NaY zeolites for transesterification of palm oil. The preparation of these catalysts involved varying the KOH loading from 15 to 35 wt% on Al_2O_3 and from 8 to 15 wt% on NaY. Their investigation identified optimal catalyst compositions of 25 wt% KOH/ Al_2O_3 and 10 wt% KOH/NaY, which achieved a biodiesel yield of 91.07% under conditions below 70 °C, within a 2–3 h reaction time, at a molar ratio of 1:15 (palm oil to methanol), and with a catalyst concentration of 3–6 wt%. The study highlighted NaY as a superior support compared to Al_2O_3 , attributable to the optimal potassium loading. Additionally, it was observed that biodiesel yield diminished when KOH loading exceeded 25 wt% on Al_2O_3 and 10 wt% on NaY. This decline in yield was attributed to the agglomeration of the active KOH phase or the occlusion of basic sites by excessive KOH, which in turn reduced the catalyst's surface area and activity. Moreover, the structure of zeolite NaY collapsed with an increase of the K content.

To mitigate the structural collapse of zeolites, Montalbo et al. (2013) prepared potassium catalysts using rice husk silica (RHS) and zeolite NaY, utilizing both acetate buffer (B) and acetate (A) solutions as potassium sources. The study found that K/NaY catalysts exhibited not only higher surface areas, but also greater stability post-impregnation and calcination compared to K/RHS catalysts, which showed structural

collapse during catalyst preparation. Consequently, NaY-supported catalysts demonstrated superior activity over those supported by RHS. Specifically, the 12K/NaY-A, prepared through the impregnation of 12 wt% K on NaY using an aqueous acetate solution, presented a reduced surface area compared to both bare NaY and the 12K/NaY-B. This reduction suggested a more significant collapse within the 12K/NaY-A zeolite structure, correlating with its incomplete conversion of *Jatropha* seed oil into biodiesel. Conversely, the 12K/NaY-B catalyst achieved complete conversion, yielding a biodiesel efficiency of 77.9%.

Another work from Supamathanon et al. (2011), They synthesized potassium-loaded catalysts on zeolite NaY using an acetate buffer solution as a potassium precursor, a strategic approach to preserve the zeolite framework. Their catalysts, tested in the transesterification of *Jatropha* seed oil, found that a 12 wt.% potassium load yielded a notable biodiesel yield of 73.4% under specific conditions. Building on this foundation, Manadee et al. (2017) explored the substitution of NaY with NaX zeolite, varying potassium content for the same process. Their findings revealed an enhanced biodiesel yield of 83% with a 12 wt.% potassium load, suggesting that NaX zeolite's superior basicity and structural integrity significantly contribute to its increased catalytic activity. These works illustrate the pivotal role of zeolite composition and potassium loading in optimizing catalyst performance for biodiesel production, highlighting a promising avenue for future research in the field.

To improve the dispersion of the active species and catalytic performance of the potassium on FAU zeolite, Rakmae et al. (2016) conducted a comparative study on catalysts for transesterification of palm oil into biodiesel. They synthesized 12 wt% potassium-supported zeolite NaY catalysts using both ultrasound-assisted impregnation with acetate buffer (K/NaY-U) and conventional impregnation methods (K/NaY) for comparison. The study revealed that the potassium precursor decomposed between 370–480 °C, forming potassium carbonate. Both catalyst types exhibited moderate to strong basic sites, but K/NaY-U demonstrated superior potassium dispersion. Notably, the K/NaY-U catalyst facilitated a faster transesterification reaction, achieving a 72% biodiesel yield in 2 hours. This finding underscores the effectiveness of ultrasound-assisted impregnation in catalyst preparation.

While previous literature indicates the effectiveness of K/NaX and K/NaY catalysts in transesterification of various oils, the catalysts in these studies were often prepared using different methods or evaluated on different oil substrates. Furthermore, there is a notable absence of studies detailing the preparation of K/NaX catalysts using ultrasound-assisted impregnation. Therefore, Kosawatthanakun et al. (2022) seeks to address this gap by comparing the physicochemical properties of K/NaX and K/NaY catalysts prepared via ultrasound-assisted impregnation from a potassium acetate buffer solution. Subsequently, their catalytic performance in the transesterification of palm oil will be evaluated under identical conditions. The results from carbon dioxide (CO₂-TPD) and the catalytic decomposition of 2-methylbut-3-yn-2-ol (MBOH) revealed that the calcined K/NaX had higher basicity than K/NaY. Both K/NaX and K/NaY are active in transesterification of palm oil, producing more than 94% of the biodiesel yields. However, the results from the second run indicated that K/NaX was a better catalyst due to the less leaching of potassium species into the produced glycerol and biodiesel.

Previous research highlights zeolite NaX as a promising support material for the transesterification reaction in biodiesel production. Consequently, this study aims to deepen the understanding of support properties by examining how the crystallinity of zeolite NaX affects the transesterification process of palm oil. The insights information are anticipated to significantly contribute to the design and improvement of catalytic performance in biodiesel production.

2.2 Development of nickel and copper catalysts in hydrogenation of methyl levulinate to gamma-valerolactone

2.2.1 Gamma-valerolactone production

Gamma-valerolactone (GVL) is an organic compound with the formula C₅H₈O₂. It is stable in water and in the presence of air, safe, biodegradable, and nontoxic chemical which can be utilized as a food additive; it can also be used as a green solvent for processing biomass, and as an efficient fuel additive (Choi et al., 2015; Manzer, 2014; Yan et al., 2015). Therefore, GVL has drawn considerable attention in

the last decade as a value-added chemical synthesized from lignocellulosic biomass (Dutta et al., 2019).

In general, GVL is primarily synthesized from levulinic acid (LA) and its esters using two main hydrogenation technologies: direct hydrogenation and transfer hydrogenation (Alonso et al., 2013; Kasar et al., 2019). The former traditionally utilizes various metal catalysts (Tan et al., 2015; Tian et al., 2015), such as palladium, ruthenium, rhodium, platinum, and rhenium (Abdelrahman et al., 2014; Galletti et al., 2012; Jones et al., 2016; Upare et al., 2011; Yan et al., 2009), in the presence of molecular hydrogen (H_2). The conventional approach for the production of GVL comprises the catalytic hydrogenation of LA followed by instantaneous lactonization of the gamma-hydroxypentanoic acid (HPA) to GVL (Chen et al., 2017) as shown in Figure 2.2.

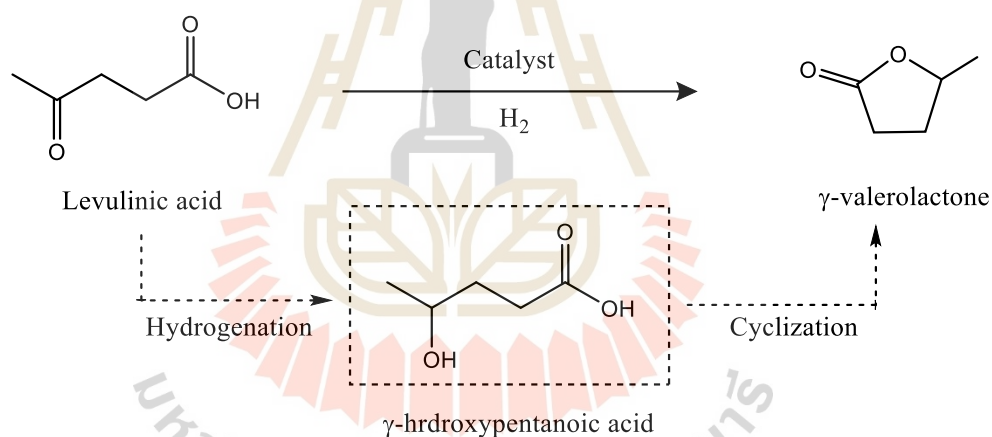


Figure 2.2 Production of GVL from LA by hydrogenation and subsequent cyclization of HPA to GVL.

However, this approach is associated with significant drawbacks, including the necessity of noble metal catalysts and the requirement for high-pressure H_2 , introducing economic challenges (Osatiashtiani et al., 2017). Conversely, an alternative transfer hydrogenation method, employing alcohols and formic acid (FA) as hydrogen donors instead of H_2 , has gained widespread adoption. While this approach mitigates the issues of corrosive formic acid (Chia et al., 2011), the utilization of alcohols as

hydrogen sources in catalytic transfer hydrogenation (CTH) of levulinic acid and its esters to GVL has emerged as a prevailing trend.

2.2.2 Alcohol as hydrogen donors

Alcohol serves as widely employed hydrogen donors in metal catalyzed CTH reactions. Secondary alcohols typically exhibit superior activity compared to primary alcohols in the dehydrogenation process over metal surfaces, facilitating efficient hydrogen transfer to the substrate. This heightened activity can be attributed to the enhanced stabilizing effect resulting from the presence of two alkyl groups, compared to one, which leads to inductive electron donation to the alpha-carbon of the alcohol during the dehydrogenation process (Aramendía et al., 2001; Panagiotopoulou et al., 2014; Scholz et al., 2013; Yang et al., 2013). Moreover, primary alcohols may irreversibly adsorb onto the metal surface. Thereby, the active sites become blocked by alkoxide species. In contrast, the adsorption of secondary alcohol, such as 2-propanol, breaks the $C_{\alpha}H$ and O-H bonds releasing of acetone (Geboers et al. 2014), as shown in Figure 2.3. Therefore, 2-propanol was chosen for this research.

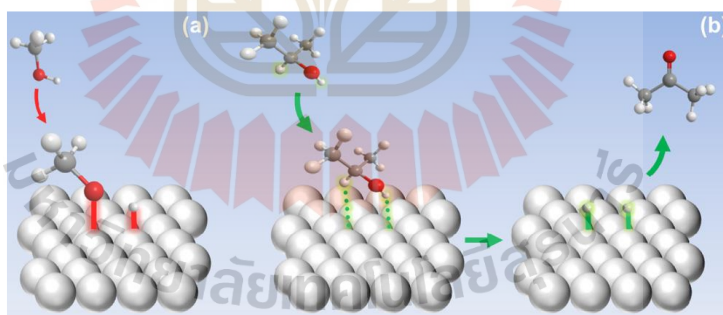


Figure 2.3 Interactions of (a) primary and (b) secondary alcohol with a Ni. Reprinted (adapted) with permission from (Geboers et al., 2014) Copyright 2013 Elsevier B.V.

2.2.3 Nickel and copper catalysts for hydrogenation of LA to GVL

There has been a notable development of solid heterogeneous and homogeneous metal catalysts for the reduction of levulinic acid, particularly focusing on noble metals such as ruthenium, platinum, and palladium. Within the category of

noble metal catalysts, Ruthenium catalysts have demonstrated exceptional performance and selectivity, achieving a 97% yield in the hydrogenation of LA in dioxane as a solvent at 423 K with 5 wt% Ru/C (Manzer, 2004; Upare et al., 2011). To reduce operational costs, non-noble metals like copper (Cu) and nickel (Ni) have been explored for this reaction (Shimizu et al., 2014; Upare et al., 2011; Zhang et al., 2015). These metals are of particular interest for catalytic applications, in the quest for the use of more earth-abundant elements, as well as for their activity in hydrogenation processes.

2.2.4 GVL production from the hydrogenation of methyl levulinate

Although, LA is the most common building block for GVL production. Ding et al. (2015) studied cellulose conversion to methyl levulinate (ML) via alcoholysis. They mentioned that when compared with LA, ML is a non-corrosive biomass derivative with a lower boiling point and viscosity. This makes ML more applicable for its separation from acidic media and more feasible for its use in further reactions. Li et al. (2017) demonstrated the production of ML with promising yields from various biomass-derived components, including cellulose, starch, sucrose, and monosaccharides, using heterogeneous zirconia-zeolite hybrid catalysts.

Alonso et al. (2013) showed their review on GVL production from ML. They mentioned that levulinate esters could be produced from hemicellulose or cellulose. For the first one, hemicellulose can be hydrolyzed to xylose and xylose can be further hydrolyzed to furfural. The hydrogenation of furfural can provide furfuryl alcohol. The alcoholysis of furfuryl alcohol can then give levulinate ester product. While the starting material is cellulose, glucose can be obtained from cellulose hydrolysis. The glucose can be hydrolyzed to hydroxymethylfurfural. It can be converted to LA via hydrolysis. Later, the esterification of LA can give levulinate ester product. After that, GVL can be produced from the CTH process which ML or its ester is hydrogenated to GVL.

Yang et al. (2016) investigated the production of GVL from ML using Cu-ZrO₂ catalysts at various temperatures. They observed that the highest GVL selectivity from ML precursor reached approximately 75% at 120 °C after 12 hours of reaction time. Another work by Sato et al. (2017), They also reported that conventional

hydrogenation of ML at 250 °C for 5 hours yielded approximately 82% GVL selectivity over Ni/Al₂O₃ catalysts.

Geboers et al. (2014) prepared alkyl gamma-hydroxypentanoates and gamma-valerolactone from alkyl levulinates by H-transfer catalyzed by Raney Ni and using 2-propanol as an H-donor and solvent. They found that, the reactivity order for the Alkyl gamma-hydroxypentanoates arranged as methyl < ethyl < 2-propyl < butyl levulinates, since a large alkyl residue is a better leaving group than a short one for nucleophilic substitution. Conversely, the results show the longer the alkyl residue, the lower the selectivity to gamma-valerolactone, as shown in Figure 2.4.

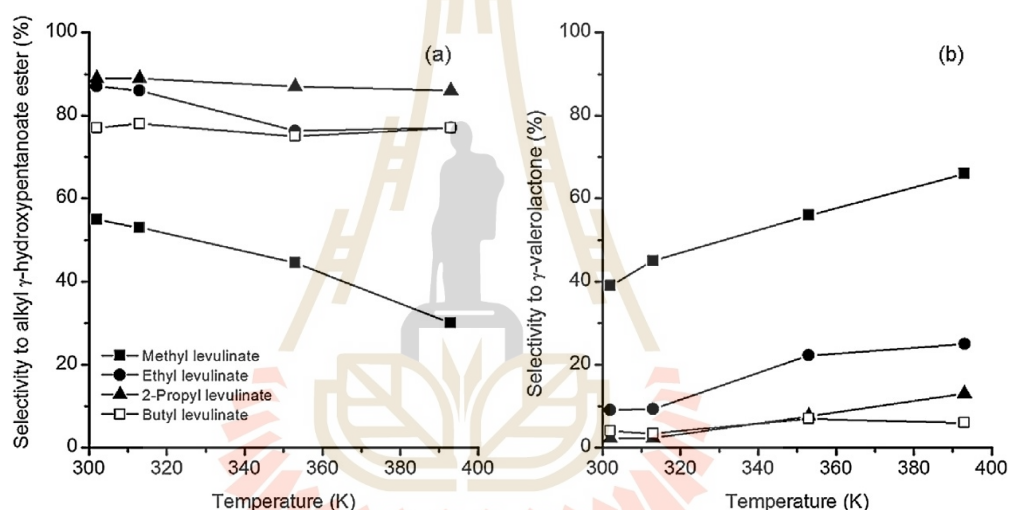


Figure 2.4 Selectivity to (a) alkyl gamma-hydroxypentanoates and (b) gamma-valerolactone in function of reaction temperature (at full conversion of substrate). Reaction mixture: substrate (1.4 mmol), Raney Ni (0.3 g, dry basis), 2-propanol (7 mL). Reprinted (adapted) with permission from (Geboers et al., 2014) Copyright 2013 Elsevier B.V.

Cai et al. (2017) studied the CTH of ethyl levulinate (EL) to GVL with 2-butanol and using 10Cu-5Ni/Al₂O₃ as a catalyst, providing a 97% yield of GVL in 12 h at 150 °C. This work focuses on the utilization of Ni and Cu catalysts for the production of GVL from levulinate esters. The effective synergy observed between Ni and Cu in bimetallic (NiCu alloy) catalysts enhances catalytic activity and stability. Notably, while Cai et al. exclusively investigated metal-supported catalysts and pure support materials, they

did not explore the individual performance of pure nickel or copper catalysts. Therefore, there exists an opportunity to extend the investigation into the promising realm of catalytic transfer hydrogenation within such a system.

Building upon the promising findings in CTH reported in earlier works for the production of valuable biochemicals from biomass (Li et al., 2016; Yang et al., 2016; Cai et al., 2017), this study aims to investigate the distinct roles of Ni and Cu in terms of catalytic activity and selectivity during the CTH process of ML to GVL. The focus is on a sole NiCu alloy catalyst, prepared, characterized, and tested without any supporting materials, utilizing 2-propanol as a hydrogen donor.

2.3 References

- Abdelrahman, O. A., Heyden, A., and Bond, J. Q. (2014). Analysis of kinetics and reaction pathways in the aqueous-phase hydrogenation of levulinic acid to form gamma-valerolactone over Ru/C. *ACS Catalysis*, 4(4), 1171-1181.
- Alonso, D. M., Wettstein, S. G., and Dumesic, J. A. (2013). Gamma-valerolactone, a sustainable platform molecule derived from lignocellulosic biomass. *Green Chemistry*, 15(3), 584-595.
- Aramendía, M. a. A., Borau, V., Jiménez, C., Marinas, J. M., Ruiz, J. R., and Urbano, F. J. (2001). Liquid-phase heterogeneous catalytic transfer hydrogenation of citral on basic catalysts. *Journal of Molecular Catalysis A: Chemical*, 171(1), 153-158.
- Barthomeuf, D. (1996). Basic zeolites: Characterization and uses in adsorption and catalysis. *Catalysis Reviews*, 38(4), 521-612.
- Boz, N., Değirmenbaşı, N., and Kalyon, D. M. (2009). Conversion of biomass to fuel: Transesterification of vegetable oil to biodiesel using KF loaded nano-gamma- Al_2O_3 as catalyst. *Applied Catalysis B-environmental*, 89, 590-596.
- Cai, B., Zhou, X.-C., Miao, Y.-C., Luo, J.-Y., Pan, H., and Huang, Y.-B. (2017). Enhanced catalytic transfer hydrogenation of ethyl levulinate to gamma-valerolactone over a robust Cu-Ni bimetallic catalyst. *ACS Sustainable Chemistry and Engineering*, 5(2), 1322-1331.

- Chen, S. S., Maneerung, T., Tsang, D. C. W., Ok, Y. S., and Wang, C.-H. (2017). Valorization of biomass to hydroxymethylfurfural, levulinic acid, and fatty acid methyl ester by heterogeneous catalysts. *Chemical Engineering Journal*, 328, 246-273.
- Chia, M., and Dumesic, J. A. (2011). Liquid-phase catalytic transfer hydrogenation and cyclization of levulinic acid and its esters to gamma-valerolactone over metal oxide catalysts. *Chemical Communications*, 47(44), 12233-12235.
- Choi, S., Song, C. W., Shin, J. H., and Lee, S. Y. (2015). Biorefineries for the production of top building block chemicals and their derivatives. *Metabolic Engineering*, 28, 223-239.
- Ding, D., Xi, J., Wang, J., Liu, X., Lu, G., and Wang, Y. (2015). Production of methyl levulinate from cellulose: selectivity and mechanism study. *Green Chemistry*, 17(7), 4037-4044.
- Dutta, S., Yu, I. K. M., Tsang, D. C. W., Ng, Y. H., Ok, Y. S., Sherwood, J., and Clark, J. H. (2019). Green synthesis of gamma-valerolactone (GVL) through hydrogenation of biomass-derived levulinic acid using non-noble metal catalysts: A critical review. *Chemical Engineering Journal*, 372, 992-1006.
- Galletti, A. M. R., Antonetti, C., De Luise, V., and Martinelli, M. (2012). A sustainable process for the production of gamma-valerolactone by hydrogenation of biomass-derived levulinic acid. *Green Chemistry*, 14(3), 688-694.
- Geboers, J., Wang, X., de Carvalho, A. B., and Rinaldi, R. (2014). Densification of biorefinery schemes by H-transfer with Raney Ni and 2-propanol: A case study of a potential avenue for valorization of alkyl levulinates to alkyl gamma-hydroxypentanoates and gamma-valerolactone. *Journal of Molecular Catalysis A: Chemical*, 388-389, 106-115.
- Highina, B., Bugaje, I., and Umar, B. (2011). Biodiesel production from *Jatropha caucis* oil in a batch reactor using zinc oxide as catalyst. *Journal of Petroleum Technology and Alternative Fuels*, 2(9), 146-149.
- Hindryawati, N., Maniam, G. P., Karim, M. R., and Chong, K. F. (2014). Transesterification of used cooking oil over alkali metal (Li, Na, K) supported rice husk silica as

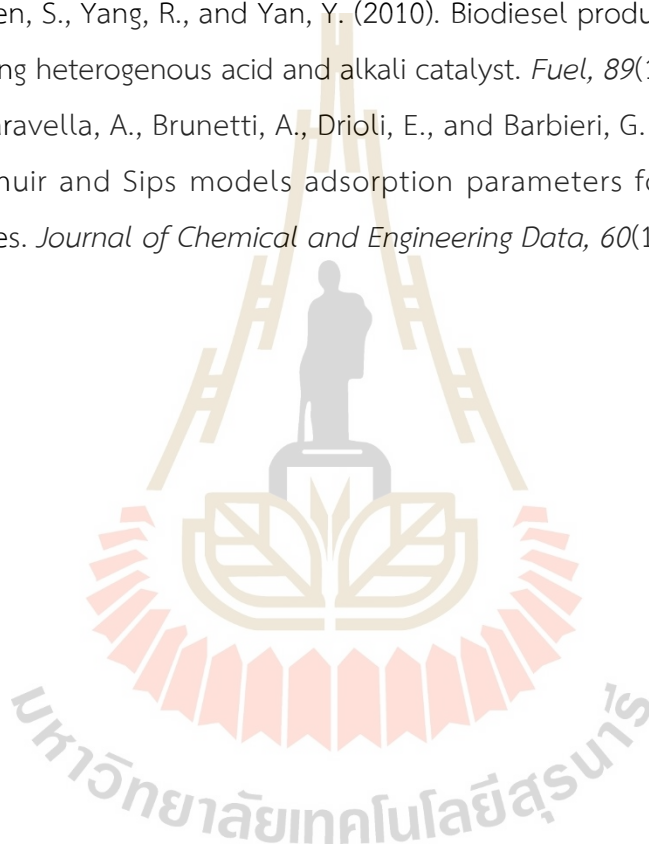
- potential solid base catalyst. *Engineering Science and Technology, an International Journal*, 17(2), 95-103.
- Ishikawa, S., Jones, D. R., Iqbal, S., Reece, C., Morgan, D. J., Willock, D. J., Miedziak, P. J., Bartley, J. K., Edwards, J. K., Murayama, T., Ueda, W., and Hutchings, G. J. (2017). Identification of the catalytically active component of Cu–Zr–O catalyst for the hydrogenation of levulinic acid to gamma-valerolactone. *Green Chemistry*, 19(1), 225-236.
- Jones, D. R., Iqbal, S., Ishikawa, S., Reece, C., Thomas, L. M., Miedziak, P. J., Morgan, D. J., Edwards, J. K., Bartley, J. K., Willock, D. J., and Hutchings, G. J. (2016). The conversion of levulinic acid into gamma-valerolactone using Cu–ZrO₂ catalysts. *Catalysis Science and Technology*, 6(15), 6022-6030.
- Kasar, G. B., Medhekar, R. S., Bhosale, P. N., and Rode, C. V. (2019). Kinetics of hydrogenation of aqueous levulinic acid over bimetallic Ru–Ni/MMT catalyst. *Industrial and Engineering Chemistry Research*, 58(43), 19803-19817.
- Kosawatthanakun, S., Pansakdanon, C., Sosa, N., Chanlek, N., Roessner, F., Prayoonpokarach, S., and Wittayakun, J. (2022). Comparative properties of K/NaX and K/NaY from ultrasound-assisted impregnation and performance in transesterification of palm oil. *ACS Omega*, 7(11), 9130-9141.
- Leung, D. Y. C., Wu, X., and Leung, M. K. H. (2010). A review on biodiesel production using catalyzed transesterification. *Applied Energy*, 87(4), 1083-1095.
- Li, H., Fang, Z., Luo, J., and Yang, S. (2017). Direct conversion of biomass components to the biofuel methyl levulinate catalyzed by acid-base bifunctional zirconia-zeolites. *Applied Catalysis B: Environmental*, 200, 182-191.
- Liu, S., McDonald, T., and Wang, Y. (2010). Producing biodiesel from high free fatty acids waste cooking oil assisted by radio frequency heating. *Fuel*, 89(10), 2735-2740.
- Ma, Y.-K., Rigolet, S., Michelin, L., Paillaud, J.-L., Mintova, S., Khoerunnisa, F., Daou, T. J., and Ng, E.-P. (2021). Facile and fast determination of Si/Al ratio of zeolites using FTIR spectroscopy technique. *Microporous and Mesoporous Materials*, 311, 110683.

- Manadee, S., Sophiphun, O., Osakoo, N., Supamathanon, N., Kidkhunthod, P., Chanlek, N., Wittayakun, J., and Prayoonpokarach, S. (2017). Identification of potassium phase in catalysts supported on zeolite NaX and performance in transesterification of Jatropha seed oil. *Fuel Processing Technology*, *156*, 62-67.
- Manzer, L. E. (2004). Catalytic synthesis of alpha-methylene-gamma-valerolactone: A biomass-derived acrylic monomer. *Applied Catalysis A: General*, *272*(1), 249-256.
- Marchetti, J. M., Miguel, V. U., and Errazu, A. F. (2007). Possible methods for biodiesel production. *Renewable and Sustainable Energy Reviews*, *11*(6), 1300-1311.
- Montalbo, K. D., Leon, R. L. d., Sophiphun, O., Manadee, S., Prayoonpokarach, S., and Wittayakun, J. (2013). Characterization and catalytic performance of potassium loaded on rice husk silica and zeolite NaY for transesterification of jatropha seed oil. *Química Nova*. *36*, 1116-1120.
- Noiroj, K., Intarapong, P., Luengnaruemitchai, A., and Jai-In, S. (2009). A comparative study of KOH/Al₂O₃ and KOH/NaY catalysts for biodiesel production via transesterification from palm oil. *Renewable Energy*, *34*(4), 1145-1150.
- Osatiashtiani, A., Lee, A. F., and Wilson, K. (2017). Recent advances in the production of gamma-valerolactone from biomass-derived feedstocks via heterogeneous catalytic transfer hydrogenation. *Journal of Chemical Technology and Biotechnology*, *92*(6), 1125-1135.
- Panagiotopoulou, P., Martin, N., and Vlachos, D. G. (2014). Effect of hydrogen donor on liquid phase catalytic transfer hydrogenation of furfural over a Ru/RuO₂/C catalyst. *Journal of Molecular Catalysis A: Chemical*, *392*, 223-228.
- Perego, C., Bosetti, A., Ricci, M., and Millini, R. (2017). Zeolite materials for biomass conversion to biofuel. *Energy and Fuels*, *31*(8), 7721-7733.
- Polisi, M., Grand, J., Arletti, R., Barrier, N., Komaty, S., Zaarour, M., Mintova, S., and Vezzalini, G. (2019). CO₂ adsorption/desorption in FAU zeolite nanocrystals: In situ synchrotron X-ray powder diffraction and in situ fourier transform infrared spectroscopic study. *The Journal of Physical Chemistry C*, *123*(4), 2361-2369.

- Rakmae, S., Keawkumay, C., Osakoo, N., Montalbo, K. D., de Leon, R. L., Kidkhunthod, P., Chanlek, N., Roessner, F., Prayoonpokarach, S., and Wittayakun, J. (2016). Realization of active species in potassium catalysts on zeolite NaY prepared by ultrasound-assisted impregnation with acetate buffer and improved performance in transesterification of palm oil. *Fuel*, *184*, 512-517.
- Refaat, A. A. (2011). Biodiesel production using solid metal oxide catalysts. *International Journal of Environmental Science and Technology*, *8*(1), 203-221.
- Romero, M. D., Ovejero, G., Rodríguez, A., and Gómez, J. M. (2005). Enhancement of the basic properties in FAU zeolites by impregnation with cesium hydroxide. *Microporous and Mesoporous Materials*, *81*(1), 313-320.
- Sánchez, M., Navas, M., Ruggera, J. F., Casella, M. L., Aracil, J., and Martínez, M. (2014). Biodiesel production optimization using gamma-Al₂O₃ based catalysts. *Energy*, *73*, 661-669.
- Scholz, D., Aellig, C., and Hermans, I. (2014). Catalytic transfer hydrogenation/hydrogenolysis for reductive upgrading of furfural and 5-(hydroxymethyl)furfural. *ChemSusChem*, *7*(1), 268-275.
- Shimada, Y., Watanabe, Y., Sugihara, A., and Tominaga, Y. (2002). Enzymatic alcoholysis for biodiesel fuel production and application of the reaction to oil processing. *Journal of Molecular Catalysis B: Enzymatic*, *17*(3), 133-142.
- Shimizu, K.-i., Kanno, S., and Kon, K. (2014). Hydrogenation of levulinic acid to gamma-valerolactone by Ni and MoO_x co-loaded carbon catalysts. *Green Chemistry*, *16*(8), 3899-3903.
- Sun, D., Ohkubo, A., Asami, K., Katori, T., Yamada, Y., and Sato, S. (2017). Vapor-phase hydrogenation of levulinic acid and methyl levulinate to gamma-valerolactone over non-noble metal-based catalysts. *Molecular Catalysis*, *437*, 105-113.
- Supamathanon, N., Wittayakun, J., and Prayoonpokarach, S. (2011). Properties of Jatropha seed oil from Northeastern Thailand and its transesterification catalyzed by potassium supported on NaY zeolite. *Journal of Industrial and Engineering Chemistry*, *17*(2), 182-185.

- Tan, J., Cui, J., Deng, T., Cui, X., Ding, G., Zhu, Y., and Li, Y. (2015). Water-promoted hydrogenation of levulinic acid to gamma-valerolactone on supported ruthenium catalyst. *ChemCatChem*, 7(3), 508-512.
- Tian, Z., Liu, C., Li, Q., Hou, J., Li, Y., and Ai, S. (2015). Nitrogen- and oxygen-functionalized carbon nanotubes supported Pt-based catalyst for the selective hydrogenation of cinnamaldehyde. *Applied Catalysis A: General*, 506, 134-142.
- Upare, P. P., Lee, J.-M., Hwang, Y. K., Hwang, D. W., Lee, J.-H., Halligudi, S. B., Hwang, J.-S., and Chang, J.-S. (2011). Direct hydrocyclization of biomass-derived levulinic acid to 2-methyltetrahydrofuran over nanocomposite copper/silica catalysts. *ChemSusChem*, 4(12), 1749-1752.
- Upare, P. P., Lee, J.-M., Hwang, D. W., Halligudi, S. B., Hwang, Y. K., and Chang, J.-S. (2011). Selective hydrogenation of levulinic acid to gamma-valerolactone over carbon-supported noble metal catalysts. *Journal of Industrial and Engineering Chemistry*, 17(2), 287-292.
- Vicente, G., Martínez, M., and Aracil, J. (2004). Integrated biodiesel production: A comparison of different homogeneous catalysts systems. *Bioresource Technology*, 92(3), 297-305.
- Wan Omar, W. N. N., and Amin, N. A. S. (2011). Biodiesel production from waste cooking oil over alkaline modified zirconia catalyst. *Fuel Processing Technology*, 92(12), 2397-2405.
- Yan, K., Yang, Y., Chai, J., and Lu, Y. (2015). Catalytic reactions of gamma-valerolactone: A platform to fuels and value-added chemicals. *Applied Catalysis B: Environmental*, 179, 292-304.
- Yan, Z.-p., Lin, L., and Liu, S. (2009). Synthesis of gamma-valerolactone by hydrogenation of biomass-derived levulinic acid over Ru/C catalyst. *Energy & Fuels*, 23(8), 3853-3858.
- Yang, Y., Xu, X., Zou, W., Yue, H., Tian, G., and Feng, S. (2016). Transfer hydrogenation of methyl levulinate into gamma-valerolactone, 1,4-pentanediol, and 1-pentanol over Cu-ZrO₂ catalyst under solvothermal conditions. *Catalysis Communications*, 76, 50-53.

- Yang, Z., Huang, Y.-B., Guo, Q.-X., and Fu, Y. (2013). RANEY® Ni catalyzed transfer hydrogenation of levulinate esters to gamma-valerolactone at room temperature. *Chemical Communications*, 49(46), 5328-5330.
- Zhang, J., Chen, J., Guo, Y., and Chen, L. (2015). Effective upgrade of levulinic acid into gamma-valerolactone over an inexpensive and magnetic catalyst derived from hydrotalcite precursor. *ACS Sustainable Chemistry and Engineering*, 3(8), 1708-1714.
- Zhang, J., Chen, S., Yang, R., and Yan, Y. (2010). Biodiesel production from vegetable oil using heterogenous acid and alkali catalyst. *Fuel*, 89(10), 2939-2944.
- Zito, P. F., Caravella, A., Brunetti, A., Drioli, E., and Barbieri, G. (2015). Estimation of Langmuir and Sips models adsorption parameters for NaX and NaY FAU zeolites. *Journal of Chemical and Engineering Data*, 60(10), 2858-2868.



CHAPTER III

INFLUENCE OF THE ZEOLITE NaX CRYSTALLINITY ON CATALYTIC PERFORMANCE OF K/NaX IN TRANSESTERIFICATION OF PALM OIL

3.1 Abstract

Zeolite NaX with various hydrothermal times (0, 4, 8, 12, and 24 h) were impregnated with potassium and employed as a catalyst in the transesterification of palm oil with methanol to explore the influence of the crystallinity of zeolite NaX on biodiesel production. The findings from XRD, N₂ sorption, SEM-EDS, FTIR, and CO₂-TPD demonstrate that prolonging the hydrothermal treatment time correlates with an enhancement in zeolite NaX crystallinity. Complete zeolite NaX crystallization was achieved with hydrothermal times of 8 h or longer. The enhanced crystallinity of zeolite NaX support led to an increase in the basicity of the K/NaX catalyst, resulting in improved catalytic performance for transesterification of palm oil. The catalysts using supports treated for 0 and 4 h, exhibited varying crystallinity, resulting in different biodiesel yields (29.7% and 43.9% with the K/HT0 and K/HT4, respectively) despite having similar surface area, functional group, and morphology. Catalysts employing fully crystallized zeolite NaX as the support yielded biodiesel about 80%. However, these catalysts could not be effectively reused due to the leaching of potassium carbonate from the support surface.

3.2 Introduction

Biodiesel, also known as fatty acid methyl ester, is a viable alternative to traditional fossil fuels due to its similar properties. It is distinguished by its biodegradability, non-toxicity, renewability, and lower emissions of CO, SO₂, particulates, and hydrocarbons (Demirbas, 2007; Muniyappa et al., 1996). Biodiesel is typically synthesized from vegetable oils or animal fats through the transesterification of triglycerides with alcohol and catalyst. Homogeneous catalysts such as NaOH and KOH are frequently used due to their efficiency and rapid reaction times (Meher et al., 2006). However, they present challenges such as the need for post-reaction washing to remove catalyst residues and difficulty in catalyst recovery (Sharma et al., 2011). As a consequence, there is growing research interest in developing heterogeneous catalysts, which are more environmentally friendly due to their ease of recovery and reuse (Mathew et al., 2021; Mukhtar et al., 2022).

The predominant heterogeneous catalysts used in biodiesel production are carbonates and oxides of alkali and alkaline earth metals, supported on materials with high porosity and surface area like SiO₂, Al₂O₃, and zeolites (Perego et al., 2017; Refaat, 2011; Romero et al., 2005; Xie et al., 2006). Sanchez et al. (2014) varied the alkali and alkaline earth oxides on gamma-Al₂O₃ supports to examine the behavior of soybean oil transesterification with different gamma-Al₂O₃-based catalysts. They concluded that K/gamma-Al₂O₃ exhibited superior performance than other metals. Hindryawati et al. (2014) also reported that potassium-based catalysts possess greater basicity and are more resistant to free fatty acid contamination in triglyceride sources compared to lithium and sodium.

Among several supported materials, zeolites faujasite such as NaX and NaY are interesting because they are aluminosilicate material with large surface areas and high thermal stability (Verboekend et al., 2016). Various investigations have explored potassium-supported zeolite catalysts for the transesterification of diverse oil feedstocks. Noiroj et al. (2009) utilized KOH on Al₂O₃ and zeolite NaY as catalysts for transesterification of palm oil with methanol. The 10 wt% potassium of KOH/NaY catalyst demonstrates considerable efficacy at temperatures below 70 °C within 3 h, achieving biodiesel yields of 91.07 %. However, the incorporation of KOH affected the

crystalline structure of the zeolite, leading to its partial collapse. Subsequently, Supamathanon et al. (2011) used the other potassium precursor, potassium acetate buffer solution pH \approx 5, to produce the catalyst with preservation of the NaY structure. This potassium precursor was found to minimize the collapse of the zeolite structure. Montalbo et al. (2013) employed potassium acetate buffer solution as a potassium precursor to evaluate K/SiO₂ and K/NaY in the transesterification of Jatropha seed oil at 65 °C for 3 h and determined that NaY-supported catalysts were more active than those supported on SiO₂. Kosawatthanakun et al. (2022) conducted a comparative analysis of K/NaX and K/NaY for transesterification of palm oil. A more pronounced collapse in K/NaY compared to K/NaX, along with a higher basicity in K/NaX, indicating its superior catalytic properties for this reaction.

Previous studies have assessed various support materials for their efficacy in catalyzing transesterification reactions, with zeolite NaX being identified as particularly efficient for this process. Therefore, this study aims to deepen our understanding of the K/NaX catalyst by investigating the influence of zeolite NaX crystallinity on the transesterification of palm oil. The insights gained are expected to substantially enhance the design and optimization of catalytic processes for biodiesel production.

3.3 Experimental

3.3.1 Chemicals

Chemicals for zeolite NaX synthesis included fumed silica (SiO₂, 99%, Sigma-Aldrich), sodium aluminate (NaAlO₂, Al₂O₃ \sim 55–56%, Riedel-deHaën) and sodium hydroxide (NaOH, 98%, Carlo-Erba). The chemicals for catalyst preparation were potassium acetate (CH₃COOK, 99.0%, Carlo-Erba) and acetic acid (CH₃COOH, 99.7%, RCI Labscan). The chemicals in catalyst testing were refined palm oil (food grade, Morakot Industries PCL., Thailand), methanol (CH₃OH, 99.9%, Carlo Erba) and hexane (CH₃(CH₂)₄CH₃, 95.0%, Carlo Erba). The chemical used as the initial standard for testing with Gas chromatography with flame ionization detector (GC-FID) was methyl nonadecanoate, (CH₃ (CH₂)₁₇COOCH₃, 98%, Sigma Aldrich).

3.3.2 Synthesis of zeolite NaX with various hydrothermal time

The synthesis methods of zeolite NaX as supports were modified from the literature (Lechert et al., 2016). Firstly, the zeolite NaX gel was prepared by creating a 27% SiO_2 solution, where deionized (DI) water 61.94 g was mixed with NaOH 10.71 g, and fumed SiO_2 27.35 g was gradually added and stirred until dissolved overnight. A 65% Al_2O_3 solution was prepared by mixing DI water 35.71 g with NaOH 12.26 g and adding NaAlO_2 42.81 g, stirring until dissolved overnight. The Na_2SiO_3 solution was then formed by mixing DI water 218.57 g with NaOH 21.12 g and adding the 27% SiO_2 solution from the previous step 78.46 g, followed by stirring until dissolved. Similarly, the NaAlO_2 solution was prepared by mixing DI water 218.57 g with NaOH 21.12 g and adding the 65% Al_2O_3 solution from the previous step 35.71 g, while stirring until dissolved. The zeolite NaX gel was created by rapidly and vigorously combining the Na_2SiO_3 and NaAlO_2 solutions, stirring for 5-10 min. The resulting mixture was divided into five polypropylene bottles (125 mL), each further stirred for 30 min. Subsequently, the bottles were tightly sealed, and the products were crystallized by varying hydrothermal times (0-24 h) at 90 °C. The final step involved recovering the product through centrifugation (4000 rpm, 5 min, 125 PP bottle), washing to achieve $\text{pH} < 10$, and drying at 100 °C for 24 h. The support materials obtained with different hydrothermal time of 0, 4, 8, 12, and 24 h, were designated as HT0, HT4, HT8, HT12, and HT24, respectively.

3.3.3 Catalyst preparation

The catalysts with an 8 wt% potassium loading were prepared using ultrasound-assisted impregnation. The support materials were dried at 100 °C overnight. For the preparation of an acetate buffer, 5.45 g of potassium acetate was dissolved in 17.50 mL, 1.00 M acetic acid and adjusted to a volume of 25.00 mL by DI water. Subsequently, 1.00 mL of the buffer was added to 1.00 g of dried zeolite and subjected to sonication at a frequency of 37 kHz and power of 80 W (Elmasonic E 30H model, Elma) for 10 min. The resulting mixture was then dried at 80 °C for 24 h and subjected to calcination at 500 °C under a static air atmosphere for 3 h. The catalysts obtained from this process were denoted as K/HT0, K/HT4, K/HT8, K/HT12, and K/HT24.

3.3.4 Catalyst characterization

The phase characteristics of the samples were investigated through X-ray diffraction (XRD) using a Bruker XRD-D8 Advance instrument with Cu K α radiation ($\lambda = 0.154$ nm). The instrument operated at a voltage of 40 kV and a current of 40 mA. XRD patterns were obtained through a 2θ scan range from 5 to 50°, employing a step size of 0.02° and a scan speed of 0.5 s-step⁻¹.

The relative percentage of crystallinity was determined using data from XRD and plotted in the OriginPro 2018 software program. The selection of 9 strong crystalline peaks were based on visual observation. The relative percentage of crystallinity was calculated by the area of 9 strong diffraction peaks of the sample compared with the patterns of the product with the highest intensity in the studied experiment (Liu et al., 2016), as defined in Equation (3.1).

$$\text{Relative crystallinity (\%)} = \left(\frac{\text{Total area of 9 strong peaks of the sample}}{\text{Total area of 9 peaks of the one with the highest intensity}} \right) 100 \quad (3.1)$$

The isotherms of all samples were determined through N₂ adsorption-desorption measurements using a BELSORP-mini II. Prior to analysis, the samples were degassing at 200 °C for 24 h. Surface areas were calculated by Brunauer–Emmett–Teller (BET) method, while micropore volumes were estimated using the t-plot method based on the desorption branch.

The morphology and particle size of all samples were examined using scanning electron microscopy (SEM) on a JEOL model JSM-6010LV. Prior to imaging, each sample powder was uniformly dispersed on a carbon tape and subsequently coated with gold through sputtering to enhance electrical conductivity and the sample surface compositions were analyzed by energy dispersive spectrometer (SEM-EDS).

The examination of functional groups and vibration bands in samples was conducted through Fourier-transform infrared spectroscopy (FTIR) using a Bruker Tensor 27 instrument operating in attenuated total reflectance (ATR) mode. Sample powders were positioned on the ATR crystal and securely compressed using a pressure tower. Spectra were captured in the 400 - 4000 cm⁻¹ region at a resolution of 4 cm⁻¹, with each spectrum representing 64 scans.

The evaluation of catalyst basicity was carried out through temperature-programmed desorption of carbon dioxide (CO₂-TPD) using a BELCAT-B chemisorption analyzer. In this process, a 50 mg sample was loaded into a tubular glass reactor and subjected to pretreatment at 300 °C under helium (He) gas flow at a rate of 50 mL·min⁻¹ for 60 min to eliminate physisorbed species. Subsequently, the sample was cooled to 70 °C, and a gas mixture of 10% CO₂/He, flowing at a rate of 50 mL·min⁻¹, was introduced into the sample cell for 30 min. Following this, the system was purged with He for 30 min and then heated to 100 °C at a rate of 10 °C·min⁻¹, held for 60 min to remove non-adsorbed CO₂. The TPD process covered a temperature range from 100 to 800 °C, with a temperature ramp of 10 °C·min⁻¹. The determination of basic site density was achieved through the integration of peak area.

3.3.5 Catalysts testing: Transesterification of palm oil

Transesterification of palm oil was performed according to the previous work. (Rakmae et al., 2016). The transesterification conditions involved a methanol to oil molar ratio of 16:1, a reaction temperature of 60 °C, reaction time of 3 h, and a catalyst to oil ratio of 4% w/w. The transesterification reactions were conducted in a 50-mL round-bottom flask equipped with a water-cooled condenser, as shown in Figure 3.1.

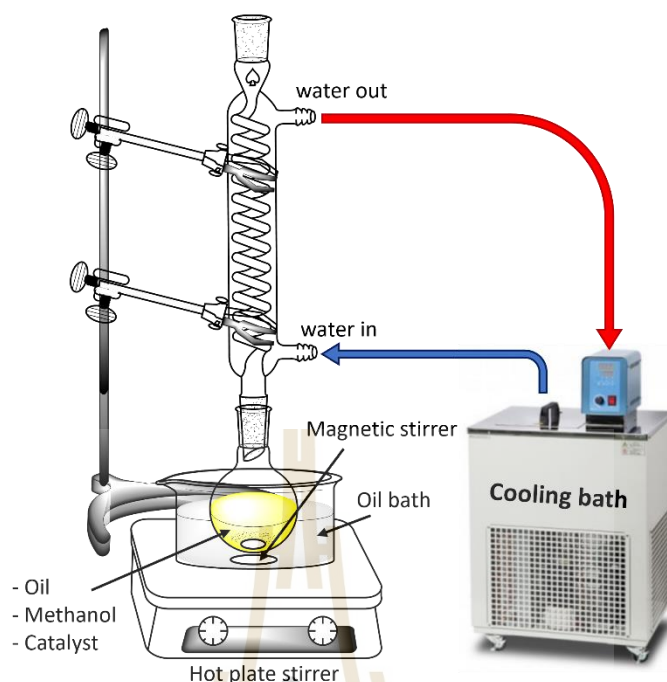


Figure 3.1 Apparatus set up for transesterification.

A mixture of 5.00 g palm oil, 0.20 g catalyst and 2.90 g methanol were magnetically stirred in a round bottom flask equipped with a condenser at 60 °C for 3 h. The product mixture was separated by vacuum filter. The liquid phase was transferred to a separatory funnel and left to undergo overnight separation. The resulting biodiesel, located in the upper layer, was collected and evaporated to eliminate methanol using a rotary evaporator.

The biodiesel yield was conducted following the biodiesel test method EN 14103 using gas chromatography (Agilent 7890 GC) equipped with a flame ionization detector (FID) and a capillary column (Agilent J&W CP-Sil 88, CP7489). The capillary column had a length of 100 m, a film thickness of 0.20 μm , and an internal diameter of 0.25 mm. Helium served as the carrier gas at a flow rate of 3 $\text{mL}\cdot\text{min}^{-1}$. Injection was carried out in split mode with a split ratio of 50:1. The injector and detector temperatures were set at 240 and 300 °C, respectively. The oven temperature underwent a series of steps: initially started at 70 °C for 4 min, then ramped up to 175 °C at a rate of 13 $^{\circ}\text{C}\cdot\text{min}^{-1}$ and held for 27 min in the first step. In the second step, the oven was heated to 215 °C with a ramp rate of 4 $^{\circ}\text{C}\cdot\text{min}^{-1}$ and held for 15 min. The final step involved raising the oven temperature to 240 °C at a ramp rate of 4 $^{\circ}\text{C}\cdot\text{min}^{-1}$

and maintaining it for 12 min. Methyl nonadecanoate, referred to C19, served as the internal standard in the analysis. The biodiesel yield was calculated using Equation (3.2) based on the literature reference (Okwundu et al., 2019; Roschat et al., 2016)

$$\text{biodiesel yield}(\%) = \left(\frac{(\sum A_{C_8-C_{24:1}}) - A_{C_{19}}}{A_{C_{19}}} \right) \left(\frac{[C_{19}](V_{C_{19}})}{m_{\text{sample}}} \right) 100 \quad (3.2)$$

Where, $\sum A_{C_8-C_{24:1}}$ represents the cumulative peak area of methyl esters from C8 to C24:1 obtained from GC-FID, and m_{sample} denotes the mass of the analyzed biodiesel sample. The GC peak area, concentration, and volume of the methyl nonadecanoate solution are denoted as $A_{C_{19}}$, $[C_{19}]$, and $V_{C_{19}}$, respectively.

3.3.6 Catalysts stability

After the reaction, the spent catalysts were washed with 10 mL of methanol and 10 mL of hexane, then dried at 90 °C overnight. These spent catalysts were reused in the transesterification reaction of palm oil under conditions identical to those used for fresh catalysts. The quantity of the products was determined using GC-FID. The spent catalysts were characterized by XRD, FTIR, and CO₂-TPD.

3.4 Results and Discussion

3.4.1 Catalysts characterization

XRD patterns illustrating the characteristics of all support samples are depicted in Figure 3.2. HT0 and HT4 contained broad peaks in the ranges 7° – 17° and 17° - 40° (Figure 3.2(a)) which are characteristic of amorphous phase. Notably, the HT4 exhibits an additional peak at 6.10°, corresponding to the 111 plane of zeolite NaX. HT8, HT12 and HT24 exhibit the same peak positions (Figure 3.2(b)) which are characteristic of zeolite NaX (JCPDS No. 38-0237). The results from this work were similar to those reported in the literature (Zhang et al., 2013) that the appearance of crystalline peaks of zeolite NaX in the XRD spectra occurs after a hydrothermal time of 3 h, and the peak intensity increases with longer hydrothermal time.

The relative crystallinity percentages of all support samples are shown in Figure 3.3. The relative crystallinity percentages are low for HT0 and HT4 and increase

significantly with hydrothermal treatment time. The results of this experiment suggest that the zeolite NaX initiates structural formation after a hydrothermal time of 4 h, with complete formation occurring at hydrothermal times from 8 h onwards.

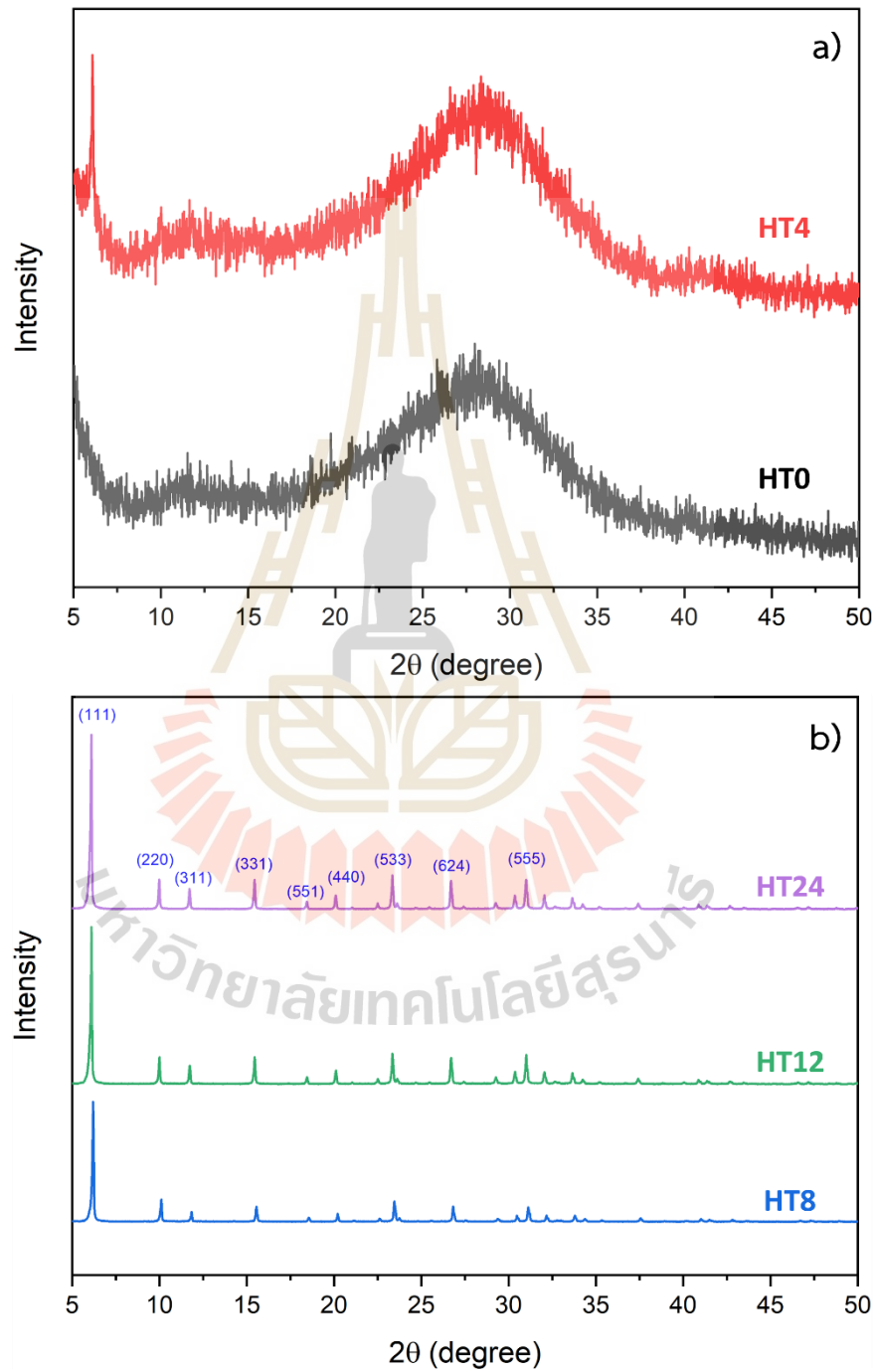


Figure 3.2 XRD patterns of a) HT0 and HT4 and b) HT8, HT12 and HT24.

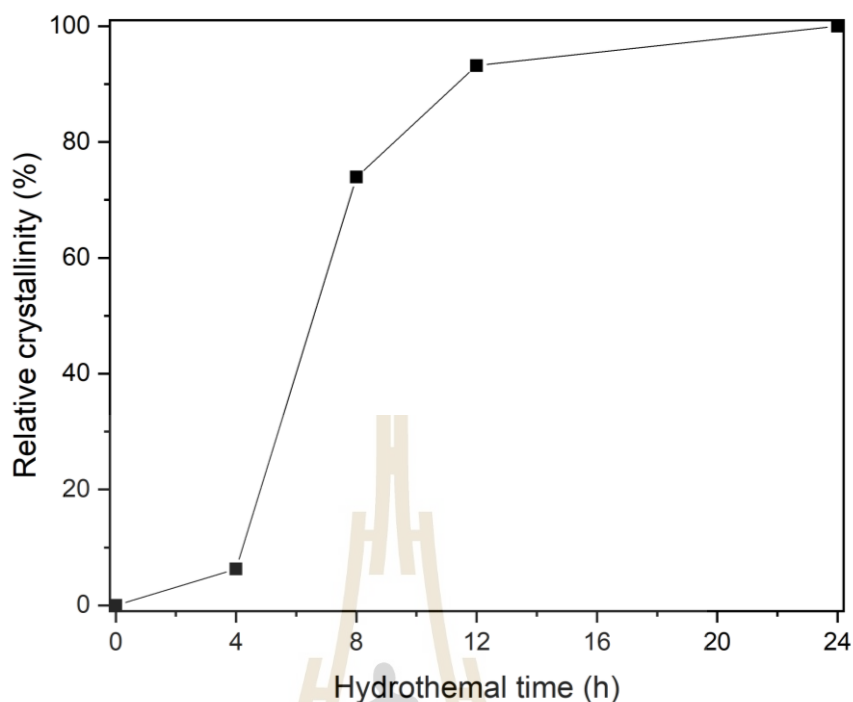


Figure 3.3 Relative crystallinity percentage of all support samples.

The XRD patterns of all catalyst samples are depicted in Figure 3.4. The K/HT0 and K/HT4 catalysts still show broad peaks (Figure 3.4(a)), but the peak at 6.10° in K/HT4 diminishes in comparison to HT4. In the case of the K/HT8, K/HT12, and K/HT24 catalysts, the characteristic peaks specific to zeolite NaX are still observable (Figure 3.4(b)). However, these catalyst samples exhibit lower intensities compared to the support samples. This observation suggests that impregnating the zeolite with a potassium buffer solution did not significantly change the NaX structure (Manadee et al., 2017). The intensity of the peaks decreased due to the partial collapse of the zeolite frameworks caused by the hydrolysis of Si-O-Al bonds (Peña et al., 2013), or due to impregnated species covering the surface of zeolite NaX, resulting in a reduction in peaks intensity.

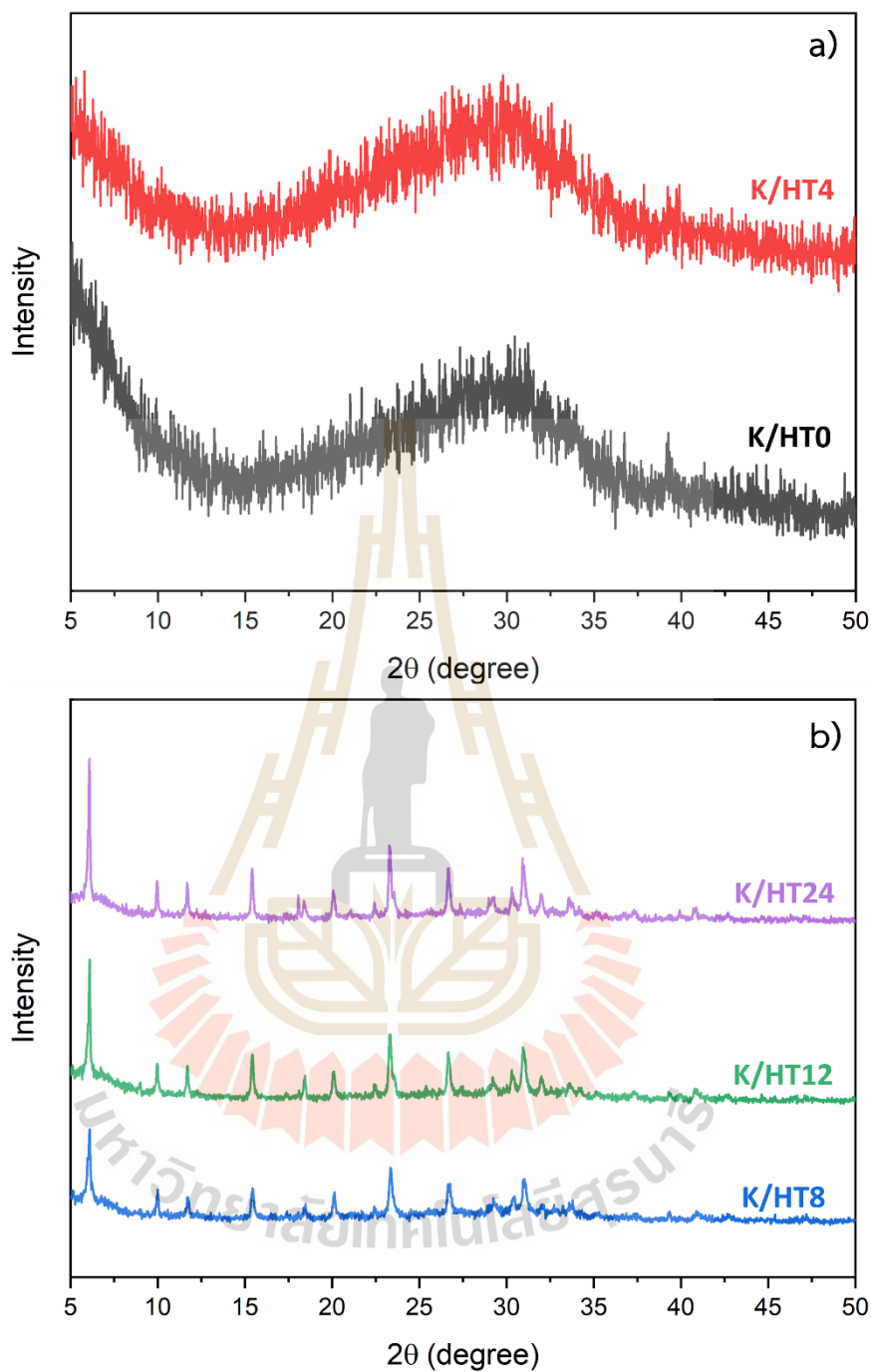
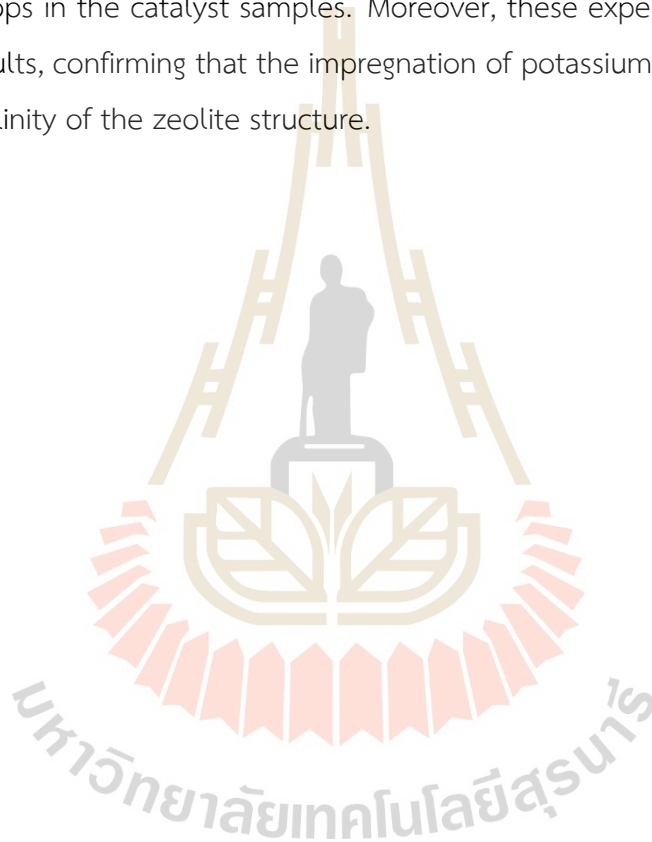


Figure 3.4 XRD patterns of a) K/HT0 and K/HT4 and b) K/HT8, K/HT12 and K/HT24.

The N_2 sorption isotherms of the supports are compared with the catalysts in Figure 3.5. The surface areas and pore volumes are summarized in Table 3.1. For the N_2 sorption isotherms of the support samples (black line), HT0 and HT4 exhibit type II isotherms, characteristic of macroporous materials, while HT8, HT12, and HT24 display

type I isotherms, indicative of microporous materials (Thommes et al., 2015). In the case of catalyst samples (red line), the N_2 sorption isotherms for each catalyst resemble those of their respective supports. However, K/HT8, K/HT12, and K/NHT24 display H2(b) hysteresis loops. The adsorbed volumes, surface areas, and pore volumes of the catalysts are smaller than those of the bare supports, possibly due to the occupation of impregnated species in the zeolite cavities, blockage of zeolite pores, and collapse of the zeolite structure (Rakmae et al., 2016). These factors contribute to the observed hysteresis loops in the catalyst samples. Moreover, these experimental findings align with XRD results, confirming that the impregnation of potassium results in a reduction in the crystallinity of the zeolite structure.



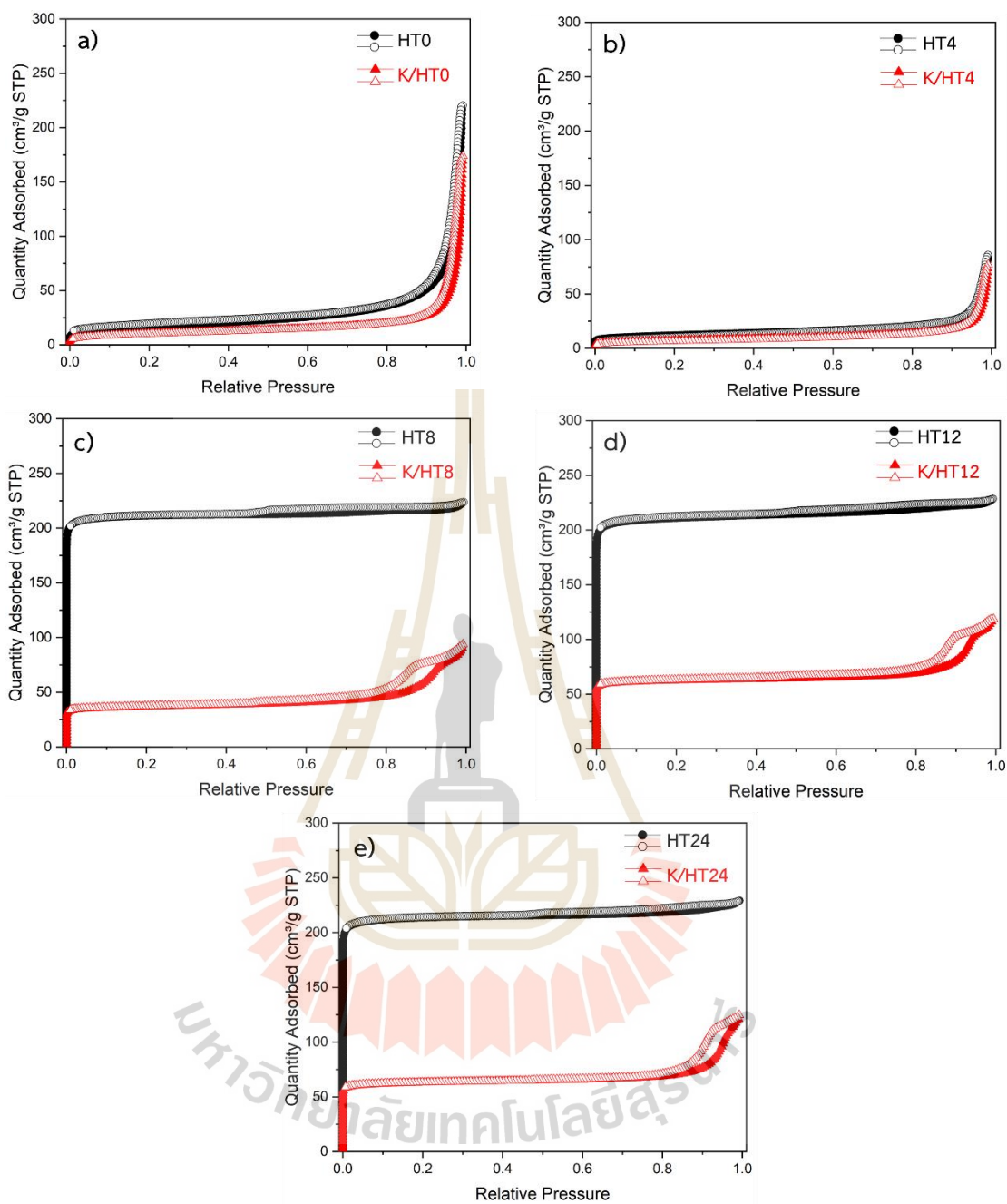


Figure 3.5 N_2 sorption isotherms of (a) HT0, (b) HT4, (c) HT8, (d) HT12, and (e) HT24 compared to their potassium catalysts; filled symbol = adsorption and hollow symbol = desorption.

Table 3.1 BET surface area and micropore volume of supports and catalysts from N₂ sorption analysis.

Sample	BET surface area (m ² ·g ⁻¹)	micropore volume (cm ³ ·g ⁻¹)
HT0	60	0.003
HT4	43	0.006
HT8	754	0.316
HT12	774	0.308
HT24	779	0.315
K/HT0	37	0.001
K/HT4	25	0.002
K/HT8	124	0.047
K/HT12	210	0.087
K/HT24	210	0.087

The morphological characteristics of the supports and catalysts were investigated by SEM, as shown in Figure 3.6. The SEM analysis of the supports (Figure 3.6(a-e)) reveals that HT0 and HT4 exhibit non-uniformly spherical with small particles forming clusters. The particle size of HT0 is approximately 20-50 nm, whereas HT4 has a larger particle size in the range of 80-120 nm. This difference is attributed to the longer hydrothermal time of HT4. For HT8, HT12, and HT24, the morphology appears as polycrystals with similar shapes and approximate sizes, each being roughly 1.2-1.8 μm in diameter. The particles exhibit a spherical form, comprised of clusters of small crystals with varying sizes and thicknesses interconnected. Additionally, it is observed that the size and thickness of the crystals progressively increase with an extended hydrothermal time. After potassium impregnation and calcination, the morphology of catalysts (Figure 3.6(f-j)) closely resembles that of the supports, albeit with a reduction in the sharpness of crystal edges.

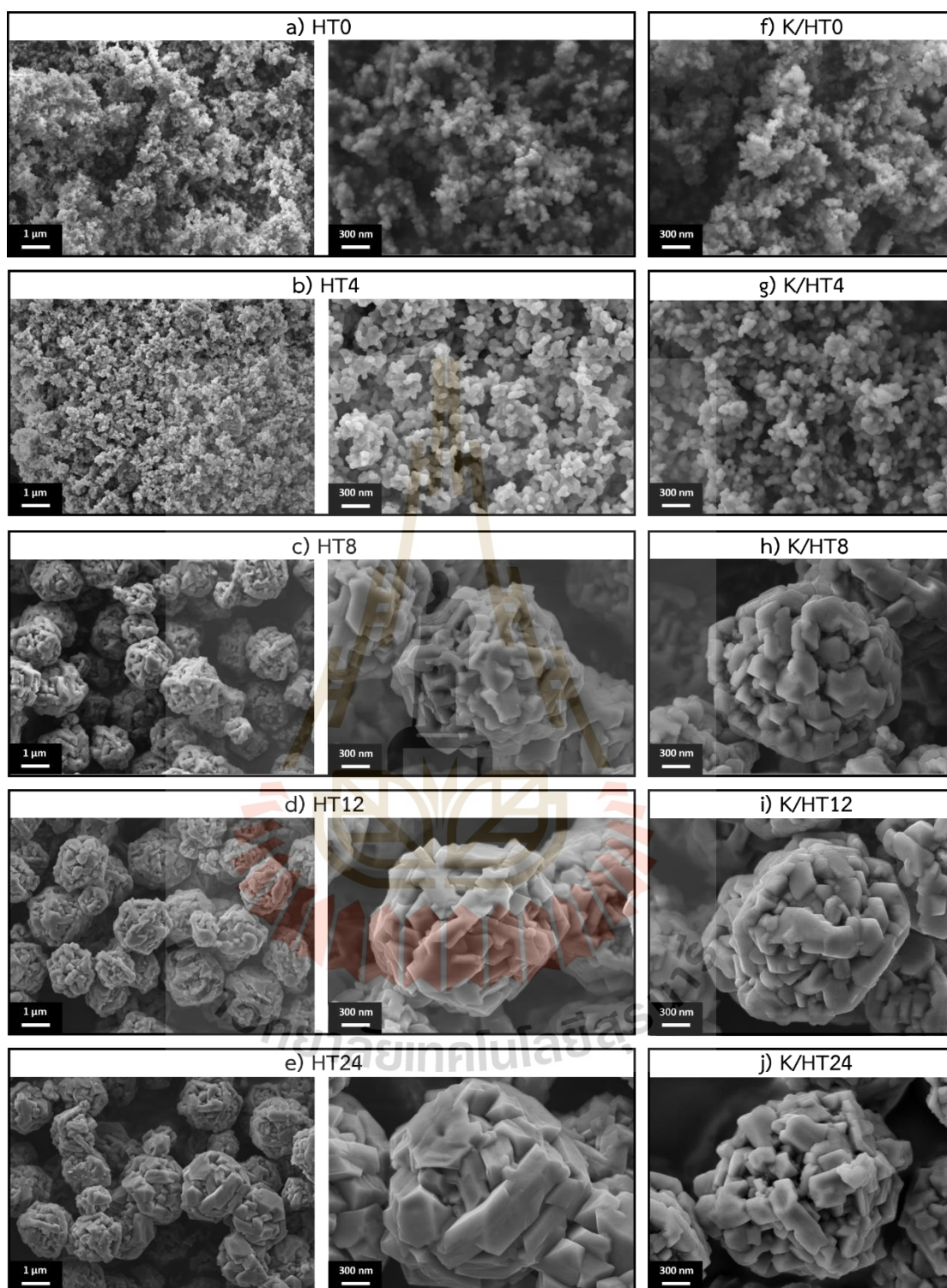


Figure 3.6 SEM images of with 10k and 30k magnification of (a) HT0, (b) HT4, (c) HT8, (d) HT12, and (e) HT24 and 30k magnification of (f) K/HT0, (g) K/HT4, (h) K/HT8, (i) K/HT12, and (j) K/HT24.

EDS element mapping of the supports and catalysts are depicted in Figure 3.7-3.11. For support materials, the results show that the synthesized supports predominantly consist of Si, Al, O, and Na. This composition confirms that the support material is pure zeolite NaX or aluminosilicate materials. In the case of the catalysts, it was observed that K is well dispersed across all support samples.

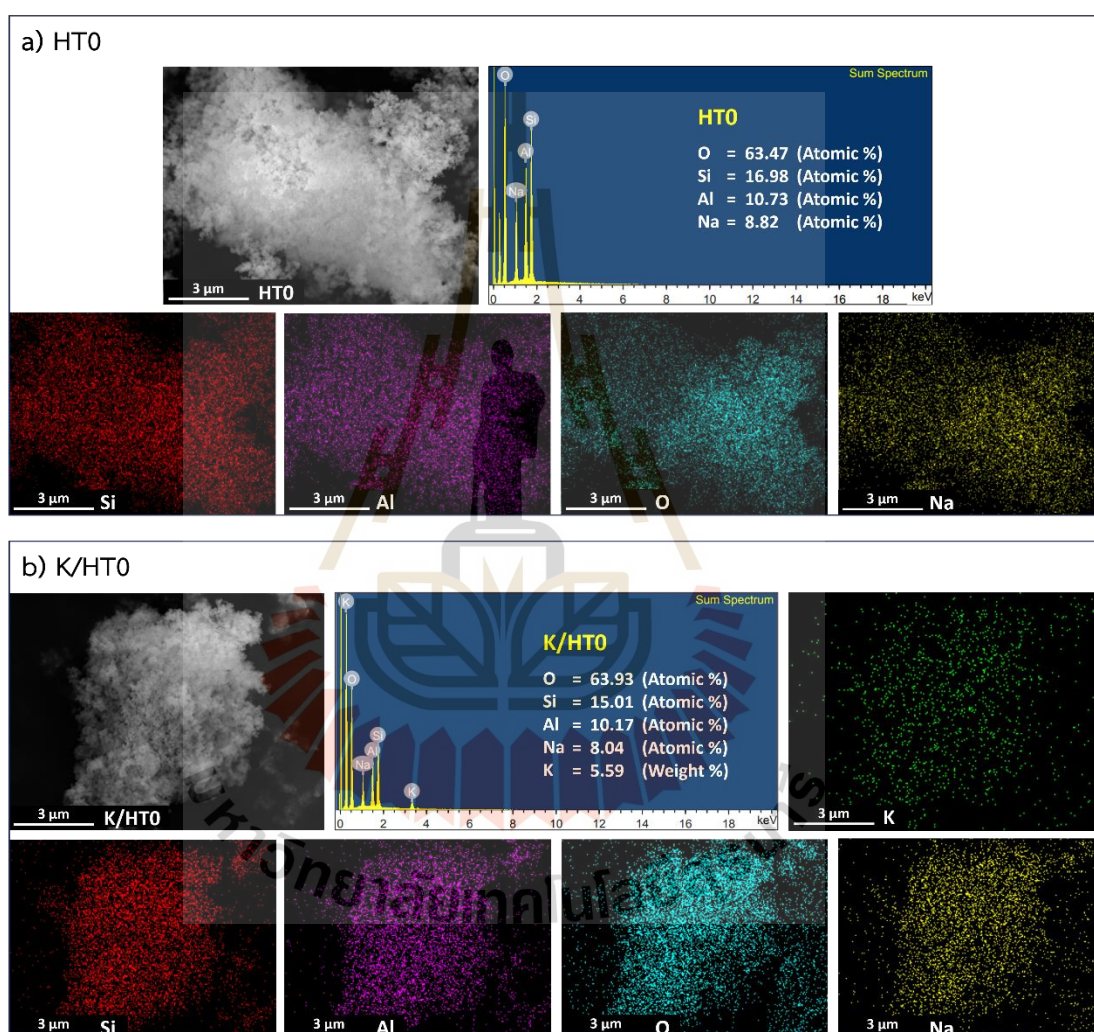


Figure 3.7 EDS elements mapping images of a) HTO and b) K/HTO.

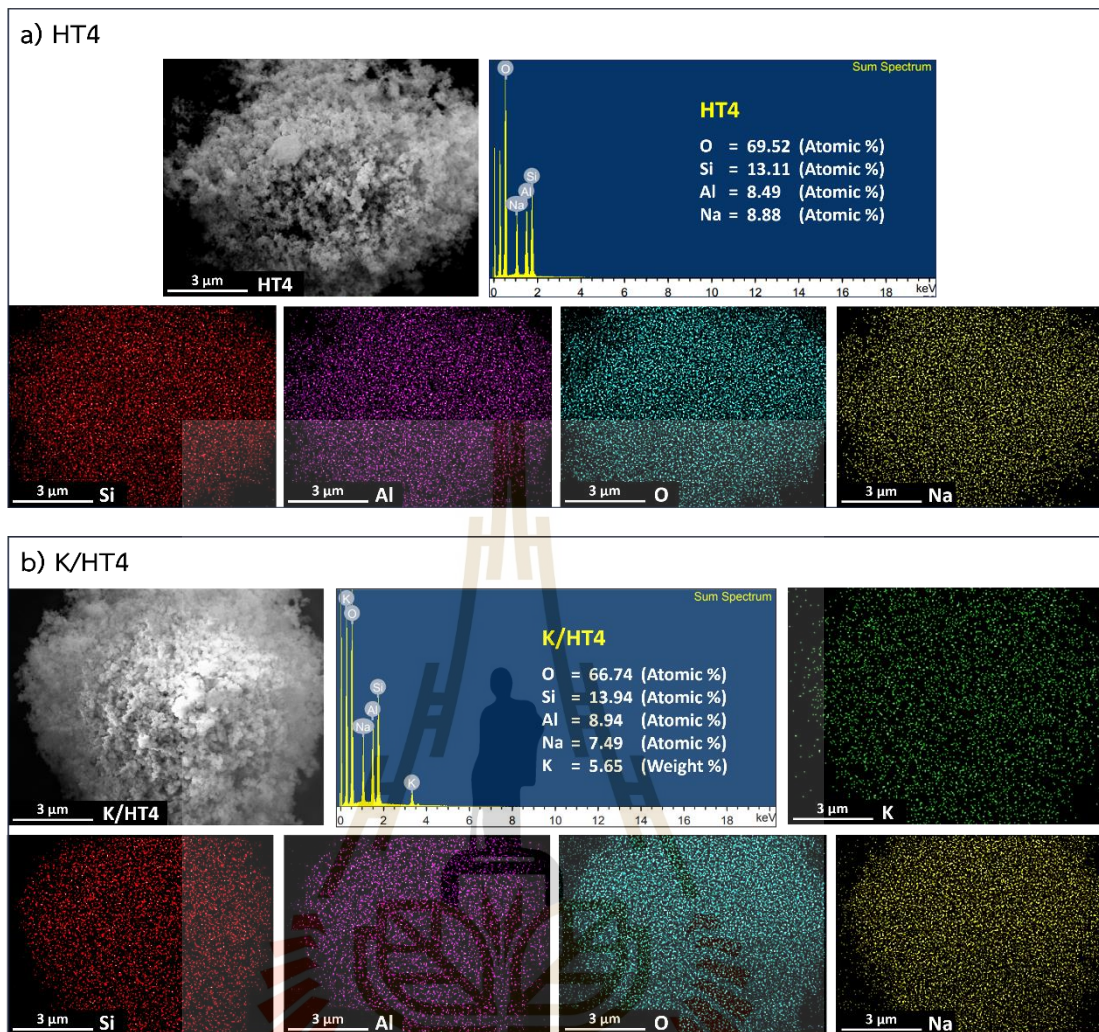


Figure 3.8 EDS elements mapping images of a) HT4 and b) K/HT4.

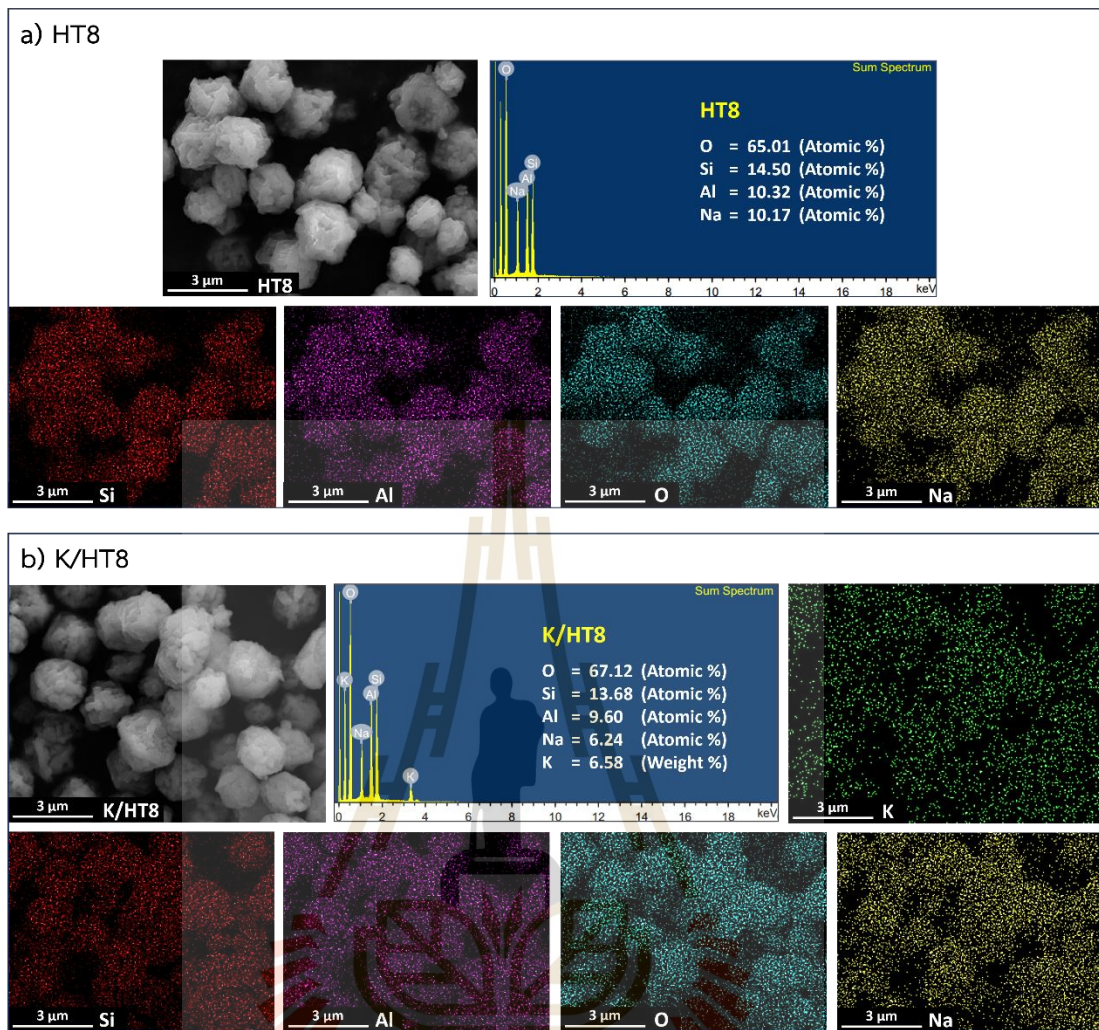


Figure 3.9 EDS elements mapping images of a) HT8 and b) K/HT8.

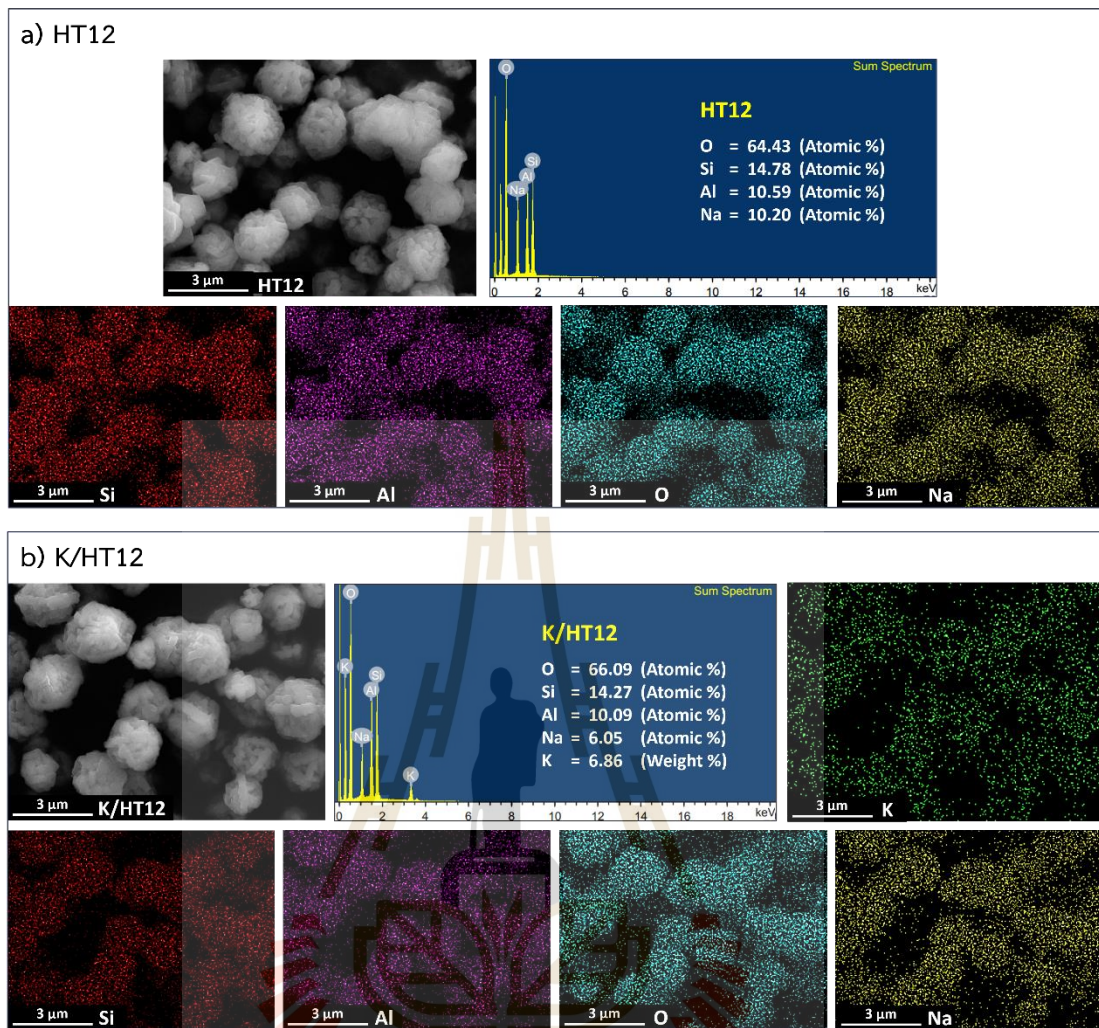


Figure 3.10 EDS elements mapping images of a) HT12 and b) K/HT12.

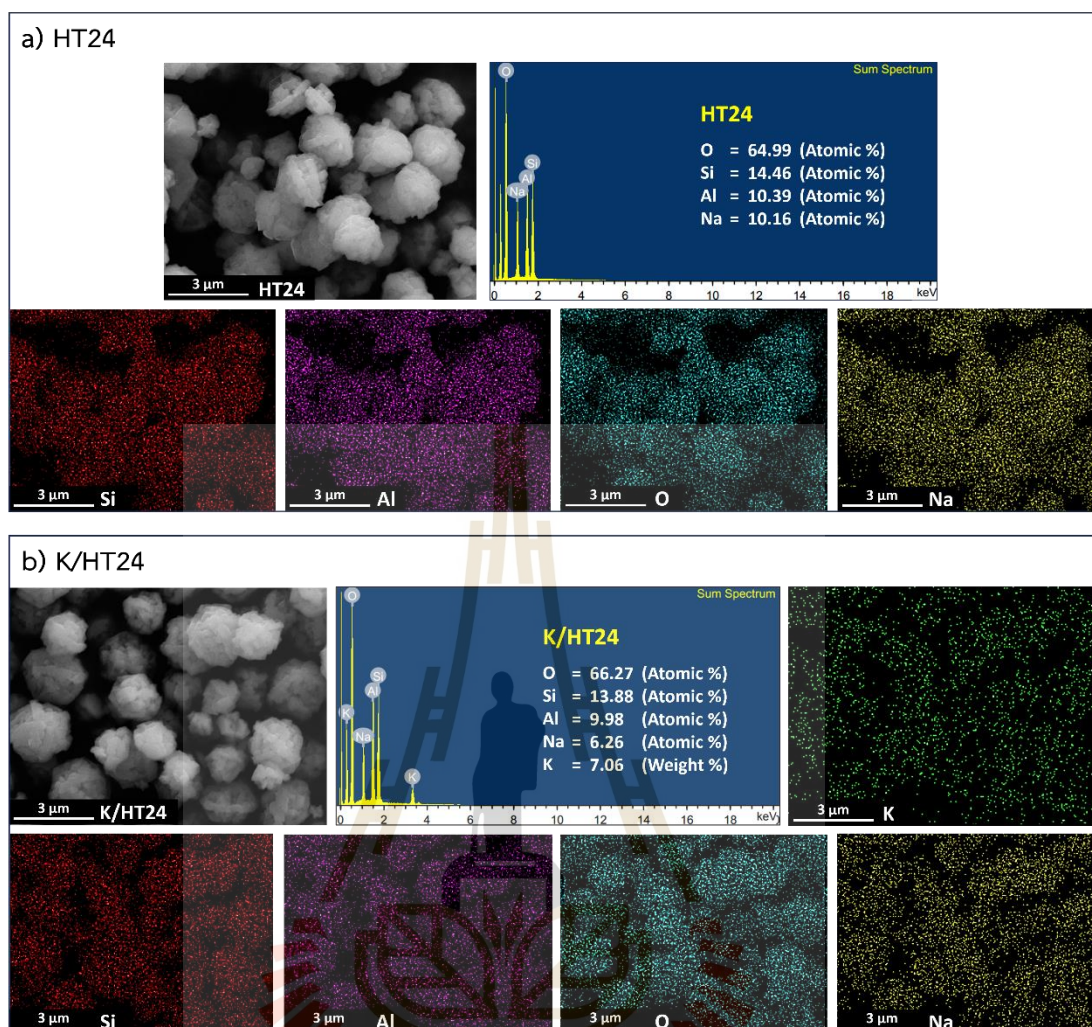


Figure 3.11 EDS elements mapping images of a) HT24 and b) K/HT24.

The elemental compositions of supports and catalysts characterized by EDS are compared in Table 3.2. For the support materials, it indicates a decrease in the Si/Al ratio when increased hydrothermal treatment time. This trend correlates with an increase in Na content as the hydrothermal time is extended. This increase is expected because Na serves as the counter ion for the substitution of Si atoms by Al, which is a crucial process in the formation of zeolite NaX. These experimental results are consistent with XRD results and confirm that the complete zeolite NaX structure begins to form at a hydrothermal time of 8 h or longer.

After loading 8 wt% potassium onto the supports, it was observed that the Na content decreased in the K/HT-8, K/HT-12, and K/HT-24 catalysts compared to their

respective supports. This phenomenon is probably due to the impregnated species tending to adsorb around the Na ions (Rybakov et al., 2015). Since EDS is a surface technique, the signal from the Na ions might be blocked, resulting in a lower observed Na content. Additionally, the measured potassium content was lower than expected, particularly in the K/HT0 and K/HT4 samples. These catalysts have a lower surface area, causing the impregnated species to agglomerate. In contrast, the K/HT8, K/HT12, and K/HT24 catalysts have a larger surface area, allowing the impregnated species to disperse more effectively.

Table 3.2 Elemental compositions of supports and catalysts characterized by EDS.

Samples	Si (Atomic%)	Al (Atomic%)	Na (Atomic%)	Si/Al	K (wt%)
HT0	16.98	10.73	8.82	1.58	-
HT4	13.11	8.49	8.88	1.54	-
HT8	14.50	10.32	10.17	1.40	-
HT12	14.78	10.59	10.20	1.39	-
HT24	14.46	10.39	10.16	1.39	-
K/HT0	15.01	10.17	8.04	1.47	5.59
K/HT4	13.94	8.97	7.49	1.55	5.65
K/HT8	13.68	9.60	6.24	1.42	6.58
K/HT12	14.27	10.09	6.05	1.40	6.86
K/HT24	13.88	9.98	6.26	1.39	7.06

The FTIR spectra of the supports, as-prepared (not calcined), and calcined catalysts are presented in Figure 3.12. The IR spectra of the supports (Figure 3.12(a)) reveal two distinct patterns. The first pattern is observed in HT0 and HT4, while the second pattern is shared by the IR spectra of HT8, HT12, and HT24. This observation is consistent with the XRD results, indicating that HT0 and HT4 possess an amorphous structure, while HT8, HT12, and HT24 exhibit a well-defined zeolite NaX structure. In the first pattern, the peak at 450 cm^{-1} is assigned to the O-T-O bending(δ) vibration (T = Si or Al) of the 4-membered ring (S4R) (Phung et al., 2014). In the second pattern, this peak shifts to 475 cm^{-1} due to the incorporation of aluminum ions. The peaks at

550 cm^{-1} , T–O–T bending vibrations of double rings (D6R) and 700 cm^{-1} , symmetric stretching (ν_s) of O–T–O (Abu-Zied, 2011) in the second pattern are sharper and distinct from the first pattern, suggesting more zeolite formation. Additionally, the peak at 975 cm^{-1} of the first pattern, asymmetric stretching of Si–O–T, shifts to 950 cm^{-1} compared to second pattern due to the incorporation of aluminium ions, confirming the formation of Al–O–Si bonds. In the presence of Al^{3+} ions as the second neighbor of the Si–O, the Al^{3+} ions attract the oxygen molecule more strongly than Si. Hence, the Si–O–Al asymmetric stretching is located at a lower wavenumber than Si–O–Si stretching (Ma et al., 2021; Madani et al., 2016).

Following the impregnation of the supports with potassium acetate buffer solution at an 8 wt% of potassium loading, The IR spectra of all as-prepared samples (Figure 3.12(b)) retained the absorption peaks within the 400–1200 cm^{-1} range, indicating the presence of the supports structure. In addition, there are new absorption bands emerged at 1567, 1416, and 1345 cm^{-1} , corresponding to the C=O antisymmetric stretching (ν_{as}), C=O symmetric stretching, and CH_3 deformation modes, respectively (Zhong et al., 2018). These absorption peaks are attributed to acetate groups.

The IR spectra of the catalysts (Figure 3.12(c)) revealed the emergence of new absorption peaks at 1455 and 1385 cm^{-1} , corresponding to the asymmetric stretching of carbonate ions (CO_3^{2-}) (Nyquist et al., 1997). This observation suggests the formation of carbonates as a result of the calcination process applied to the as-prepared catalysts. The absorption peaks previously observed at 1567, 1416, and 1345 cm^{-1} are no longer present due to their decomposition (Strydom et al., 2015). Furthermore, the IR spectra in the 400–1200 cm^{-1} range exhibited continued observability, indicating the preservation of the support structure.

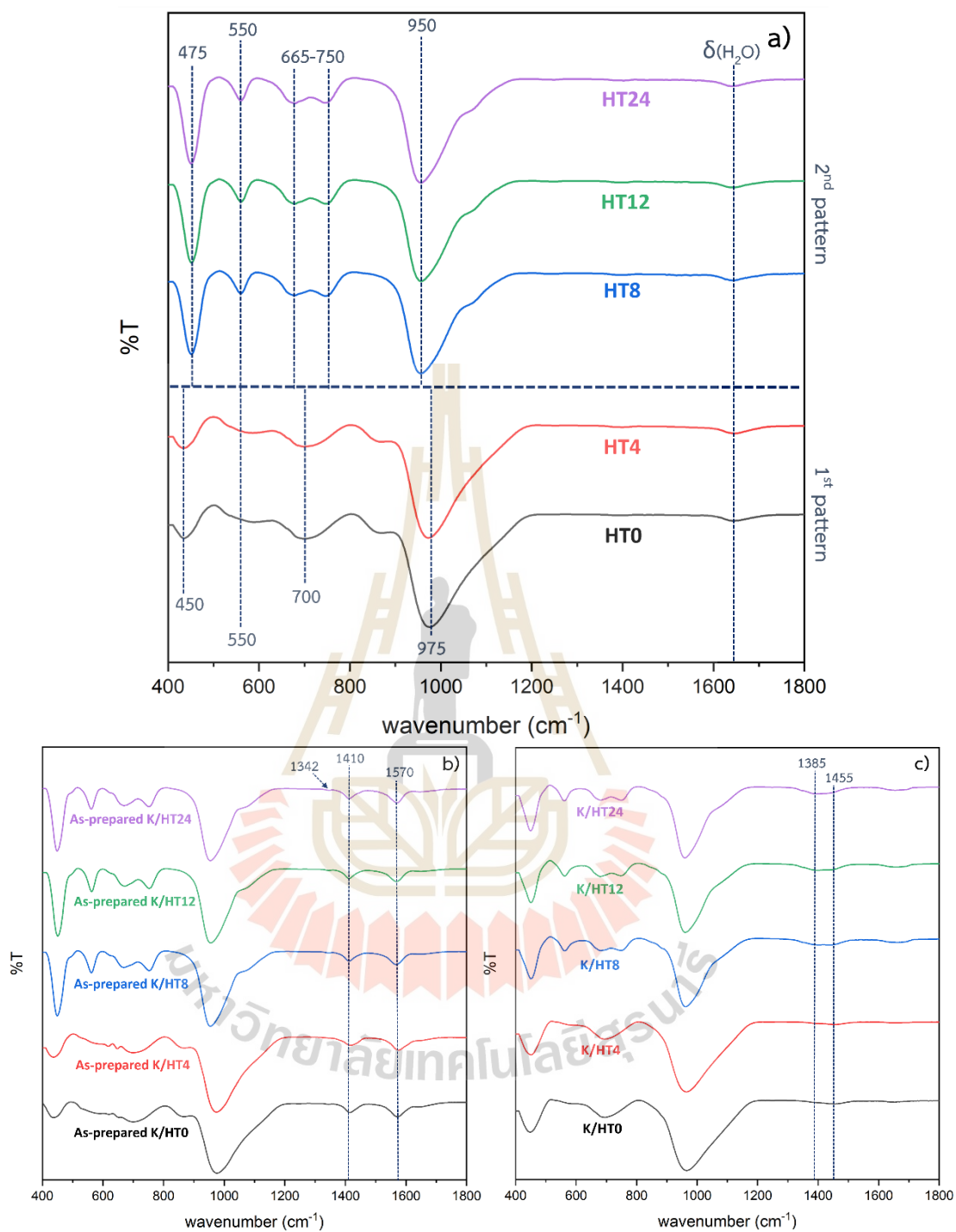


Figure 3.12 FTIR spectra of (a) supports, (b) as-prepared, and (c) calcined catalysts.

The CO₂-TPD profiles of both supports and catalysts are presented in Figure 3.13, while the calculated basicity values are tabulated in Table 3.3. Regarding the support samples (Figure 3.13(a)), HT0 and HT4 exhibit a single peak at 500 °C. In contrast, HT8, HT12, and HT24 display broad peaks around 200 °C and 400 °C. This difference can be attributed to their differing structural characteristics. In the case of the catalyst samples (Figure 3.13(b)), K/HT0 demonstrates a broad peak around 500 °C, whereas K/HT4 exhibits a broad peak around 700 °C. The desorbed amounts from both K/HT0 and K/HT4 catalysts were relatively low, suggesting limited accessibility to the basic sites (Montalbo et al., 2013) and a higher desorption temperature, implying a stronger basicity. For K/HT8, K/HT12, and K/HT24, the CO₂-TPD profiles share a common feature of a high peak at 750 °C. The larger peak area indicates the presence of a higher amount of basic site.

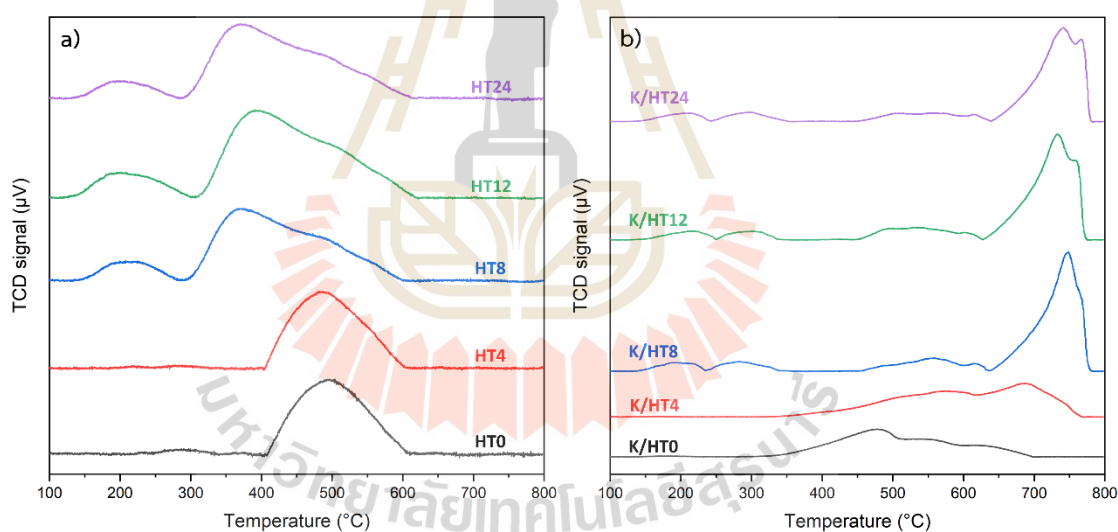


Figure 3.13 CO₂-TPD profiles of a) supports and b) catalysts.

Table 3.3 Basicity of calcined catalysts.

Catalysts	Basicity (mmol·g ⁻¹)
K/HT0	0.346
K/HT4	0.449
K/HT8	1.049
K/HT12	1.034
K/HT24	1.090

3.4.2 Catalysts performance on transesterification of palm oil

The GC chromatograms and the results of biodiesel yield from potassium supported on zeolite NaX with varying degrees of crystallinity are presented in Figure 3.14(a-f). Yields exceeding 75% are achieved when the support material forms a well-defined zeolite NaX structure or when the hydrothermal time exceeds 8 h. Interestingly, K/HT0 and K/HT4, which have similar surface areas, slightly different relative percentage crystallinity, and similar functional groups, exhibit significantly different yields. This correlates with the CO₂-TPD results, indicating that K/HT4 possesses stronger and more abundant basic sites compared to K/HT0.

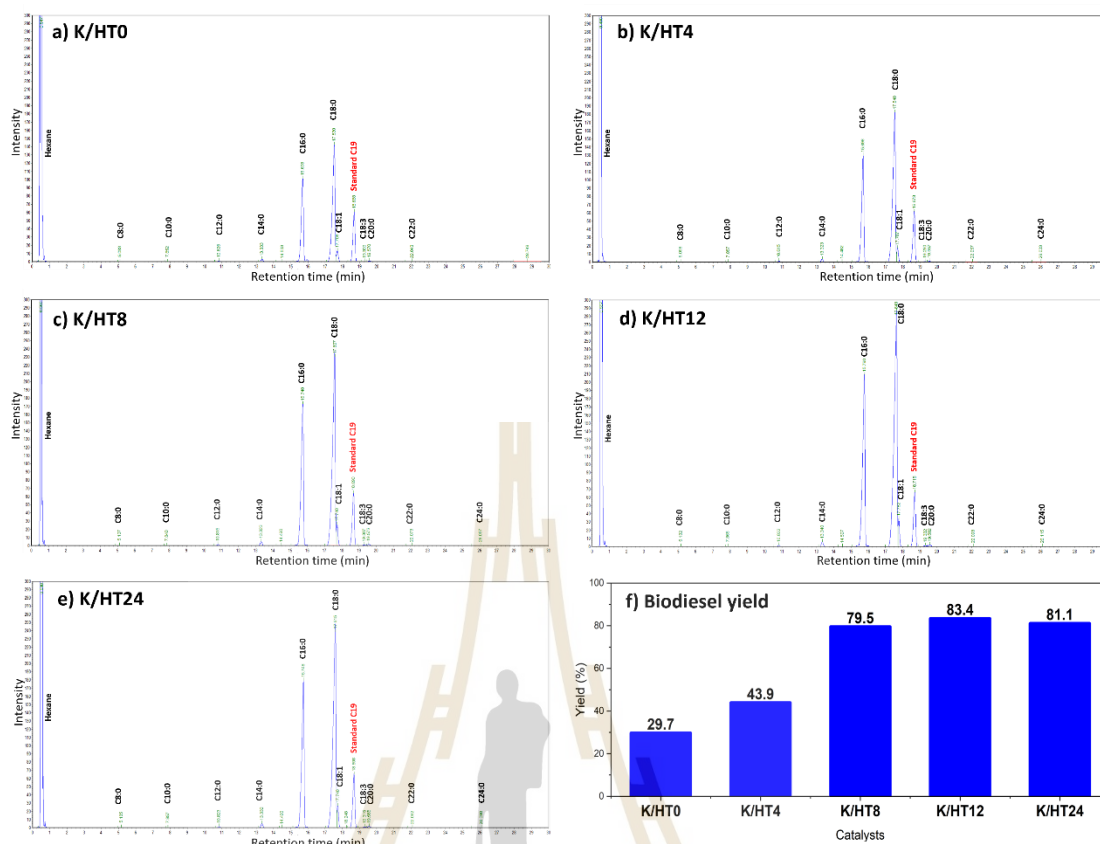


Figure 3.14 GC chromatograms of biodiesel products from the conversion of palm oil obtained from a) K/HT0, b) K/HT4, c) K/HT8, d) K/HT12, e) K/HT24, and f) biodiesel yield at 60 °C for 3 h.

3.4.3 Catalysts stability

The catalysts K/HT8, K/HT12, and K/HT24 demonstrated effective catalytic activity in the transesterification reaction of palm oil with methanol. Therefore, these catalysts were further evaluated for their reusability. However, experimental results indicated that they could not efficiently catalyze subsequent reactions, yielding biodiesel less than 5% (Figure 3.15(a)). Characterization of the spent catalysts using XRD, FTIR, and CO₂-TPD were conducted.

The XRD results for both fresh and spent catalysts are illustrated in Figure 3.15(b), indicate that their patterns are similar, confirming the stability of the zeolite under reaction conditions. However, a notable difference in peak intensities was observed, with fresh catalysts exhibiting lower intensities compared to their spent

counterparts. This observation suggests that potassium carbonate on the surface of zeolite NaX was leached out by methanol (Malins, 2018; Zhang et al., 2022).

The FTIR spectra of the spent catalysts compared with those of the fresh catalysts are shown in Figure 3.15(c). It demonstrates persistence in the IR spectra within the 400-1200 cm^{-1} range, suggesting similarity and indicating the structural integrity of the supports. However, carbonate peaks exhibited reduced intensities indicating changes after the catalytic test. These observations are in agreement with the findings from XRD analysis of spent catalysts.

The comparison of CO_2 -TPD profiles for fresh and spent catalysts is presented in Figure 3.15(d). The peak at 750 $^\circ\text{C}$, indicative of a strong base and a primary peak for these catalysts, showed a reduced peak area. This observation suggests that potassium carbonate on the surface of the supports leached out after the reaction. The remaining peaks likely originated from potassium carbonate impregnated within the pores of zeolite NaX. The inability of the spent catalysts to effectively catalyze the reaction may be attributed to the small pore size of zeolite NaX, which restricts access of reactants to the catalyst's active phase. Furthermore, the CO_2 -TPD profile of the spent catalysts revealed new broad peaks between 350-550 $^\circ\text{C}$, possibly due to the decomposition of potassium carbonate into another species with lesser basicity, which does not significantly affect the transesterification reaction of palm oil.

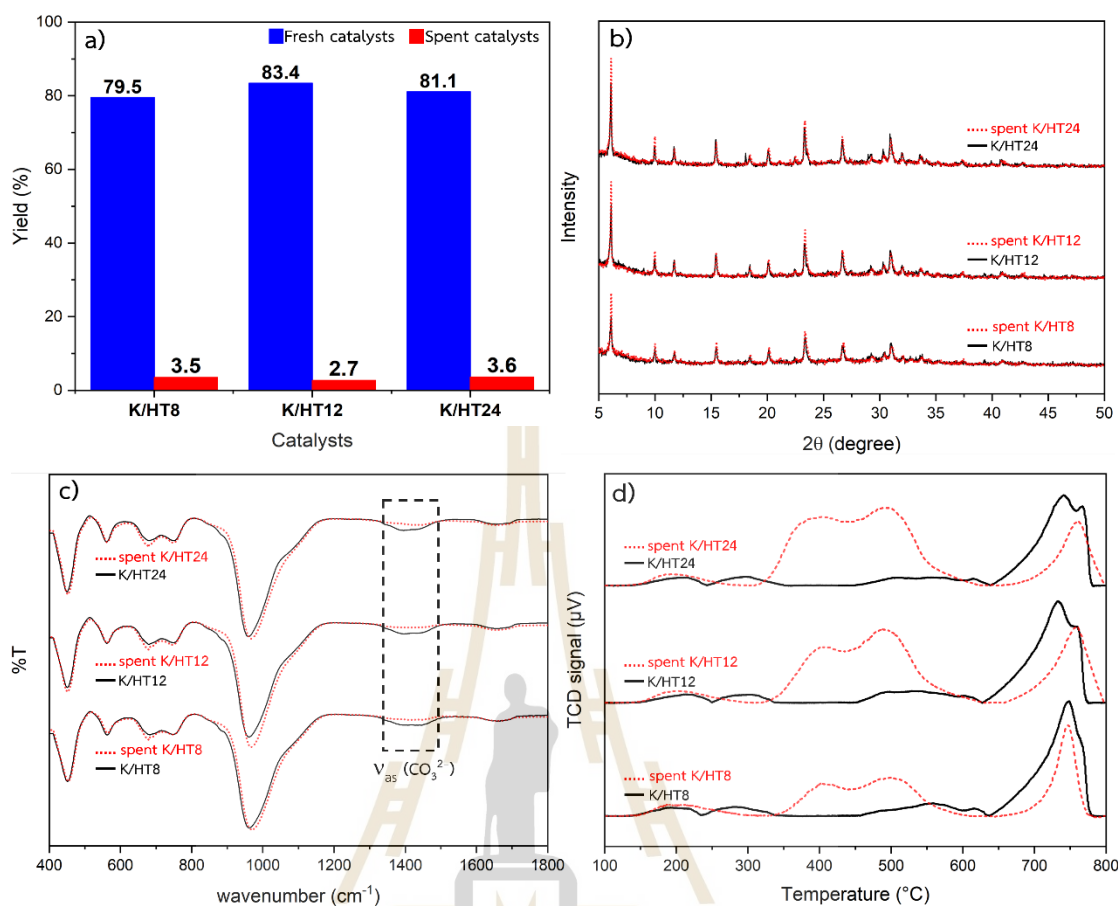


Figure 3.15 Comparison between fresh and spent catalysts by a) biodiesel yield, b) XRD, c) FTIR, and d) CO₂-TPD.

3.5 Conclusions

Zeolite NaX samples with varying degrees of crystallinity were prepared through the modification of hydrothermal treatment times, ranging from 0, 4, 8, 12, to 24 h. These samples exhibited distinct properties including crystallinity, surface area, morphology, elemental composition, and functional groups. HT0 and HT4 demonstrated similar characteristics, although the onset of crystallization in the zeolite occurred after 4 h of hydrothermal treatment. Complete zeolite crystallization was achieved with hydrothermal treatment times of 8 h or longer, resulting in similar characteristics for the HT8, HT12 and HT24.

Subsequently, these support samples were impregnated with potassium acetate buffer through ultrasound-assisted impregnation to compare their catalytic

efficiency in the transesterification reaction of palm oil. The calcination process transformed the potassium precursor into potassium carbonate. It was observed that catalysts using supports treated for 0 and 4 h, despite having similar surface areas and functional groups, produced significantly different biodiesel yields. This finding correlated with the results of XRD and CO₂-TPD analyses, which revealed that the K/HT4 possessed higher crystallinity, stronger base strength, and a greater quantity of basic sites compared to the K/HT0. Hence, it is evident that biodiesel yield increases with higher crystallinity or longer hydrothermal treatment of the zeolite NaX support.

For the catalysts K/HT8, K/HT12, and K/HT24, these catalysts exhibited similar properties in terms of crystallinity, morphology, functional groups, and basicity. They effectively facilitated the transesterification reaction, with each catalyst achieving biodiesel yields of $\approx 80\%$. However, the spent catalysts could not be effectively reused for the reactions. This inefficiency is attributed to the leaching of potassium carbonate from the support surfaces by methanol.

3.6 References

- Abu-Zied, B. M. (2011). Cu²⁺-acetate exchanged X zeolites: Preparation, characterization and N₂O decomposition activity. *Microporous and Mesoporous Materials*, 139(1), 59-66.
- Demirbas, A. (2007). Importance of biodiesel as transportation fuel. *Energy Policy*, 35(9), 4661-4670.
- Hindryawati, N., Maniam, G. P., Karim, M. R., and Chong, K. F. (2014). Transesterification of used cooking oil over alkali metal (Li, Na, K) supported rice husk silica as potential solid base catalyst. *Engineering Science and Technology, an International Journal*, 17(2), 95-103.
- Kosawatthanakun, S., Pansakdanon, C., Sosa, N., Chanlek, N., Roessner, F., Prayoonpokarach, S., and Wittayakun, J. (2022). Comparative properties of K/NaX and K/NaY from ultrasound-assisted impregnation and performance in transesterification of palm oil. *ACS Omega*, 7(11), 9130-9141.

- Liu, Z., Shi, C., Wu, D., He, S., and Ren, B. (2016). A simple method of preparation of high silica zeolite Y and its performance in the catalytic cracking of cumene. *Journal of Nanotechnology*, 2016, 1486107.
- Lechert, H., and Staelin, P. (2016). Linde Type X. In S. Mintova (Ed.), *Verified syntheses of zeolitic materials* (third ed., pp. 220-222): The synthesis commission of the international zeolite association.
- Ma, Y-K., Rigolet, S., Michelin, L., Paillaud, J.-L., Mintova, S., Khoerunnisa, F., and Ng, E-P. (2021). Facile and fast determination of Si/Al ratio of zeolites using FTIR spectroscopy technique. *Microporous and Mesoporous Materials*, 311, 110683.
- Madani, A., Nakhaei, M., Karami, P., Rajabzadeh, G., Salehi, S., and Bagheri, H. (2016). Sol-gel dip coating of yttria-stabilized tetragonal zirconia dental ceramic by aluminosilicate nanocomposite as a novel technique to improve the bonding of veneering porcelain. *International Journal of Nanomedicine*, 11, 3215-3223.
- Malins, K. (2018). The potential of K_3PO_4 , K_2CO_3 , Na_3PO_4 and Na_2CO_3 as reusable alkaline catalysts for practical application in biodiesel production. *Fuel Processing Technology*, 179, 302-312.
- Manadee, S., Sophiphun, O., Osakoo, N., Supamathanon, N., Kidkhunthod, P., Chanlek, N., Wittayakun, J., and Prayoonpokarach, S. (2017). Identification of potassium phase in catalysts supported on zeolite NaX and performance in transesterification of Jatropha seed oil. *Fuel Processing Technology*, 156, 62-67.
- Mathew, G. M., Raina, D., Narisetty, V., Kumar, V., Saran, S., Pugazhendi, A., Sindhu, R., Pandey, A., and Binod, P. (2021). Recent advances in biodiesel production: Challenges and solutions. *Science of The Total Environment*, 794, 148751.
- Meher, L. C., Vidya Sagar, D., and Naik, S. N. (2006). Technical aspects of biodiesel production by transesterification: a review. *Renewable and Sustainable Energy Reviews*, 10(3), 248-268.
- Montalbo, K., de Leon, R., Sophiphun, O., Manadee, S., Prayoonpokarach, S., and Wittayakun, J. (2013). Characterization and catalytic performance of potassium loaded on rice husk silica and zeolite NaY for transesterification of jatropha seed oil. *Química Nova*, 36, 1116-1120.

- Mukhtar, A., Saqib, S., Lin, H., Hassan Shah, M. U., Ullah, S., Younas, M., Rezakazemi, M., Ibrahim, M., Mahmood, A., Asif, S., and Bokhari, A. (2022). Current status and challenges in the heterogeneous catalysis for biodiesel production. *Renewable and Sustainable Energy Reviews*, 157, 112012.
- Muniyappa, P. R., Brammer, S. C., and Nouredini, H. (1996). Improved conversion of plant oils and animal fats into biodiesel and co-product. *Bioresource Technology*, 56(1), 19-24.
- Noiroj, K., Intarapong, P., Luengnaruemitchai, A., and Jai-In, S. (2009). A comparative study of KOH/Al₂O₃ and KOH/NaY catalysts for biodiesel production via transesterification from palm oil. *Renewable Energy*, 34(4), 1145-1150.
- Nyquist, R. A., and Kagel, R. O. (2012). Handbook of infrared and raman spectra of inorganic compounds and organic salts: Infrared spectra of inorganic compounds (Vol. 4), Academic press.
- Okwundu, O. S., El-Shazly, A. H., and Elkady, M. (2019). Comparative effect of reaction time on biodiesel production from low free fatty acid beef tallow: A definition of product yield. *SN Applied Sciences*, 1(2), 140.
- Peña, R., Romero, R., Martínez, S. L., Natividad, R., and Ramírez, A. (2013). Characterization of KNO₃/NaX catalyst for sunflower oil transesterification. *Fuel*, 110, 63-69.
- Perego, C., Bosetti, A., Ricci, M., and Millini, R. (2017). Zeolite materials for biomass conversion to biofuel. *Energy and Fuels*, 31(8), 7721-7733.
- Phung, T. K., Carnasciali, M. M., Finocchio, E., and Busca, G. (2014). Catalytic conversion of ethyl acetate over faujasite zeolites. *Applied Catalysis A: General*, 470, 72-80.
- Rakmae, S., Keawkumay, C., Osakoo, N., Montalbo, K. D., de Leon, R. L., Kidkhunthod, P., Chanlek, N., Roessner, F., Prayoonpokarach, S., and Wittayakun, J. (2016). Realization of active species in potassium catalysts on zeolite NaY prepared by ultrasound-assisted impregnation with acetate buffer and improved performance in transesterification of palm oil. *Fuel*, 184, 512-517.
- Refaat, A. A. (2011). Biodiesel production using solid metal oxide catalysts. *International Journal of Environmental Science and Technology*, 8(1), 203-221.

- Romero, M. D., Ovejero, G., Rodríguez, A., and Gómez, J. M. (2005). Enhancement of the basic properties in FAU zeolites by impregnation with cesium hydroxide. *Microporous and Mesoporous Materials*, 81(1), 313-320.
- Roschat, W., Siritanon, T., Yoosuk, B., and Promarak, V. (2016). Biodiesel production from palm oil using hydrated lime-derived CaO as a low-cost basic heterogeneous catalyst. *Energy Conversion and Management*, 108, 459-467.
- Rybakov, A. A., Bryukhanov, I. A., Larin, A. V., and Zhidomirov, G. M. (2015). Carbonates in zeolites: Formation, properties, reactivity. *International Journal of Quantum Chemistry*, 115(24), 1709-1717.
- Sánchez, M., Navas, M., Ruggera, J. F., Casella, M. L., Aracil, J., and Martínez, M. (2014). Biodiesel production optimization using gamma-Al₂O₃ based catalysts. *Energy*, 73, 661-669.
- Sharma, Y. C., Singh, B., and Korstad, J. (2011). Latest developments on application of heterogenous basic catalysts for an efficient and eco-friendly synthesis of biodiesel: A review. *Fuel*, 90(4), 1309-1324.
- Strydom, C. A., Collins, A. C., and Bunt, J. R. (2015). The influence of various potassium compound additions on the plasticity of a high-swelling South African coal under pyrolyzing conditions. *Journal of Analytical and Applied Pyrolysis*, 112, 221-229.
- Supamathanon, N., Wittayakun, J., and Prayoonpokarach, S. (2011). Properties of Jatropha seed oil from Northeastern Thailand and its transesterification catalyzed by potassium supported on NaY zeolite. *Journal of Industrial and Engineering Chemistry*. 17(2), 182-185.
- Thommes, M., Kaneko, K., Neimark, A. V., Olivier, J. P., Rodriguez-Reinoso, F., Rouquerol, J., and Sing, K. S. W. (2015). Physisorption of gases, with special reference to the evaluation of surface area and pore size distribution (IUPAC Technical Report). *Pure and Applied Chemistry*, 87(9-10), 1051-1069.
- Verboekend, D., Nuttens, N., Locus, R., Van Aelst, J., Verolme, P., Groen, J. C., Perez-Ramirez, J., and Sels, B. F. (2016). Synthesis, characterisation, and catalytic evaluation of hierarchical faujasite zeolites: Milestones, challenges, and future directions. *Chemical Society Reviews*. 45(12), 3331-3352.

- Xie, W., Peng, H., and Chen, L. (2006). Transesterification of soybean oil catalyzed by potassium loaded on alumina as a solid-base catalyst. *Applied Catalysis A: General*, 300(1), 67-74.
- Zhang, T., Li, B., Li, H., Liu, Y., Li, J., Zhao, B., and Wang, J. (2022). The efficient and green synthesis of biodiesel from crude oil without degumming catalyzed by sodium carbonate supported MoS_2 . *RSC Advances*, 12(38), 24456-24464.
- Zhang, X., Tang, D., Zhang, M., and Yang, R. (2013). Synthesis of NaX zeolite: Influence of crystallization time, temperature and batch molar ratio $\text{SiO}_2/\text{Al}_2\text{O}_3$ on the particulate properties of zeolite crystals. *Powder Technology*, 235, 322-328.
- Zhong, X.-H., Liu, Y., Xu, T., and Liu, W.-Y. (2018). Influencing factors of intercalation of potassium acetate into dickite using immersion method. *Journal of Alloys and Compounds*, 742, 996-1001.



CHAPTER IV

THE CATALYTIC BEHAVIOR OF NICKEL AND COPPER MONO/BIMETALLIC CATALYSTS IN HYDROGENATION OF METHYL LEVULINATE TO GAMMA-VALEROLACTONE

4.1 Abstract

Recently various supported bimetallic catalysts have been employed as effective catalysts for gamma-valerolactone (GVL) production from levulinic acid or its esters. However, previous reports have shown synergetic roles of active metals and supports as important keys for superior catalytic performance. This work focuses on the role of bimetallic formation between nickel (Ni) and copper (Cu). The experimental results suggest that both Ni and nickel-copper alloy (NiCu) catalysts are good for hydrogenation of methyl levulinate (ML) to an intermediate species, gamma-hydroxypentanoate (HPA). However, only NiCu has a better tendency to accelerate the conversion of HPA to GVL via cyclization process. The NiCu catalyst provided a good performance even at lower temperatures as 140 °C giving 75% of GVL yield within 6 h. In contrast, Ni catalyst showed a comparative performance only at 200 °C, but it exhibited inadequate GVL yield (28%) at 160 °C and gave no catalytic activity below this temperature. Activation energy from experimental study of cyclization step over Ni is about two times larger than that of NiCu (E_a^{K2} values are 121.7 and 56.0 kJ·mol⁻¹·K⁻¹ for Ni and NiCu, respectively) provided strong evidence of superior GVL production over NiCu catalyst.

4.2 Introduction

An increase in energy demand leads to a great challenge for exploring new renewable energy sources. Currently, wind, solar, and thermoelectric sources are considered promising alternatives for sustainable energy. However, with their current energy generation capacities, fossil fuel is still the main energy source. In addition, biomass has been identified as another renewable source of energy that shows high potential for reducing fossil fuel consumption. Lignocellulosic biomass is an abundant material which can be transformed into biofuels and various chemical platforms via biorefinery technology (Alonso et al., 2012; Huber et al., 2006; Kumar et al., 2009; Li et al., 2016) in particular, building block products such as 5-hydroxymethylfurfural (Rosatella et al., 2011), levulinic acid (LA) (Fitzpatrick et al., 2006; Rackemann et al., 2011), and levulinate ester (Amarasekara et al., 2014; Mascal et al., 2010; Peng et al., 2011). These building blocks can be further converted into many value-added products, for example, dimethylfuran, 5-ethoxymethylfurfural, and gamma-valerolactone (GVL) (Climent et al., 2014). Among various products from biomass, GVL has been highly focused in the past few years because of its unique physical and chemical properties as well as its versatile applications (Geboers et al., 2014; Obregon et al., 2014; Putrakumar et al., 2015; Yan et al., 2013). GVL could be used directly as an excellent solvent due to its renewable, non-toxic, and biodegradable characters (Alonso et al., 2013; Fegyverneki et al., 2010; Horvath et al., 2008; Liguori et al., 2015). It has been used as a fuel additive in a similar manner to ethanol. In addition, GVL is considered an interesting precursor to produce bio-based polymers (Chalid et al., 2012; Lee et al., 1998). It is well-known that the production of GVL involves hydrogenation process where LA or its ester could be transformed to GVL in the presence of H₂ gas (Serrano-Ruiz et al., 2010). However, many investigations have shown that the GVL production from LA or its derivatives does not require an external H₂ source. Some catalysts for hydrogenation reactions are also active for catalyzing the decomposition of formic acid (Deng et al., 2009; Hengne et al., 2012). It was proposed that the formic acid decomposed into H₂ and CO₂, H₂ being the reducing agent.

Since the past few years, solid heterogeneous and homogenous metal catalysts have been developed for the reduction of LA, especially noble metals such as

ruthenium (Galletti et al., 2012), platinum (Yan et al., 2009), and palladium (Upare et al., 2011). Among the noble metal catalysts, ruthenium catalysts have shown high performance and selectivity with 97% yield hydrogenation of LA in dioxane as a solvent at 423 K with 5 wt% Ru/C (Manzer, 2004; Upare et al., 2011). For reducing the operation cost, the non-noble metals like copper (Cu) and nickel (Ni) have been tested in this reaction (Shimizu et al., 2014; Upare et al., 2011; Zhang et al., 2015). The high performance of Cu catalyst was achieved by copper chromium combination, where 91% yield of GVL at above 99% conversion of LA (Yan et al., 2013).

Although, LA is the most common building block for GVL production. In 2015, Ding et al. (2015) studied cellulose conversion to methyl levulinate (ML) via alcoholysis. They mentioned that when compared with LA, ML is a non-corrosive biomass derivative with a lower boiling point and viscosity. This makes ML more applicable for its separation from acidic media and more feasible for its use in further reactions. Li et al. (2017) has demonstrated ML production with promising yields from various biomass-derived components including cellulose, starch, sucrose, and monosaccharides using heterogeneous zirconia-zeolite hybrid catalysts. This could pave the way for efficient GVL production from biomass in the future. Yang et al. (2016) prepared GVL from ML using Cu-ZrO₂ as catalysts at various temperatures. They found that the highest GVL selectivity obtained from ML precursor was around 75% at 120 °C after 12 h of reaction time. Another work by Sato et al. (2017) also indicated that the conventional hydrogenation of ML at 250 °C for 5 h gave about 82% of GVL selectivity over Ni/Al₂O₃ catalysts. Cai et al. (2017) studied the catalytic transfer hydrogenation of ethyl levulinate (EL) to GVL with 2-butanol and using 10Cu-5Ni/Al₂O₃ as a catalyst, providing a 97% yield of GVL in 12 h at 150 °C. The common aspect of this work and Cai et al. is that the Ni and Cu catalysts were employed for GVL production from levulinate esters. The good synergy between Ni and Cu provided bimetallic catalysts with high catalytic activity and stability. However, Cai et al. have only studied the metal-supported catalysts and pure support materials, not the performance of the pure nickel or copper catalyst. Therefore, it is worth to expand the promising catalytic transfer hydrogenation (CTH) in such system.

According to the promising CTH reported in previous works for valuable biochemical production from biomass (Li et al., 2016; Yang et al., 2016; Cai et al., 2017), the focus of this work is to study the role of Ni and Cu in terms of catalytic activity and selectivity during CTH process of ML to GVL. The sole nickel-copper alloy (NiCu) catalyst without any supporting materials was prepared, characterized, and tested using 2-propanol as a hydrogen donor.

4.3 Experimental

4.3.1 Chemicals

Chemicals used for Ni metal, Cu metal, and NiCu alloy synthesis included Nickel(II) nitrate hexahydrate ($\text{Ni}(\text{NO}_3)_2 \cdot 6\text{H}_2\text{O}$, $\geq 98\%$, Ajax Finchem Pty), Copper(II) nitrate trihydrate ($\text{Cu}(\text{NO}_3)_2 \cdot 3\text{H}_2\text{O}$, $\geq 98\%$, Ajax Finchem Pty). The chemical for catalytic transfer hydrogenation was ML ($\text{CH}_3\text{COCH}_2\text{CH}_2\text{COOCH}_3$, $\geq 98\%$, Sigma-Aldrich). The chemical used as H-donor for the reaction was Isopropyl alcohol ($(\text{CH}_3)_2\text{CHOH}$, $\geq 99.8\%$, Fisher Scientific UK). The chemical used as solvent for testing with Gas chromatography with flame ionization detector (GC-FID) was ethyl alcohol ($\text{CH}_3\text{CH}_2\text{OH}$, $\geq 99.8\%$, Carlo Erba).

4.3.2 Preparation of Ni metal, Cu metal and NiCu alloy catalysts

Ni metal catalyst was prepared by dissolving 12.21 g $\text{Ni}(\text{NO}_3)_2 \cdot 6\text{H}_2\text{O}$ in 10.0 mL of Deionized (DI) water and stirred until a clear solution was obtained. For Cu metal catalyst, 10.15 g of $\text{Cu}(\text{NO}_3)_2 \cdot 3\text{H}_2\text{O}$ was dissolved in 10 mL of DI water. For the preparation of NiCu alloy catalyst, a 1:1 molar ratio solution was prepared by dissolving 6.11 g of $\text{Ni}(\text{NO}_3)_2 \cdot 6\text{H}_2\text{O}$ and 5.07 g of $\text{Cu}(\text{NO}_3)_2 \cdot 3\text{H}_2\text{O}$ in 10 mL of DI water. Each sample was transferred to a crucible and dried at 200 °C with a heating rate of 10 °C·min⁻¹ for 2 h, followed by calcination at 800 °C for 5 h at the same heating rate.

After calcination, the catalysts were reduced at 500 °C (heating rate of 3 °C·min⁻¹) for 3 h in a quartz tube reactor within a mixed H₂ and N₂ atmosphere (50:50 %vol) at a total flow rate of 40 mL·min⁻¹ prior to the catalytic test.

4.3.3 Catalysts characterization

The crystal structure of catalysts was analyzed by X-ray diffraction (XRD, D8 ADVANCE, Bruker, Ltd., Germany) equipped with monochromatic light source $\text{CuK}\alpha$ radiation operating at 40kV and 40 mA, measuring from $2\theta = 10 - 80^\circ$ with step intervals of 0.02° and time intervals of 0.5 s.

The optimal reduction temperature for the catalysts was obtained from temperature-programmed reduction of H_2 (H_2 -TPR) analysis (PULSAR, Quantachrome, USA). Each sample was pretreated in a He flow of $30 \text{ mL}\cdot\text{min}^{-1}$ at 120°C with the ramping rate of $10^\circ\text{C}\cdot\text{min}^{-1}$ for 60 min and then cooled to 40°C . The gas feed was then switched to 5% H_2 in Ar with a flow rate of $30 \text{ mL}\cdot\text{min}^{-1}$ and held at 40°C for 30 min, before increasing the temperature at a rate of $10^\circ\text{C}\cdot\text{min}^{-1}$ to 850°C .

The surface morphology of the catalysts was observed by scanning electron microscope (S3400N, Hitachi, Japan) and the catalyst surface compositions were analyzed by energy dispersive spectrometer (SEM-EDS).

The bulk elemental composition of the alloy catalyst was determined by X-ray fluorescence (XRF) (Micro-XRF, Orbis, USA) analysis.

4.3.4 Catalysts testing: Hydrogenation of ML

The reaction was carried out in a 70 mL Teflon lined stainless steel autoclave comprised of 0.58 mL of ML in 24 mL 2-propanol and 1.0 g of catalyst. The reaction mixture was heated up to desired temperature range varying from $120 - 200^\circ\text{C}$ and held under continuous stirring for a certain period. After cooling, the mixture was filtered and diluted with ethanol with a dilution factor of 10, which was then analyzed by GC-FID (DBWAX column with length $30.0 \text{ m} \times \text{ID } 0.25 \text{ mm}$). The initial column temperature was held at 50°C for 3 min then ramped up to 210°C at the rate of $40^\circ\text{C}\cdot\text{min}^{-1}$ for 5.5 min. The ML conversion and GVL yields were calculated by Equations (4.1) and (4.2), respectively:

$$\text{ML conversion (\%)} = \left(\frac{\text{mole of initial ML} - \text{mole of final ML}}{\text{mole of initial ML}} \right) 100 \quad (4.1)$$

$$\text{GVL yield (\%)} = \left(\frac{\text{mole of obtained GVL}}{\text{mole of initial ML}} \right) 100 \quad (4.2)$$

4.4 Results and discussion

4.4.1 Catalysts characterization

Figure 4.1 presents the XRD patterns of the as-prepared catalysts and catalysts. Figure 4.1(a) illustrates the patterns of the as-prepared catalysts. For CuO, the peaks are observed at 2θ values of 32.5, 35.5, 38.7, 48.8, 53.4, 58.3, 61.6, 66.3, 68.0, 72.3, and 74.9°. For NiO, characteristic peaks are evident at 37.14, 43.18, 62.72, 75.38, and 79.3°. The XRD pattern of the NiCuO demonstrates a combination of peaks corresponding to both CuO and NiO. This finding aligns with the research from literature (Wang et al., 2015), which identified NiCuO as a mixed phase of CuO and NiO.

The XRD analysis of Cu, Ni, and NiCu alloy, as shown in Figure 4.1(b), have very similar pattern indicating the FCC structure. The Cu metal showed three diffraction peaks at 43.2, 50.4, and 74.0°. The Ni metal show diffraction peaks at 44.5, 51.8, and 76.4°. The NiCu alloy also showed three diffraction peaks at 44.1, 51.3, and 75.5°. It could be observed clearly that all values of NiCu peaks were in between the peak positions of Cu and Ni, indicating the formation of alloy structure.

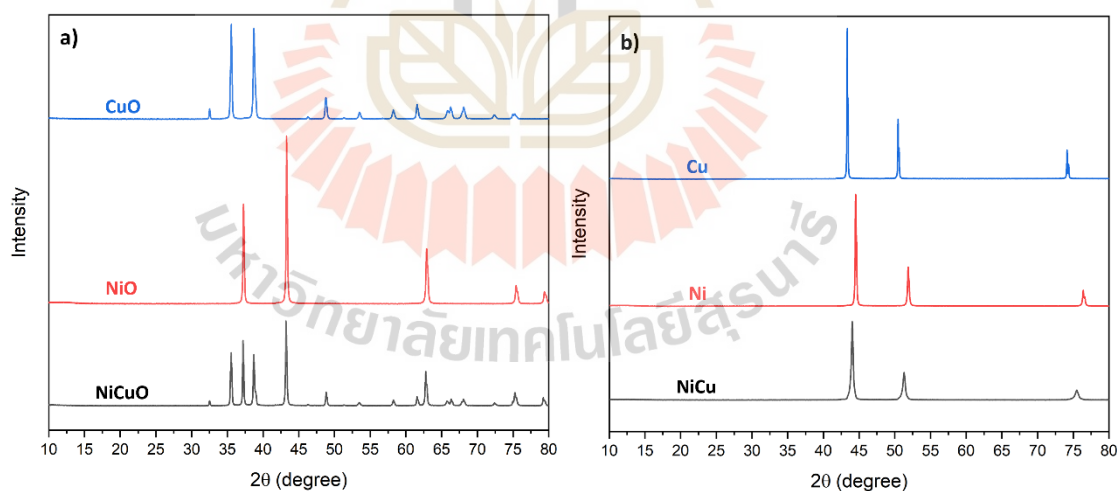


Figure 4.1 XRD of the a) as-prepared catalysts and b) catalysts.

Figure 4.2 shows TPR of the as-prepared catalysts. The reduction of CuO (Figure 4.2(a)) and NiCuO (Figure 4.2(c)) was completed at 400 °C, and NiO (Figure 4.2(b)) at 500 °C, hence the catalyst reduction temperature of 500 °C employed as shown in the methodology section.

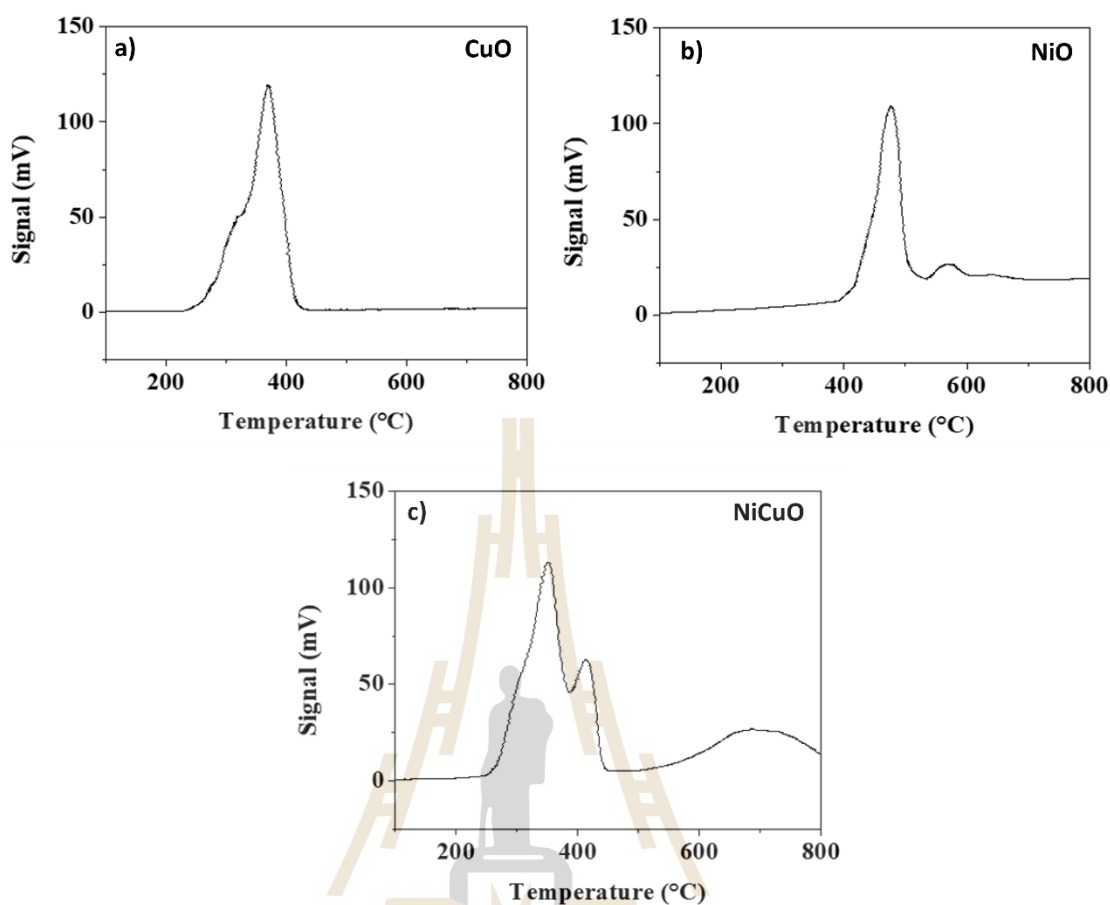


Figure 4.2 H₂-TPR profile of (a) CuO (b) NiO and (c) NiCuO samples.

SEM analysis of the catalysts (Figure 4.3(a-c)) showed that Ni and NiCu were highly dispersed compared to the agglomerated Cu catalyst. Furthermore, the NiCu alloy particles were smaller compared to the Ni metal. EDS element mapping (Table 4.1 and Figure 4.3(d)) of the NiCu alloy showed that Ni tended to disperse on the surface of the catalyst, with 60% of Ni on the surface. XRF result (Table 4.1) revealed that the bulk element of NiCu catalyst is nearly 50% of Ni and Cu, thus confirming that Ni has a slight tendency to accumulate near the surface of the alloy.

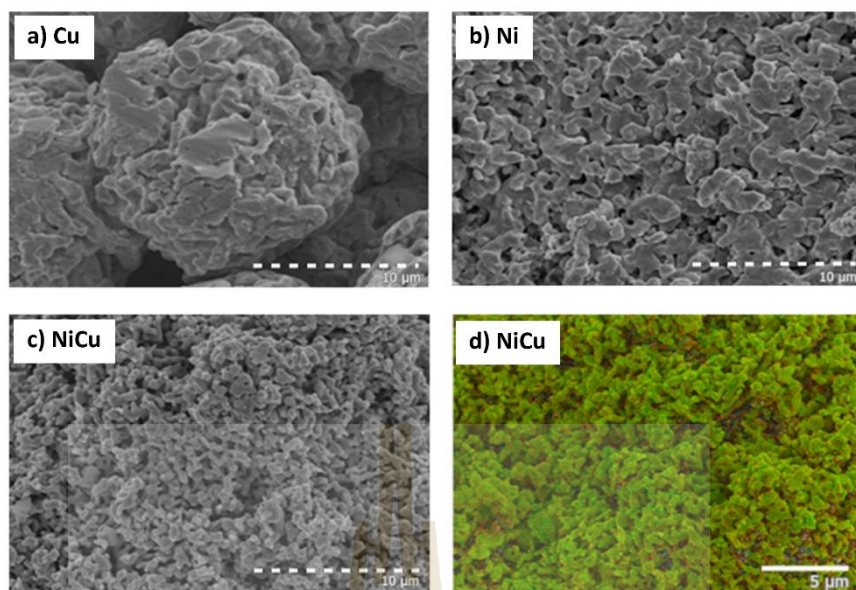


Figure 4.3 SEM images of catalysts (a) Cu metal (b) Ni metal and (c) NiCu alloy catalyst and the EDS element mapping of (d) NiCu alloy (green indicates Ni and Cu is represented by orange).

Table 4.1 Elemental compositions of NiCu catalyst characterized by EDS and XRF.

Catalyst	EDS		XRF	
	Cu (%)	Ni (%)	Cu (%)	Ni (%)
NiCu	40.0	60.0	50.7	49.3

4.4.2 Catalytic behaviors of metal and alloy catalysts

ML conversion to GVL was conducted using Cu, Ni, and NiCu catalysts at 200 °C for 4 h. As displayed in Figure 4.4, Cu had no catalytic performance in ML conversion, similar to the blank test. However, Ni and NiCu showed high catalytic performance indicating promising ML conversion (80% for Ni and 100% for NiCu) and a good GVL yield of 80% for Ni and 100% for NiCu. Although both Ni and NiCu showed their potential for GVL production from ML, the NiCu seemed to exhibit a better conversion and superior GVL selectivity.

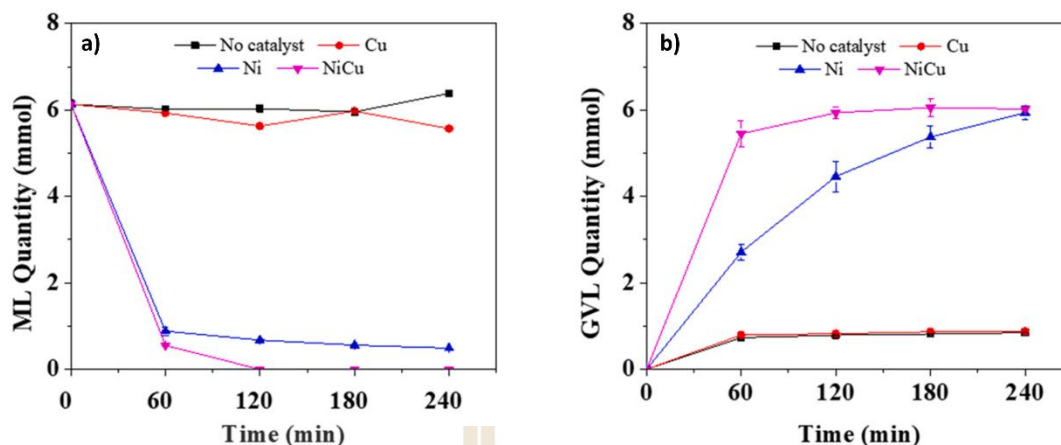


Figure 4.4 Quantity profile of (a) ML and (b) GVL at 200 °C for no catalyst, Cu metal, Ni metal, and NiCu alloy.

Figure 4.5 shows the amount of reactant (ML), intermediate (HPA), product (GVL), and byproduct (methanol, MeOH) during ML hydrogenation when Ni and NiCu catalysts were used with period of 0–180 min. The results clearly showed that the NiCu catalyst system is significantly more effective at producing GVL than the Ni catalyst. The Ni catalyst system exhibits good ML conversion and comparatively high HPA yields for all temperatures, which correlates to the lower GVL yield. Therefore, the Ni catalyst can convert ML to the intermediate but is not selective to the conversion of HPA to GVL. On the other hand, the NiCu catalyst provided roughly twice the GVL yield and half the HPA yield compared to Ni. Despite the good performance in ML conversion of both catalysts, NiCu is able to cyclize the intermediate product, which leads to the GVL formation. Ni is less effective at this process, leading to the high HPA yield, which is exacerbated at lower temperatures.

The reaction pathway is highly selective, with a preference of the formation of GVL. Hence, variation of the temperature from 160 °C to 200 °C when the NiCu catalyst was used had a small effect on the final GVL yield after 3 h (77%, 82%, and 100% at 160 °C, 180 °C and 200 °C, respectively), as shown in Figure 4.5 (a, b, and c, respectively). However, the increase of temperature could improve the reaction rate in terms of ML conversion (0.026, 0.031, 0.051 mmol·min⁻¹, respectively). As shown in Figure 4.5(c), the complete conversion of ML could be achieved within 2 h at 200 °C. Both NiCu (Figure 4.5(c)) and Ni (Figure 4.5(f)) displayed competitive performance at 200 °C, yielding 100%

and 80% GVL respectively. However, Ni catalyst (Figure 4.5(d and e)) showed much poorer performance at the lower temperatures of 160 °C (28% yield), and 180 °C (55% yield).

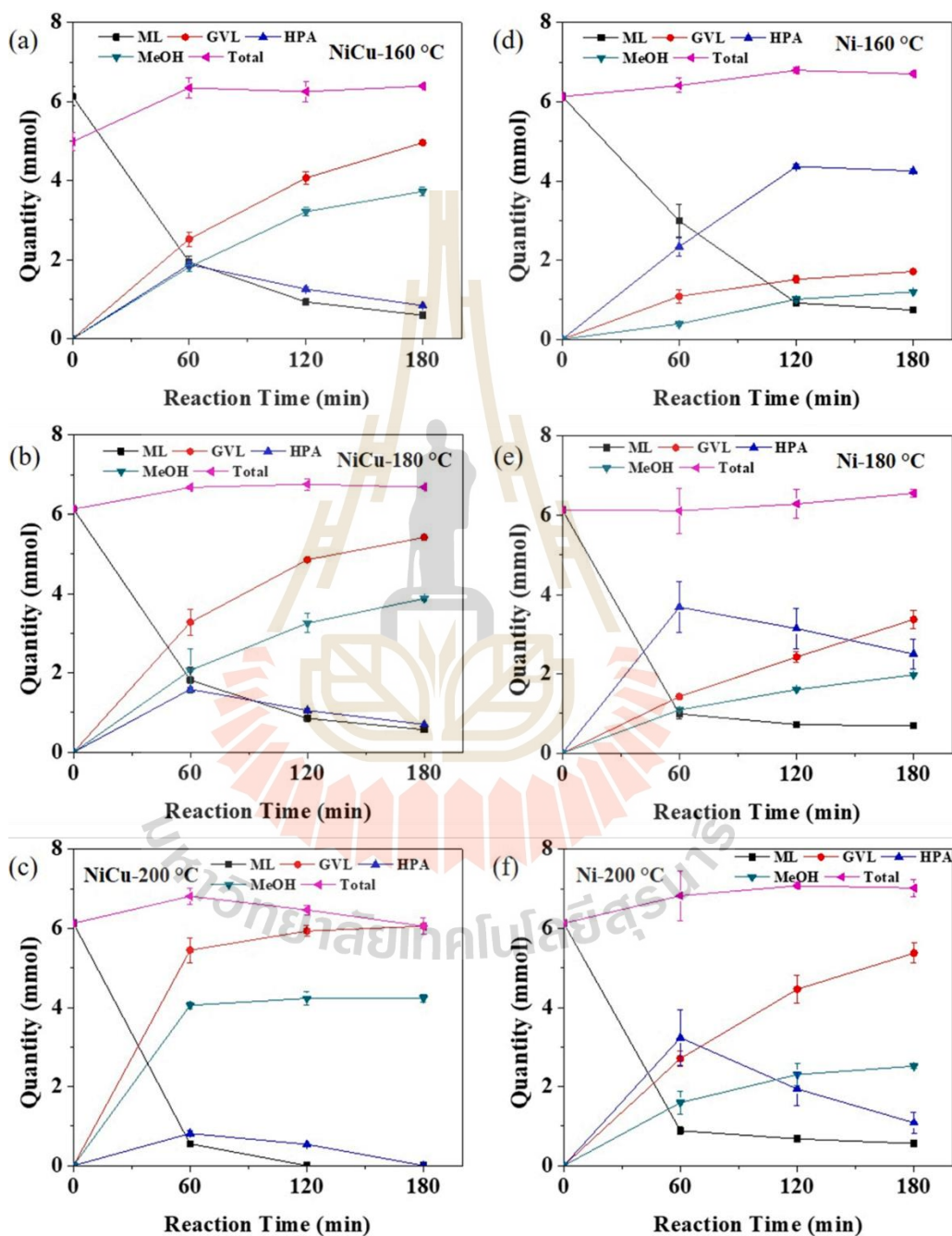


Figure 4.5 Quantity of reactant, product, and intermediate from the hydrogenation of ML in 2-propanol over time using NiCu catalyst at (a) 160 °C (b) 180 °C (c) 200 °C and Ni catalyst at (d) 160 °C (e) 180 °C and (f) 200 °C.

As NiCu catalyst showed superior performance at the lower temperature of 160 °C, it was of interest to study the reaction at even lower temperatures to determine its versatility. Thus, the experiment was conducted at the temperatures of 120 °C and 140 °C and the results are displayed in Figure 4.6. At the temperatures 140 °C and below, NiCu could still produce GVL after an initial period of 2 h. The reaction at 140 °C for 6 h produced a good GVL yield of 75%, whereas at 120 °C, a significantly lower yield of 45% was obtained. Hence, 140 °C is a viable temperature for the production of GVL from the NiCu catalyst system.

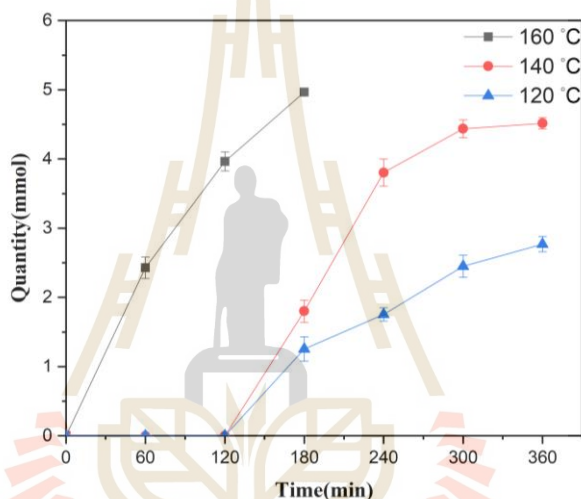


Figure 4.6 A comparison of GVL quantity produced over NiCu catalyst at temperatures of 120–160 °C.

The rate constant (k) and the activation energy (E_a) for the conversion of ML to GVL were calculated from the experimental data (Figure A1 and A2) and displayed in Table 4.2. The conversion of ML to GVL has two key reaction steps as shown in Figure 4.7, with hydrogenation of ML to the intermediate HPA (k_1), followed by the ring-closing process (cyclization) where HPA is converted into GVL (k_2). The rate constants and activation energy were calculated via the Arrhenius equation according to the research performed by (Negahdar et al., 2017). Thus, the rate constants were calculated for each reaction step at 160 °C, 180 °C, and 200 °C, and the activation energies for the catalysts were determined. It was found that the second-order calculations exhibited the best fit for the hydrogenation and cyclization processes.

The hydrogenation activation energy ($E_a^{k_1}$) for both Ni and NiCu catalysts are relatively competitive at 31.5 and 30.7 $\text{kJ}\cdot\text{mol}^{-1}\cdot\text{K}^{-1}$ respectively. Those values correspond to the similar ML conversion rate as shown in Figure 4.5, with both catalysts exhibiting good performance for ML hydrogenation.

Theoretically, the hydrogenation of ML produces an equivalent quantity of the HPA intermediate, followed by an equal molar concentration of GVL after cyclization. Calculation of $E_a^{k_2}$ from the obtained k_2 values show significantly higher activation energy for the Ni catalyst (121.7 $\text{kJ}\cdot\text{mol}^{-1}\cdot\text{K}^{-1}$) in comparison to that of the NiCu catalyst (56.0 $\text{kJ}\cdot\text{mol}^{-1}\cdot\text{K}^{-1}$). This supports the experimental data (Figure 4.5) where Ni catalyst shows higher yields of HPA at 160 °C and 180 °C in comparison to the NiCu catalyst. At 200 °C, the high thermal energy enables Ni to produce GVL from HPA cyclization at a comparable rate to NiCu. However, the lower activation energy of NiCu enables the cyclization process to occur even at the lower temperatures of 120 °C and 140 °C as shown in Figure 4.6, where GVL was not produced when the employed catalyst was Ni.

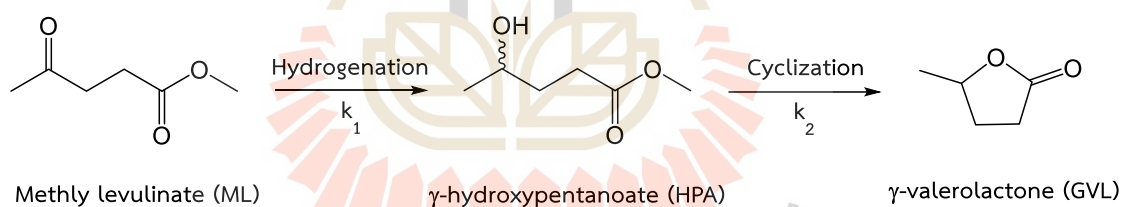


Figure 4.7 Reaction scheme for GVL formation from ML.

Table 4.2 Kinetic calculations for Ni and NiCu catalyst.

Rate constant	Catalyst	k (min^{-1})			E_a ($\text{kJ}\cdot\text{mol}^{-1}\cdot\text{K}^{-1}$)	R^2
		433 K	453 K	473 K		
k_1	Ni	0.0078	0.0153	0.0162	31.5	0.83
	NiCu	0.0097	0.0121	0.0249	30.7	0.94
k_2	Ni	0.0046	0.0173	0.0806	121.7	0.99
	NiCu	0.00549	0.1014	0.1014	56.0	0.99

4.5 Conclusion

We have shown that GVL could be produced from ML in 2-propanol as a medium via catalytic transfer hydrogenation using NiCu alloy as a catalyst compared with Ni catalysts. At high temperature of 200 °C, either Ni or NiCu achieved high ML conversion and GVL yield. Nevertheless, the NiCu catalyst provided a good performance even at lower temperatures as 140 °C giving 75% of GVL yield within 6 h. In contrast, Ni catalyst showed a comparative performance only at 200 °C, but it exhibited inadequate GVL yield (28%) at 160 °C and gave no catalytic activity below this temperature.

4.6 References

- Alonso, D. M., Wettstein, S. G., and Dumesic, J. A. (2012). Bimetallic catalysts for upgrading of biomass to fuels and chemicals. *Chemical Society Reviews*, 41(24), 8075-8098.
- Alonso, D. M., Wettstein, S. G., and Dumesic, J. A. (2013). Gamma-valerolactone a sustainable platform molecule derived from lignocellulosic biomass. *Green Chemistry*, 15(3), 584- 595.
- Amarasekara, A. S., and Wiredu, B. (2014). Acidic ionic liquid catalyzed one-pot conversion of cellulose to ethyl levulinate and levulinic acid in ethanol-water solvent system. *BioEnergy Research*, 7(4), 1237-1243.
- Cai, B., Zhou, X.-C., Miao, Y.-C., Luo, J.-Y., Pan, H., and Huang, Y.-B. (2017). Enhanced catalytic transfer hydrogenation of ethyl levulinate to gamma-valerolactone over a robust Cu–Ni bimetallic catalyst. *ACS Sustainable Chemistry and Engineering*, 5(2), 1322-1331.
- Chalid, M., Heeres, H. J., and Broekhuis, A. A. (2012). Green polymer precursors from biomass-based levulinic acid. *Procedia Chemistry*, 4, 260-267.
- Climent, M. J., Corma, A., and Iborra, S. (2014). Conversion of biomass platform molecules into fuel additives and liquid hydrocarbon fuels. *Green Chemistry*, 16(2), 516-547.

- Deng, L., Li, J., Lai, D.-M., Fu, Y., and Guo, Q.-X. (2009). Catalytic conversion of biomass-derived carbohydrates into gamma-valerolactone without using an external H₂ supply. *Angewandte Chemie International Edition*, 48(35), 6529-6532.
- Ding, D., Xi, J., Wang, J., Liu, X., Lu, G., and Wang, Y. (2015). Production of methyl levulinate from cellulose: selectivity and mechanism study. *Green Chemistry*, 17(7), 4037-4044.
- Fedorov, A. V., Kukushkin, R. G., Yeletsky, P. M., Bulavchenko, O. A., Chesalov, Y. A., and Yakovlev, V. A. (2020). Temperature-programmed reduction of model CuO, NiO and mixed CuO–NiO catalysts with hydrogen. *Journal of Alloys and Compounds*, 844, 156135.
- Fegyverneki, D., Orha, L., Láng, G., and Horváth, I. T. (2010). Gamma-valerolactone based solvents. *Tetrahedron*, 66(5), 1078-1081.
- Fitzpatrick, S. W. (2006). The biofine technology: a bio-refinery concept based on thermochemical conversion of cellulosic biomass. *Feedstocks for the Future*, 921, 271-287: American Chemical Society.
- Galletti, A. M. R., Antonetti, C., De Luise, V., and Martinelli, M. (2012). A sustainable process for the production of gamma-valerolactone by hydrogenation of biomass-derived levulinic acid. *Green Chemistry*, 14(3), 688-694.
- Geboers, J., Wang, X., de Carvalho, A. B., and Rinaldi, R. (2014). Densification of biorefinery schemes by H-transfer with Raney Ni and 2-propanol: A case study of a potential avenue for valorization of alkyl levulinates to alkyl gamma-hydroxypentanoates and gamma-valerolactone. *Journal of Molecular Catalysis A: Chemical*, 388-389, 106-115.
- Hengne, A. M., Biradar, N. S., and Rode, C. V. (2012). Surface species of supported ruthenium catalysts in selective hydrogenation of levulinic esters for bio-refinery application. *Catalysis Letters*, 142(6), 779-787.
- Horváth, I. T., Mehdi, H., Fábos, V., Boda, L., and Mika, L. T. (2008). Gamma-valerolactone: A sustainable liquid for energy and carbon-based chemicals. *Green Chemistry*, 10(2), 238-242.

- Huber, G. W., Iborra, S., and Corma, A. (2006). Synthesis of transportation fuels from biomass: chemistry, catalysts, and engineering. *Chemical Reviews*, 106(9), 4044-4098.
- Kumar, P., Barrett, D. M., Delwiche, M. J., and Stroeve, P. (2009). Methods for pretreatment of lignocellulosic biomass for efficient hydrolysis and biofuel production. *Industrial and Engineering Chemistry Research*, 48(8), 3713-3729.
- Lee, C. W., Urakawa, R., and Kimura, Y. (1998). Copolymerization of gamma-valerolactone and beta-butyrolactone. *European Polymer Journal*, 34(1), 117-122.
- Li, H., Fang, Z., Luo, J., and Yang, S. (2017). Direct conversion of biomass components to the biofuel methyl levulinate catalyzed by acid-base bifunctional zirconia-zeolites. *Applied Catalysis B: Environmental*, 200, 182-191.
- Li, H., He, J., Riisager, A., Saravanamurugan, S., Song, B., and Yang, S. (2016). Acid-base bifunctional zirconium n-alkyltriphosphate nanohybrid for hydrogen transfer of biomass-derived carboxides. *ACS Catalysis*, 6(11), 7722-7727.
- Liguori, F., Moreno-Marrodan, C., and Barbaro, P. (2015). Environmentally friendly synthesis of gamma-valerolactone by direct catalytic conversion of renewable sources. *ACS Catalysis*, 5(3), 1882-1894.
- Manzer, L. E. (2004). Catalytic synthesis of alpha-methylene-gamma-valerolactone: A biomass-derived acrylic monomer. *Applied Catalysis A: General*, 272(1), 249-256.
- Mascal, M., and Nikitin, E. B. (2010). High-yield conversion of plant biomass into the key value-added feedstocks 5-(hydroxymethyl)furfural, levulinic acid, and levulinic esters via 5-(chloromethyl)furfural. *Green Chemistry*, 12(3), 370-373.
- Negahdar, L., Al-Shaal, M. G., Holzhäuser, F. J., and Palkovits, R. (2017). Kinetic analysis of the catalytic hydrogenation of alkyl levulinates to gamma-valerolactone. *Chemical Engineering Science*, 158, 545-551.
- Obregón, I., Corro, E., Izquierdo, U., Requies, J., and Arias, P. L. (2014). Levulinic acid hydrogenolysis on Al₂O₃-based Ni-Cu bimetallic catalysts. *Chinese Journal of Catalysis*, 35(5), 656-662.

- Peng, L., Lin, L., Li, H., and Yang, Q. (2011). Conversion of carbohydrates biomass into levulinate esters using heterogeneous catalysts. *Applied Energy*, 88(12), 4590-4596.
- Putrakumar, B., Nagaraju, N., Kumar, V. P., and Chary, K. V. R. (2015). Hydrogenation of levulinic acid to gamma-valerolactone over copper catalysts supported on gamma-Al₂O₃. *Catalysis Today*, 250, 209-217.
- Rackemann, D. W., and Doherty, W. O. (2011). The conversion of lignocellulosics to levulinic acid. *Biofuels, Bioproducts and Biorefining*, 5(2), 198-214.
- Rosatella, A. A., Simeonov, S. P., Frade, R. F. M., and Afonso, C. A. M. (2011). 5-Hydroxymethylfurfural (HMF) as a building block platform: Biological properties, synthesis and synthetic applications. *Green Chemistry*, 13(4), 754-793.
- Serrano-Ruiz, J. C., Wang, D., and Dumesic, J. A. (2010). Catalytic upgrading of levulinic acid to 5-nonanone. *Green Chemistry*, 12(4), 574-577.
- Shimizu, K.-i., Kanno, S., and Kon, K. (2014). Hydrogenation of levulinic acid to gamma-valerolactone by Ni and MoO_x co-loaded carbon catalysts. *Green Chemistry*, 16(8), 3899-3903.
- Sun, D., Ohkubo, A., Asami, K., Katori, T., Yamada, Y., and Sato, S. (2017). Vapor-phase hydrogenation of levulinic acid and methyl levulinate to gamma-valerolactone over non-noble metal-based catalysts. *Molecular Catalysis*, 437, 105-113.
- Upare, P. P., Lee, J. M., Hwang, Y. K., Hwang, D. W., Lee, J. H., Halligudi, S. B., Hwang, J. S., and Chang, J. S. (2011). Direct hydrocyclization of biomass-derived levulinic acid to 2-methyltetrahydrofuran over nanocomposite copper/silica catalysts. *ChemSusChem*, 4(12), 1749-1752.
- Upare, P. P., Lee, J.-M., Hwang, D. W., Halligudi, S. B., Hwang, Y. K., and Chang, J.-S. (2011). Selective hydrogenation of levulinic acid to gamma-valerolactone over carbon-supported noble metal catalysts. *Journal of Industrial and Engineering Chemistry*, 17(2), 287-292.
- Wang, Y., Qu, F., Liu, J., Wang, Y., Zhou, J., and Ruan, S. (2015). Enhanced H₂S sensing characteristics of CuO-NiO core-shell microspheres sensors. *Sensors and Actuators B: Chemical*, 209, 515-523.

- Yan, K., and Chen, A. (2013). Efficient hydrogenation of biomass-derived furfural and levulinic acid on the facilely synthesized noble-metal-free Cu–Cr catalyst. *Energy*, *58*, 357-363.
- Yan, K., and Chen, A. (2014). Selective hydrogenation of furfural and levulinic acid to biofuels on the ecofriendly Cu–Fe catalyst. *Fuel*, *115*, 101-108.
- Yan, K., Jarvis, C., Lafleur, T., Qiao, Y., and Xie, X. (2013). Novel synthesis of Pd nanoparticles for hydrogenation of biomass-derived platform chemicals showing enhanced catalytic performance. *RSC Advances*, *3*(48), 25865-25871.
- Yan, Z.-p., Lin, L., and Liu, S. (2009). Synthesis of gamma-valerolactone by hydrogenation of biomass-derived levulinic acid over Ru/C catalyst. *Energy and Fuels*, *23*(8), 3853-3858.
- Yang, Y., Xu, X., Zou, W., Yue, H., Tian, G., and Feng, S. (2016). Transfer hydrogenation of methyl levulinate into gamma-valerolactone, 1,4-pentanediol, and 1-pentanol over Cu–ZrO₂ catalyst under solvothermal conditions. *Catalysis Communications*, *76*, 50-53.
- Zhang, J., Chen, J., Guo, Y., and Chen, L. (2015). Effective upgrade of levulinic acid into gamma-valerolactone over an inexpensive and magnetic catalyst derived from hydrotalcite precursor. *ACS Sustainable Chemistry and Engineering*, *3*(8), 1708-1714.

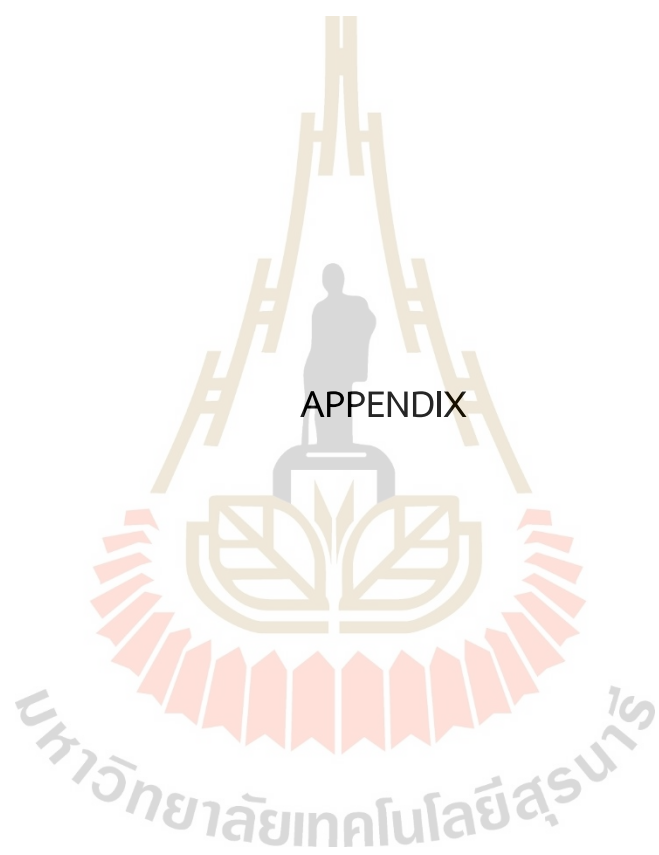
CHAPTER V

CONCLUSIONS

Zeolite NaX samples with varied crystallinity were synthesized by adjusting hydrothermal time from 0 to 24 h. HT0 and HT4 displayed similar characteristics, with crystallization beginning after 4 h. Complete zeolite crystallization occurred with treatment times of 8 hours or longer. Impregnation with potassium acetate buffer and subsequent calcination transformed the precursor into potassium carbonate. Catalysts employing zeolite NaX with higher crystallinity exhibited stronger and higher basicity, consequently enhancing catalytic efficiency in transesterification reactions, despite possessing similar surface areas, morphology, elemental compositions, and functional groups. K/HT8, K/HT12, and K/HT24 effectively facilitated the transesterification reaction, each achieving biodiesel yields about 80%. However, the spent catalysts proved ineffective for reuse due to the leaching of potassium carbonate from the support surfaces by methanol.

The synthesis of gamma-valerolactone (GVL) from methyl levulinate (ML) utilizing 2-propanol as a solvent via catalytic transfer hydrogenation has been successfully demonstrated, employing NiCu alloy as a catalyst in comparison to Ni catalysts. Both Ni and NiCu catalysts exhibited significant ML conversion rates and GVL yields under high-temperature conditions (200 °C). Notably, the NiCu catalyst displayed superior performance even at lower temperatures, achieving a GVL yield of 75% within a 6 h, reaction temperature at 140 °C. Conversely, the Ni catalyst demonstrated comparable performance solely at 200 °C, yielding inadequate GVL (28%) at 160 °C and exhibiting no catalytic activity below this temperature.

This thesis has provided a deeper understanding and data for the development of catalysts such as K/NaX and NiCu alloy for the conversion of both liquid and solid biomass into high-value chemicals such as biodiesel and GVL.



APPENDIX

APPENDIX

**SUPPORTING INFORMATION FOR KINETIC STUDY OF NICKEL AND
COPPER MONO/BIMETALLIC CATALYSTS IN HYDROGENATION OF
METHYL LEVULINATE TO GAMMA-VALEROLACTONE**

Kinetic chart of k_1 and k_2 from Ni and NiCu catalysts

Note that the data points selected represent where the rates are the most constant, which leads to the most linear plots – applies to Figure A1 and A2.

Rate constants (k_1 and k_2) are plotted according to the second-order rate law due to good fit and correlation. Figure A.1(a, b, c) and A.2(a, b, c) were plotted as 1/concentration by time for both ML and HPA.

Due to the simultaneous production and consumption of HPA, the quantity of the intermediate product was calculated from the amount of ML converted and the concentration of GVL produced in as shown in equation below:

$$\text{HPA conc. (mol)} = (\text{starting ML}) - (\text{current GVL} + \text{current HPA})$$

The rate constant k_2 was calculated by the rate in which HPA was consumed. However, as the HPA was both produced and consumed simultaneously, the HPA concentration obtained in the equation is an assumption that was deduced from the 100 % selectivity in converting ML to GVL.

The activation energy was obtained from the rearranged Arrhenius equation in Figure A.1(d) and A.2(d)

$$\ln k = \frac{-E_a}{RT} - \ln A \quad (\ln A = \text{intercept on y-axis})$$

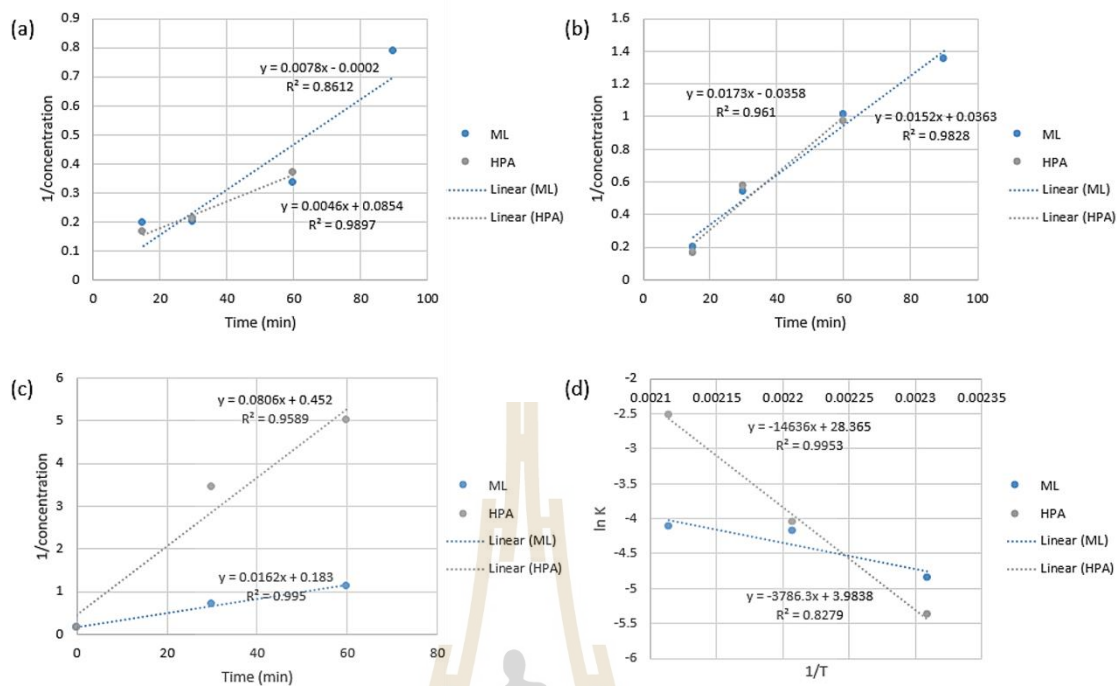


Figure A.1 Kinetic chart of k_1 and k_2 Ni catalyst at the temperatures of (a) 160 °C (b) 180 °C and (c) 200 °C and (d) the Ea calculation plot of $\ln k$ by $1/T$

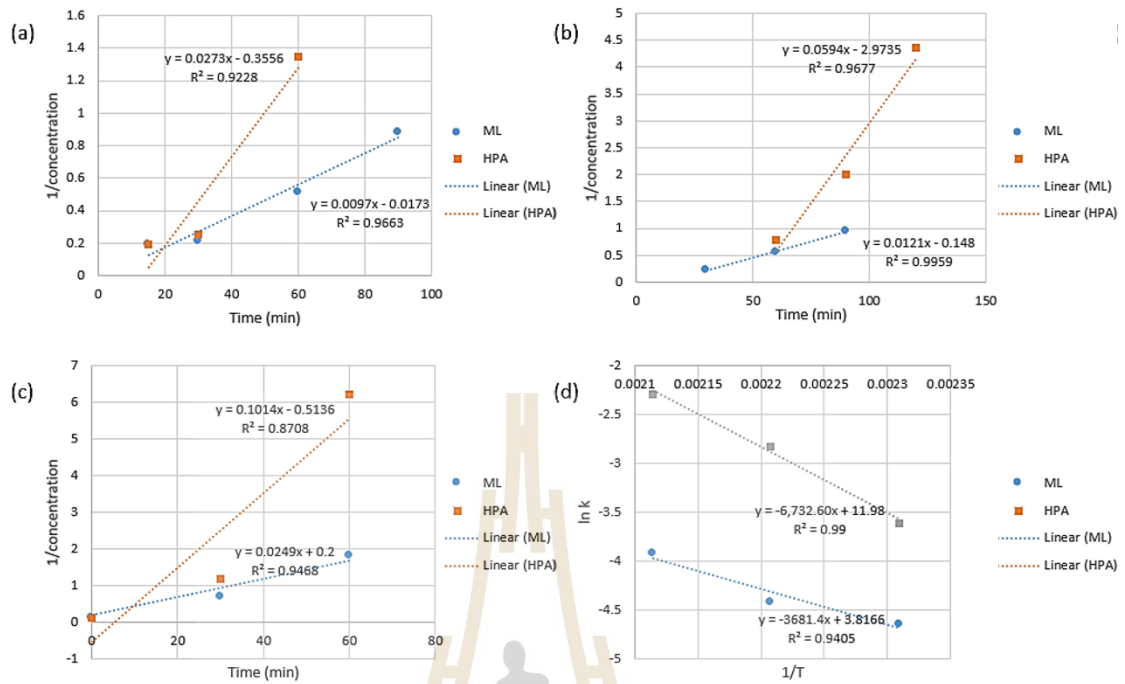


Figure A.2 Kinetic chart of k_1 and k_2 NiCu catalyst at the temperatures of (a) 160 °C (b) 180 °C and (c) 200 °C and (d) the E_a calculation plot of $\ln k$ by $1/T$

CURRICULUM VITAE

CHAIANUN PANSAKDANON

Place of Birth Surin, Thailand

Education

- 2012-2016 B.Sc. in Chemistry (1st Class Honors)
Ubon Ratchathani University, Ubon Ratchathani, Thailand
- 2016-2023 Ph.D. candidate in Chemistry
Suranaree University of Technology, Nakhon Ratchasima, Thailand

Scholarship

- 2012-2020 Science Achievement Scholarship of Thailand, SAST
- October-December 2018 German Academic Exchange Service, DAAD
Carl von Ossietzky Universität Oldenburg, Germany

Publications

1. Chitpakdee, C., Boonyoung, P., Pansakdanon, C., Suttisintong, K., Faungnawakij, K., Khemthong, P., Youngjan, S., Kraithong W., Sattayaporn, S., Tanthanuch, W., Kidkhunthod, P., Tanwongwan, W., Wittayakun, J., Kunaseth, M., Kuboon, S. (2023). *Applied Catalysis A: General*, 660, 119230
2. Kosawatthanakun, S., Pansakdanon, C., Sosa, N., Chanlek, N., Roessner, F., Prayoonpokarach, S., Wittayakun, J. (2022). *ACS Omega*, 7(11), 9130-9141.
3. Osakoo, N., Pansakdanon, C., Sosa, N., Deekamwong, K., Keawkumay, C., Rongchapo, W., Chanlek, N., Jitcharoen, J., Prayoonpokarach, S., Wittayakun, J. (2017). *Materials Chemistry and Physics*, 193, 470-476.